Technical Report 1371

Minimizing Residual Vibrations in Flexible Systems

Bert Whitney Rappole, Jr.

MIT Artificial Intelligence Laboratory

This blank page was inserted to preserve pagination.

Minimizing Residual Vibrations in Flexible Systems

by

Bert Whitney Rappole, Jr.

B.S.M.E., Stanford University
(June, 1990)

SUBMITTED IN PARTIAL FULFILLMENT
OF THE REQUIREMENTS FOR THE DEGREE OF

MASTER OF SCIENCE

at the

MASSACHUSETTS INSTITUTE OF TECHNOLOGY

May, 1992

Signature of Author 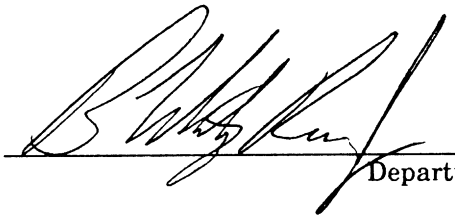
Department of Mechanical Engineering

Approved by 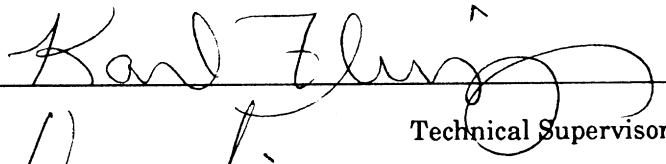
Dr. Karl Flueckiger
Technical Supervisor, Draper Laboratory

Certified by 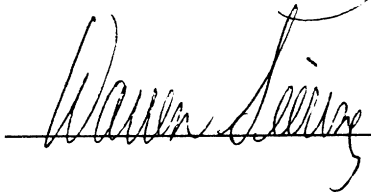
Professor Warren P. Seering
Thesis Supervisor

Accepted by _____
Ain A. Sonin
Chairman, Departmental Graduate Committee

This empty page was substituted for a blank page in the original document.

Minimizing Residual Vibrations in Flexible Systems

by

Bert Whitney Rappole, Jr.

Submitted to the Department of Mechanical Engineering
on May 21, 1992, in partial fulfillment of the requirements
for the degree of Master of Science.

Abstract

Residual vibrations degrade the performance of many systems. Due to the lightweight and flexible nature of space structures, controlling residual vibrations is especially difficult. Also, systems such as the Space Shuttle Remote Manipulator System have frequencies that vary significantly based upon configuration and loading. Recently, a technique of minimizing vibrations in flexible structures by command input shaping was developed. This document presents research completed in developing a simple, closed-form method of calculating input shaping sequences for two-mode systems and a system to adapt the command input shaping technique to known changes in system frequency about the workspace. The new techniques were tested on a three-link, flexible manipulator.

A closed-form solution was found for calculating sequences for undamped, two-mode systems. The new sequences will have a time delay up to 25% less than sequences generated using previous methods. An approximate solution was found for calculating two-mode sequences for systems with significant damping. Simplified equations for the multiple-mode cases, based upon the two-mode solution, are presented, and some possible solution methods are explained. A similarity between input shaping sequences and windows used in data acquisition is noticed.

For adapting to frequency variations about the workspace, a method was developed for determining the system frequencies based upon system configuration by interpolating values from a table, calculating new sequences using the two-mode solution, and implementing the sequence. New sequences are generated in this manner at each time step of the servo loop.

Experiments were performed on the Flexbot, a three-link, flexible manipulator. The tests showed that the new, two-mode sequences were more effective at reducing residual vibrations than previous methods of calculating sequences. Experiments testing the adaptive shaping techniques were inconclusive. The adaptive scheme was able to significantly improve the vibration reduction for certain slews but performed worse in other moves.

Thesis Supervisor:
Professor Warren P. Seering

Minimizing Residual Vibrations in Flexible Systems

by

Bert Whitney Rappole, Jr.

Submitted to the Department of Mechanical Engineering
on May 21, 1982, in partial fulfillment of the requirements
for the degree of Master of Science.

Abstract

Residual vibrations degrade the performance of many systems. Due to the lightweight and flexible nature of space structures, controlling residual vibrations is especially difficult. Also, systems such as the Space Shuttle Remote Manipulator System have frequencies that vary significantly based upon configuration and loading. Recently, a technique of minimizing vibrations in flexible structures by command input shaping was developed. This document presents research completed in developing a simple, closed-form method of calculating input shaping sequences for two-mode systems and a system to adapt the command input shaping technique to known changes in system frequency about the workspace. The new techniques were tested on a three-link, flexible manipulator.

A closed-form solution was found for calculating sequences for undamped, two-mode systems. The new sequences will have a time delay up to 25% less than sequences generated using previous methods. An approximate solution was found for calculating two-mode sequences for systems with significant damping. Simplified equations for the multiple-mode cases, based upon the two-mode solution, are presented, and some possible solution methods are explained. A similarity between input shaping sequences and windows used in data acquisition is noticed.

For adapting to frequency variations about the workspace, a method was developed for determining the system frequencies based upon system configuration by interpolating values from a table, calculating new sequences using the two-mode solution, and implementing the sequence. New sequences are generated in this manner at each time step of the servo loop.

Experiments were performed on the Flexbot, a three-link, flexible manipulator. The tests showed that the new, two-mode sequences were more effective at reducing residual vibrations than previous methods of calculating sequences. Experiments testing the adaptive shaping techniques were inconclusive. The adaptive scheme was able to significantly improve the vibration reduction for certain slews but performed worse in other moves.

Thesis Supervisor:
Professor Warren P. Seering

Acknowledgment

May 21, 1992

This thesis was prepared at The Charles Stark Draper Laboratory, Inc., under Draper IR&D Purchase Order #DL-H-404169.

Publication of this thesis does not constitute approval by Draper or the sponsoring agency of the findings or conclusions contained herein. It is published for the exchange and stimulation of ideas.

I hereby assign my copyright of this thesis to The Charles Stark Draper Laboratory, Inc., Cambridge, Massachusetts.

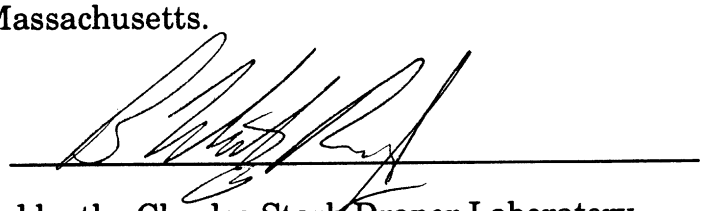

Permission is hereby granted by the Charles Stark Draper Laboratory, Inc., to the Massachusetts Institute of Technology to reproduce any or all of this thesis.

Acknowledgment

May 21, 1992

This thesis was prepared at The Charles Stark Draper Laboratory, Inc., under Draper IR&D Purchase Order #DL-H-404169.

Publication of this thesis does not constitute approval by Draper or the sponsoring agency of the findings or conclusions contained herein. It is published for the exchange and stimulation of ideas.

I hereby assign my copyright of this thesis to The Charles Stark Draper Laboratory, Inc., Cambridge, Massachusetts.

Permission is hereby granted by the Charles Stark Draper Laboratory, Inc., to the Massachusetts Institute of Technology to reproduce any or all of this thesis.

Acknowledgments

There are many people who I would like to thank for their help and support during my two years here.

At Draper, I thank Karl Flueckiger, Martha Demeo, and Joe Turnbull for their advice, and Noel Nistler and Steve Stephanides for keeping my office lively.

At the AI lab: without Brian Avery and Andy Christian, I would not have been able to complete my research. I thank Tim Tuttle and Jim Hyde for getting me out of the lab on occasion. Ken Chang, Sarath Krishnaswamy, Mike Caine, Erik Vaaler, and Lukas Ruecker all made life at MIT enjoyable.

My thesis advisor, Warren, was supportive at every turn. I appreciate his help in finding direction in my research and in solidifying my perspective on life.

I would like to thank all the Slimers and the Mechanical Engineering IM Volleyball team, especially Amy, Gunter, Steve, Evan, and Craig. We should have won the championship, again.

My life at MIT would not have been complete without my longtime roommate Chris and my friend Kai, who both decided to join me on the East Coast these past two years.

Most of all, I would like to thank my parents. Without their support and love, I could not have survived.

Acknowledgments

There are many people who I would like to thank for their help and support during my two years here.

At Draper, I thank Karl Flueckiger, Martha Demeo, and Joe Turnbull for their advice, and Noel Nistler and Steve Stephanides for keeping my office lively.

At the AI lab: without Brian Avery and Andy Christian, I would not have been able to complete my research. I thank Tim Tuttle and Jim Hyde for getting me out of the lab on occasion. Ken Chang, Sarath Krishnaswamy, Mike Caine, Erik Vaaler, and Lukas Buecker all made life at MIT enjoyable.

My thesis advisor, Warren, was supportive at every turn. I appreciate his help in finding direction in my research and in solidifying my perspective on life.

I would like to thank all the Slimers and the Mechanical Engineering IM Volleyball team, especially Amy, Gunter, Steve, Evan, and Craig. We should have won the championship, again.

My life at MIT would not have been complete without my longtime roommate Chris and my friend Kai, who both decided to join me on the East Coast these past two years.

Most of all, I would like to thank my parents. Without their support and love, I could not have survived.

Table of Contents

Acknowledgments 5

Table of Contents 9

List of Figures 11

List of Tables 15

1. Introduction 17
   - 1.1 Motivation and Background 17
   - 1.2 Previous Work 18
   - 1.3 Current Research 21

2. Basic Command Input Shaping 23
   - 2.1 Basic Theory 24
   - 2.2 Sensitivity of Input Shaping to Modelling Errors 26
   - 2.3 Multiple-Mode Formulations 27
   - 2.4 Conclusions 31

3. Expansion of Input Shaping Theory 33
   - 3.1 Direct Solutions for Multiple Modes 33
   - 3.2 The Two-Mode, Symmetric Solution 34
     - 3.2.1 Solution for Simple Constraints 35
     - 3.2.2 Solution for Simple and Derivative Constraints 37
   - 3.3 Analytic Solutions for the Higher-Mode Problem 39
   - 3.4 Domain of Direct-Solution Sequences 41
     - 3.4.1 Sequences with Positive Impulses 41
     - 3.4.2 Sequences with Negative Impulses 44
   - 3.5 Time Delay of Direct-Solution Sequences 46
     - 3.5.1 Comparison of Direct-Solution and Convolved Sequences 46
     - 3.5.2 Lengthening Sequences to Keep Positive Impulses 48
   - 3.6 Approximate, Damped Solution 54
   - 3.7 Similarities of Input Shaping and Windowing 58

4. Implementation on a Real System 63
   - 4.1 Introduction 63
   - 4.2 Selection of a Flexible System 64
   - 4.3 The Flexbot as a Flexible System 64
     - 4.3.1 Hardware Changes: 64
     - 4.3.2 Software Changes: 65
   - 4.4 Analysis of Vibrational Workspace 69
   - 4.5 Implementation of Command Shaping Techniques 74

4.5.1 Varying Frequencies 74
4.5.2 Accessing Frequency Data 74
4.5.3 Discretization Problems 75
4.5.4 Buffering Method 80
4.6 Conclusions 81

5. Experimentation and Results 83
5.1 Introduction 83
5.2 Experimental Set Up 84
5.3 Constant-Frequency Moves 88
5.3.1 Move with Tuned Shapers 88
5.3.2 Constant-Frequency Move with Poorly Tuned Sequences 93
5.4 Varying-Frequency Moves 97
5.4.1 Varying-Frequency Move Close to Tuned-Frequency Position 99
5.4.2 Varying-Frequency Move not at Tuned-Frequency Position 107
5.5 Effect of Varying Prefiltering Sequences 108
5.6 Comparison of Windowing Sequences. 109
5.7 Conclusions 110

6. Conclusions 113
6.1 Summary 113
6.2 Suggested Work 115

References 117

List of Figures

2-1 Block Diagram of System Using Input Shaping 24
2-2 Two-Impulse Sequence 26
2-3 Three-Impulse Sequence 27
2-4 Comparison of the Insensitivity of Undamped Two-Impulse and Three-Impulse Sequences. 28
2-5 Sequence for Four Modes Generated by Convolving Three-Impulse Sequences for 1.0, 2.3, 3.9, and 4.8 Hz. 29
2-6 Sequence for Four Modes Generated by Direct-Solution of Simple and Derivative Constraints for 1.0, 2.3, 3.9, and 4.8 Hz. 30
2-7 Insensitivity of Direct-Solution Sequence Shown in Figure 2-6. 31
2-8 Insensitivity of Convolved Sequence Shown in Figure 2-5. 32

3-1 Examples of Sequences found using Hyde's method 34
3-2 Time-Shifted, Symmetric Sequence for Two Modes, Using Simple Constraints 35
3-3 Three-Impulse, Direct-Solution Sequence for Two Modes. 36
3-4 Time-Shifted, Symmetric Sequence for Two-Mode System, Using Simple and Derivative Constraints 37
3-5 Five-Impulse, Direct-Solution Sequence for Two Modes. 38
3-6 Variation of Second Impulse Amplitude with Frequency Ratio Three-Impulse Sequence 42
3-7 Variation of Second Impulse Amplitude with Frequency Ratio Five-Impulse Sequence 43
3-8 Two-Mode Sequence for 1.0 and 3.7 Hz, with Negative Impulses 44
3-9 Insensitivity of Two-Mode Sequence for 1.0 and 3.7 Hz, with Negative Impulses 45
3-10 Comparison of Time Delay Caused by Convolved and Direct-Solution Shapers- 47
3-11 Insensitivity of a Three-Impulse Shaper 48
3-12 Variation of Time Delay with Choice of Z 49
3-13 Insensitivity Curve for Five-Impulse Sequence for 1.0 and 2.5 Hz. 50
3-14 Two-Mode Convolved Sequence, 1.0 and 2.5 Hz. 51
3-15 Two-Mode Direct-Solution Sequence, 1.0 and 2.5 Hz. 51
3-16 Insensitivity of Convolved Sequence for 1.0 and 2.5 Hz, ... 52
3-17 Sequence Generated by Convolving Two-Mode, Symmetric Solutions for 1.0 and 2.3 Hz and 3.9 and 4.8 Hz 53
3-18 Insensitivity of Sequence in Figure 3-18. 53
3-19 Insensitivity of Undamped Sequence, from Table 3-1 57
3-20 Insensitivity of Approximate, Damped Sequence, from Table 3-2 57
3-21 Insensitivity of Exact, Damped Sequence, from Table 3-3. 57

3-22 Parzen and Square Windows 58
3-23 Three-Impulse Convolved Sequences for 1.0, 2.0, 4.0, and 8.0 Hz. 60
3-24 Two-Impulse Convolved Sequences for 1.0, 2.0, 4.0, and 8.0 Hz. 60
3-25 Insensitivity of Three-Impulse, Convolved Sequences Shown in Figure 3-23 61
3-26 Insensitivity of Two-Impulse, Convolved Sequences Shown in Figure 3-24 61

4-1 The Flexbot. 66
4-2 Interaction of Boards in VMEbus 67
4-3 Definition of Flexbot Joint Angles 69
4-4 Variation of First Frequency with Joint Angles 72
4-5 Variation of Second Frequency with Joint Angles 72
4-6 Variation of Third Frequency with Joint Angles 73
4-7 Variation of fourth Frequency with Joint Angles 73
4-8 Sequence for 7.576 Hz Discretized to 125 Hz Timing Loop 75
4-9 Sequence for 7.575 Hz Discretized to 125 Hz Timing Loop 76
4-10 Shaped Command With Varying Sequences--The Wrong Way 77
4-11 Method of Extrapolating Sequences. 77
4-12 Continuous Time Sequence, 7.575 Hz, 125 Hz Timing Loop 78
4-13 Extrapolated Sequence for 7.575 Hz, 125 Hz Timing Loop 78
4-14 Insensitivity Curve for 7.575 Hz Continuous Sequence, from Fig. 4-12 79
4-15 Insensitivity Curve for 7.575 Hz Sequence Extrapolated to 125 Hz Timing Loop, from Fig. 4-13 79
4-16 Insensitivity Curves for 7.575 and 7.576 Hz Sequence Moved to Closest Time Step, 125 Hz Timing Loop 80
4-16 Buffering Technique used for Multiple Sequences 81

5-1 Data Collection in Experimental Set Up 84
5-2 Joint Position Data 85
5-3 Data Used for FFT Calculation 86
5-4 Detail of ResidualAcceleration for Shaped, 15°/sec Slew, Using Long-2M3 Sequence, from {30,60,10} to {-30,10,60}. 90
5-5 Detail of Residual Acceleration for Shaped, 15°/sec Slew, Using Adaptive Long-2M3 Sequence, from {30,60,10} to {-30,10,60}. 90
5-6 Detail of Residual Acceleration of Idle Robot. Recorded Two Minutes After Last Commanded Motion. 90
5-7 Accelerometer Time Trace for Constant Frequency Move, No Shaping. 91
5-8 Accelerometer Time Trace for Constant Frequency Move, Long-2M3 Sequence 91
5-9 FFT Magnitude of Unshaped, Constant Frequency Move 92
5-10 FFT Magnitude of Constant Frequency Move Using Long-2M3 Sequence. 92

5-11 FFT Magnitude of Unshaped Slew from {30,80,80} to {-30,80,80} at 50°/sec 94
5-12 FFT Magnitude of Long-2M5 Slew from {30,80,80} to {-30,80,80} at 50°/sec. 94
5-13 Variation of Third Frequency with Position with Testing Paths Marked. 98
5-14 Variation in Filtering Sequence During 30°/sec Slew from {30,60,10} to {-30,10,60} 99
5-15 Acceleration of Unshaped, 15°/sec Slew from {30,60,10} to {-30,10,60} 102
5-16 Acceleration of Shaped, 15°/sec Slew Using Long-2M3 Sequence, from {30,60,10} to {-30,10,60}. 102
5-17 Acceleration of Shaped, 15°/sec Slew, Using Adaptive Long-2M3 Sequence, from {30,60,10} to {-30,10,60} 102
5-18 In-Plane Acceleration from Unshaped move from {30,60,10} to {-30,10,60} at 30°/sec. 105
5-19 In-Plane Acceleration from Long-2M5 move from {30,60,10} to {-30,10,60} at 30°/sec. 105
5-20 In-Plane Acceleration from Adaptive-Long-2M5 move from {30,60,10} to {-30,10,60} at 30°/sec 105
5-21 FFT Magnitude of In-Plane Acceleration of Unshaped Move from {30,60,10} to {-30,10,60} at 30°/sec 106
5-22 FFT Magnitude of In-Plane Acceleration of Long-2M5 Move from {30,60,10} to {-30,10,60} at 30°/sec 106
5-23 FFT Magnitude of In-Plane Acceleration of Adaptive-Long-2M5 Move from {30,60,10} to {-30,10,60} at 30°/sec. 106
5-24 FFT Magnitude of Unshaped Response, 50°/sec Velocity Move from {0,80,80} to {30,45,45} 108
5-25 FFT Magnitude of Adaptive-Long-2M3 Shaper, 50°/sec Velocity Move from {0,80,80} to {30,45,45}. 108
5-26 FFT Magnitude of Long-2M3 Shaper, 50°/sec Velocity Move from {0,80,80} to {30,45,45}. 109
5-27 Sequence for Window Tests Three-Impulse Sequences 110

5-11 PPT Magnitude of Unshaped Slew from (30,80,80) to (-30,80,80) at 80°/sec 94
5-12 PPT Magnitude of Long-2M3 Slew from (30,80,80) to (-30,80,80) at 80°/sec 94
5-13 Variation of Third Frequency with Position with Testing Paths Marked 98
5-14 Variation in Filtering Sequence During 80°/sec Slew from (30,60,10) to (-30,10,60) 99
5-15 Acceleration of Unshaped, 15°/sec Slew from (30,60,10) to (-30,10,60) 102
5-16 Acceleration of Shaped, 15°/sec Slew Using Long-2M3 Sequence, from (30,60,10) to (-30,10,60) 102
5-17 Acceleration of Shaped, 15°/sec Slew, Using Adaptive Long-2M3 Sequence, from (30,60,10) to (-30,10,60) 102
5-18 In-Plane Acceleration from Unshaped move from (30,60,10) to (-30,10,60) at 80°/sec. 105
5-19 In-Plane Acceleration from Long-2M3 move from (30,60,10) to (-30,10,60) at 80°/sec. 105
5-20 In-Plane Acceleration from Adaptive-Long-2M3 move from (30,60,10) to (-30,10,60) at 80°/sec. 105
5-21 PPT Magnitude of In-Plane Acceleration of Unshaped Move from (30,60,10) to (-30,10,60) at 80°/sec. 106
5-22 PPT Magnitude of In-Plane Acceleration of Long-2M3 Move from (30,60,10) to (-30,10,60) at 80°/sec. 106
5-23 PPT Magnitude of In-Plane Acceleration of Adaptive-Long-2M3 Move from (30,60,10) to (-30,10,60) at 80°/sec. 106
5-24 PPT Magnitude of Unshaped Response, 80°/sec Velocity Move from (0,80,80) to (30,45,45) 108
5-25 PPT Magnitude of Adaptive-Long-2M3 Shaper, 80°/sec Velocity Move from (0,80,80) to (30,45,45) 108
5-26 PPT Magnitude of Long-2M3 Shaper, 80°/sec Velocity Move from (0,80,80) to (30,45,45) 109
5-27 Sequence for Window Tests Three-Impulse Sequence 110

List of Tables

3-1 Direct-Solution, Five-Impulse Sequence 56
3-2 Approximate, Five-Impulse Sequence for 1.0 Hz, ... 56
3-3 Exact, Five-Impulse Sequence for 1.0 Hz, ... 56

4-1 Description of Boards in VMEbus. 67

5-1 Types of Shaping Sequences Used in Tests 89
5-2 Vibration Reduction in Constant Frequency Move, {30,30,30} to {-30,30,30} at 15°/sec. 95
5-3 Vibration Reduction in Constant Frequency Move, {30,80,80} to {-30,80,80} at 50°/sec 96
5-4 Vibration Reduction in Variable Frequency Move, {30,60,10} to {-30,10,60} at 15°/sec. 101
5-5 Vibration Reduction in Variable Frequency Move, {30,60,10} to {-30,10,60} at 30°/sec 103
5-6 Vibration Reduction in Variable Frequency Move, {30,60,10} to {-30,10,60} at 50°/sec. 1077
5-7 Results of Windowing Tests 110

List of Tables

3-1 Direct-Solution, Five-Impulse Sequence 56
3-2 Approximate, Five-Impulse Sequence for 1.0 Hz, ... 56
3-3 Exact, Five-Impulse Sequence for 1.0 Hz, ... 56

4-1 Description of Bands in VME/bus. 67

5-1 Types of Shaping Sequences Used in Tests 89
5-2 Vibration Reduction in Constant Frequency Move, {30,30,30} to {-30,30,30} at 15°/sec. 96
5-3 Vibration Reduction in Constant Frequency Move, {30,80,80} to {-30,80,80} at 80°/sec 98
5-4 Vibration Reduction in Variable Frequency Move, {30,60,10} to {-30,10,60} at 15°/sec. 101
5-5 Vibration Reduction in Variable Frequency Move, {30,60,10} to {-30,10,60} at 30°/sec 108
5-6 Vibration Reduction in Variable Frequency Move, {30,60,10} to {-30,10,60} at 50°/sec. 1077
5-7 Results of Windowing Tests 110

Introduction

Chapter 1

This thesis presents the development and implementation of an improved method of reducing residual vibration in flexible systems. The method presented here is a form of command input shaping. The command input shaping theory is enhanced to accommodate systems with multiple-modes of vibration and to adapt to variations in system frequency about the workspace. This chapter describes the motivation for the work, summarizes previous research in reducing vibration, and explains the organization for the rest of the document.

1.1 Motivation and Background

Vibrations are problematic in most mechanical systems. Common methods of reducing the negative effect of vibrations include structurally stiffening the system, increasing the damping of the system, and reducing the speed at which the system operates. With the advent of high-speed computer control, another method has appeared--minimizing vibrations with computer-control algorithms. Many applications could be better solved with light, quick

systems using smart controllers to reduce vibrations, than with massive, slow structures requiring no control. The high cost of space travel severely limits the weight of space-based systems, and the large, lightweight nature of space structures makes them especially prone to vibration problems. For example, the Space Shuttle's Remote Manipulator System (RMS) is a fifty-foot arm that has a lowest vibrational frequency of 0.5 Hz when unloaded. Typically, 50% of the operating time for the RMS is spent waiting for vibrations to dissipate. A control scheme that allows systems such as the RMS to move without exciting its vibratory modes would be welcomed. The applications of such a system are not limited to space structures. A method of minimizing residual vibrations would permit the design of lighter, faster, and cheaper systems without the need to worry about vibration problems.

1.2 Previous Work

Controlling flexible structures has been a popular area of study for the past decade. The proposed space station has pushed even more effort into finding a successful method of moving flexible systems without exciting vibrations. The previous research can be split into three main areas. First, several people have investigated the possibility of incorporating flexible links and joints into a model.

Asada, Ma, and Tokumaru [1] developed a model of a two-link system, that accounted for joint and link flexibility. In simulation they were able to obtain relatively good performance in moving the system without exciting endpoint vibrations.

Eisler, Segalman, and Robinett [7] derived a model of a two-link, flexible system that incorporated Finite Element models of the links and joints. Using this model, they were able to numerically integrate to generate torque

trajectories that would minimize vibration at the end of the slew. They were able to increase performance noticeably on a simple two-link system.

Keene [32] has been working to develop a flexible model of the Space Shuttle Remote Manipulator System (RMS) during maneuvers with large payloads. The large payload assumption--for example, docking with the proposed space station--allows the arm to be modeled as a massless spring. The first attempts showed some promise in using derived end-point feedback, based upon the flexible model, however the resulting system was very sensitive to modelling errors.

Most of the attempts at incorporating flexibility into the system model have proven to be difficult to implement and very sensitive to system parameters.

The second area of research has been in filtering input commands to avoid exciting vibrations.

Smith [20] described a method of posicast control that can be used to eliminate a single frequency of vibration. He split commands into two discrete pulses, spaced over one-half period of vibration to cancel vibrations. This method is successful in reducing vibrations, but is sensitive to errors in frequency and reduces one mode of vibration only.

Aspinwall [2] uses a finite, Fourier series expression to modify the forcing function and reduce vibrations. His attempts were successful, but required a time delay twice the period of vibration to eliminate vibration.

Farrenkopf [8] generates maneuver profiles that attempt to minimize the amount of energy dumped into flexing and the magnitude of the flexing during a move. He uses the Calculus of Variations to generate the commands. The technique required moves at least 5 times the period of the

lowest flexural mode to significantly reduce vibrations at the end of the slew without causing excitation during the move.

Swigert [21] uses a linear model of a flexible system to produce a torque profile that minimizes the modal amplitude or the derivative of modal amplitude. When the derivative term is minimized, sensitivity to modelling errors is decreased.

Meckl [12] derived a shaping method that uses a versine (1- sine) shaped function to eliminate certain frequencies from the input.

Singer [18] used a linear model of a flexible system to develop a computationally simple algorithm for constraining the modal displacements and derivatives of modal displacements to zero at the end of a move. Singer's algorithm uses discrete impulses to eliminate the vibration. The impulse sequences cause a time delay of one cycle of vibration. This method, which has come to be known as input shaping forms the basis of the research presented in this document, will be described more fully in Chapter 2.

Singhose [19] developed an algorithm based upon Singer's work that further improved the insensitivity of the shaping technique to modelling errors at the cost of not constraining the residual vibration to zero at the desired frequency, but permitting a small amount to remain.

Hyde [10] expanded Singer's equations to numerically solve for impulse sequences for systems with up to five modes of vibration. His work will also be discussed in Chapter 2.

Tzes and Yurkovich [23] developed an on line modal identification scheme--TTFE--to identify the frequency characteristics of a single-link flexible structure on-line. In conjunction with Englehart [24], they were able to significantly reduce the endpoint vibration when input shaping sequences were used in conjunction with TTFE.

Magee [11] proposes a smoothing algorithm to account for vibrations induced when an input-shaping sequence is varied during a move. His efforts proved successful in driving a 20 ft. two-link, hydraulic robot.

Other people have tested the input shaping theories, including Christian [6], who compared shaping techniques with controlled acceleration profiles; Murphy and Watanabe [14], who performed a digital analysis of input shaping and determined that shaping can be described as a type of notch filtering that places zeros to cancel the closed-loop system's poles; Banerjee [31], who demonstrated that shaping effectively reduced vibration in a simulation of the Space Shuttle carrying two, 150m flexible antenna; and Seth, Rattan, and Brandstetter [34], who implemented input shaping on a Coordinate Measuring Machine with some success.

Finally, there is interdisciplinary research into Controlled Structured Interaction (CSI). CSI attempts to study the way structures interact, and concerns itself mainly with space structures. NASA has established a group that is attempting to find solutions to vibration problems in the proposed space station. They are using the technologies described above as well as doing study on active damping methods and designing to minimize vibration problems [33]. One of the NASA-CSI functions has been developing the Mid-Deck Active Control Experiment (MACE), a test article for CSI theories. [13].

1.3 Current Research

This document presents research done in two areas. First, a new method of calculating input shaping sequences for two-frequencies of vibration is presented. The new method is closed-form, and produces sequences with up to 25% savings in time delay over previous methods. Second, an adaptive input shaping method is designed to provide good vibration reduction in

systems with large variations in frequency. The new sequences and the adaptive method of shaping are both tested on the Flexbot, a three-joint spatial manipulator. The remainder of this document is divided into five chapters.

Chapter 2 describes the basic command input shaping theory as developed by Singer [18] and Hyde [10].

Chapter 3 presents the theory for the new command input shaping sequences for two frequencies of vibration. Also a comparison is made between the shape of certain convolved-sequences and several standard data-windowing curves.

Chapter 4 describes the Flexbot, the experimental system used for verifying the new shaping techniques. The variation in vibrational frequency of the Flexbot is mapped and a method of accessing the frequency data and implementing the changes on-line using adaptive-shaping is developed.

Chapter 5 presents the results of experiments performed on the Flexbot. Tests were run comparing the new, two-mode sequences with sequences generated by previous methods. Experimental data was collected comparing the method of adaptive shaping to methods that do not account for variations in frequency.

Chapter 6 discusses the conclusions that arise from the experimental data and proposed areas for continued research.

Basic Command Input Shaping

Chapter 2

Command input shaping was developed several years ago to provide a simple algorithm for reducing residual vibration in flexible systems. The method of input shaping was originally developed by Singer [18]. Several other researchers have preceded me in continuing the development of input shaping theory[10, 19]. I have chosen to implement some new techniques in command shaping theory that will improve the ability of the method to eliminate vibration with the shortest time delay. Before discussing my new additions, I will present a brief overview of the general method. This chapter is not intended to present every detail of input shaping theory. All of the material presented here is paraphrased from Singer [18] and Hyde[10]. I am including it to refresh the reader's memory of the basic theory and to present the basic constraint equations that form the basis of my derivations in Chapter 3.

Input shaping is a vibration reducing scheme that uses linear vibration theory to generate sequences of impulses, which, when convolved with commands to a plant, result in minimal residual vibration at selected frequencies. The method imposes a time delay on the system equal to the length of the sequence used. Input shaping does not require feedback, so it will not cause stability problems. A block diagram of a typical system is shown in Figure 2-1, with the input shaper outside the feedback loop. The commanded inputs are fed open-loop through the shaper to the plant. We see from this diagram that input shaping depends upon prior knowledge of the closed-loop system--the user chooses the frequencies at which to eliminate vibration. If the closed-loop dynamics of the plant change, the input shaping sequence must account for the change.

2.1 Basic Theory

Singer[18] developed the input shaping technique from a second-order, linear model of a vibratory system. The response of a second-order system, with natural frequency ω and damping ratio ζ, to a single impulse at time t_i with amplitude A_i is

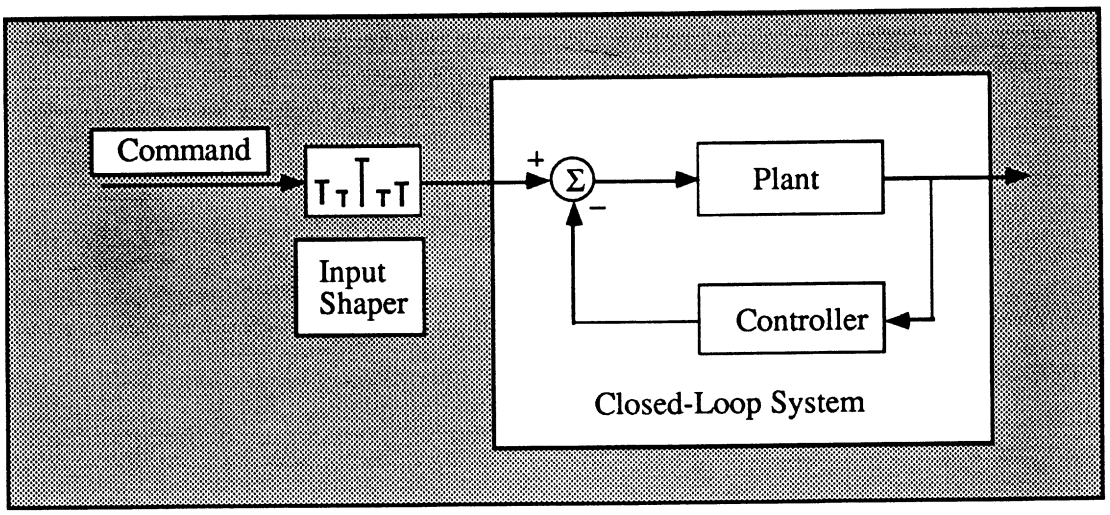

Figure 2-1: Block Diagram of System Using Input Shaping

$$y(t) = \frac{A_i \omega}{\sqrt{1-\zeta^2}} e^{-\zeta \omega (t - t_i)} \sin\left[(t - t_i)\omega\sqrt{1-\zeta^2}\right] \tag{2-1}$$

We can now find the response of the same system to a finite series of n impulses.

$$B_1 \sin(\omega t - \varphi_1) + \ldots B_n \sin(\omega t - \varphi_n) = B_{amp} \sin(\omega t - \psi) \tag{2-2}$$

where

$$B_i = \frac{A_i \omega}{\sqrt{1-\zeta^2}} e^{-\zeta \omega (t - t_i)} \tag{2-3}$$

$$\varphi_i = t_i \omega \sqrt{1-\zeta^2} \tag{2-4}$$

$$B_{amp} = \sqrt{\left(\sum_{i=1}^{n} B_i \sin(\varphi_i)\right)^2 + \left(\sum_{i=1}^{n} B_i \cos(\varphi_i)\right)^2} \tag{2-5}$$

To eliminate vibration at the conclusion of a series of impulses, the value of B_{amp} must be zero. This condition is satisfied by independently constraining both terms inside the square root in Eq. 2-5 to zero.

$$\sum_{i=1}^{n} A_i e^{-\zeta \omega (t - t_i)} \sin\left(t_i \omega \sqrt{1-\zeta^2}\right) = 0 \tag{2-7}$$

$$\sum_{i=1}^{n} A_i e^{-\zeta \omega (t - t_i)} \cos\left(t_i \omega \sqrt{1-\zeta^2}\right) = 0 \tag{2-8}$$

Two additional constraints are added.

$$t_1 = 0 \tag{2-9}$$

$$\sum_{i=1}^{n} A_i = 1 \tag{2-10}$$

The former minimizes the time delay of the shaper. The latter guarantees that there will not be a gain associated with the shaper. Singer's method also constrains the resulting values of the A_i to be positive. This additional constraint insures that high frequencies will not be excited by the shaper (see [18]). Each impulse is specified by two values: a time and an amplitude. With the four constraints listed, we generate a sequence with two impulses as shown in Figure 2-2.

In an effort to create sequences that are insensitive to modelling errors, Additional constraints are added by setting the derivative of both Eq. 2-7 and

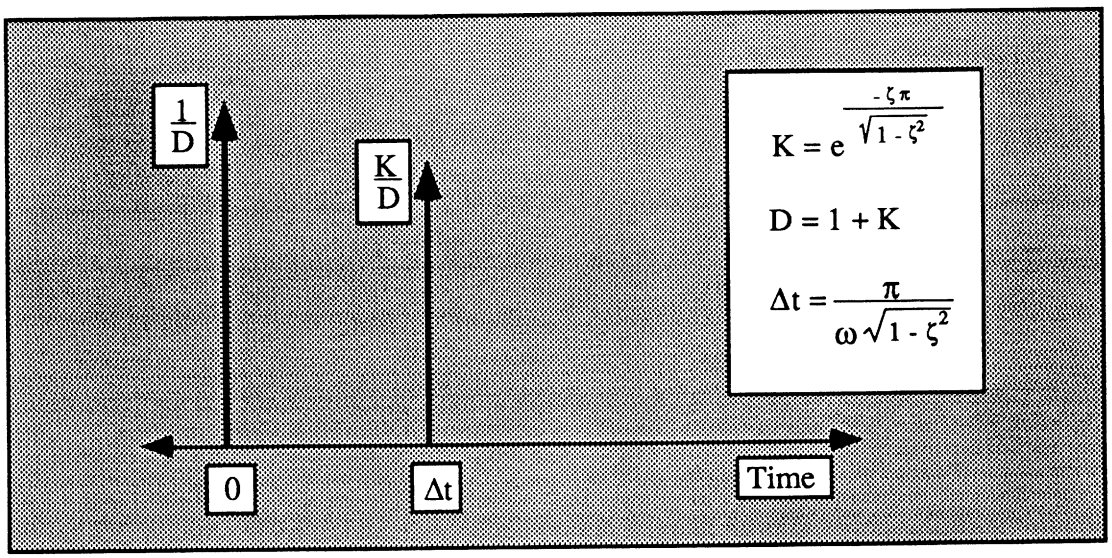

Figure 2-2: Two-Impulse Sequence

Eq. 2-8 with respect to frequency equal to zero, we will decrease the resulting sequence's sensitivity to modelling errors:

$$\sum_{i=1}^{n} A_i t_i e^{-\zeta \omega (t - t_i)} \sin\left(t_i \omega \sqrt{1-\zeta^2}\right) = 0 \qquad (2\text{-}11)$$

$$\sum_{i=1}^{n} A_i t_i e^{-\zeta \omega (t - t_i)} \cos\left(t_i \omega \sqrt{1-\zeta^2}\right) = 0 \qquad (2\text{-}12)$$

Taking the derivative of Eqs. 2-7 and 2-8 with respect to damping ratio results in the same equations. The sequence generated with these two additional constraints will have three impulses as shown in Figure 2-3. The sequences can be made "arbitrarily insensitive" to modelling errors by adding higher order derivative terms. For a complete derivation of these equations see [18].

2.2 Sensitivity of Input Shaping to Modelling Errors

Sensitivity of the shaping sequences to modelling errors is an important issue. The frequencies of vibration are likely to change with position and loading of the robot, and damping ratio is difficult to measure accurately.

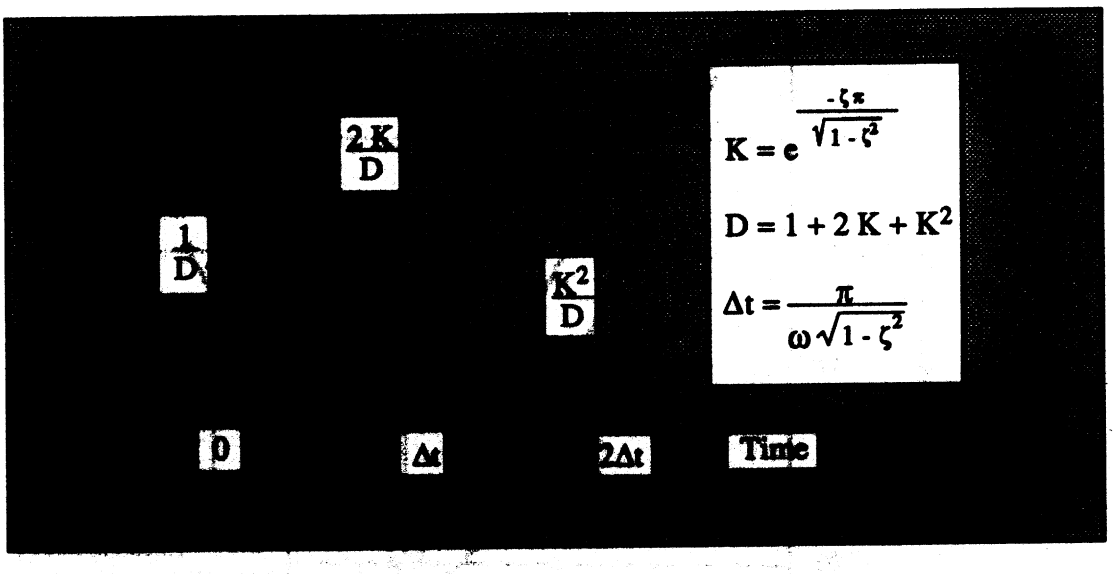

Figure 2-3: Three-Impulse Sequence

Singer defines the insensitivity to frequency errors for the single-frequency system.

$$I\left[\frac{\omega_s}{\omega_f}\right] = \sqrt{\left[\sum_{i=1}^{n} A_i e^{-\zeta\omega t_i} \sin\left(t_i\omega\sqrt{1-\zeta^2}\right)\right]^2 + \left[\sum_{i=1}^{n} A_i e^{-\zeta\omega t_i} \cos\left(t_i\omega\sqrt{1-\zeta^2}\right)\right]^2} \qquad (2\text{-}13)$$

Insensitivity corresponds to the amplitude of residual vibration that will remain in a system with natural frequency ω_s and damping ratio ζ_s when a filter with times t_i and amplitudes A_i calculated for natural frequency ω_f and damping ratio ζ_f is implemented. The insensitivity of both a two impulse sequence and a three impulse sequence is shown in Figure 2-4. The two-impulse sequence will keep the residual vibration below 5% of the unshaped amplitude for frequency-modelling errors of less than 5%. A three-impulse sequence will provide comparable vibration reduction for modelling errors of 15%.

2.3 Multiple-Mode Formulations

Singer addresses the issue of systems with more than one frequency of vibration. Since input shaping is a linear operation, shapers can be convolved

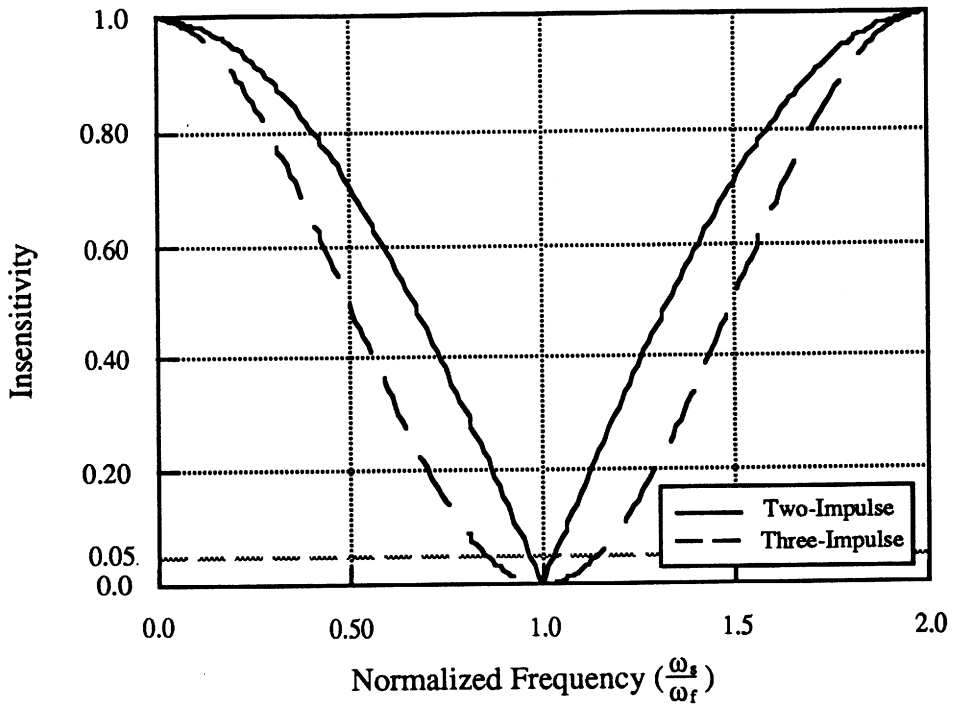

Figure 2-4: Comparison of the Insensitivity of Undamped Two-Impulse and Three-Impulse Sequences.

together. In this manner many different frequencies can be eliminated simultaneously. Unfortunately, the number of individual impulses in the resulting sequence, N, will grow exponentially with the number of frequencies being shaped, m.

$$N = n^m \tag{2-14}$$

A sequence for four modes generated in this fashion is shown in Figure 2-5.

Another drawback of this method is that the total time delay of the sequence is equal to the sum of the damped periods of vibration. A sequence for m modes generated by convolving three-impulse shapers together will have a time delay of

$$t_N = \sum_{j=1}^{m} \frac{2\pi}{\omega_j \sqrt{1 - \zeta_j^2}} \tag{2-15}$$

where ω_j and ζ_j are the frequency and damping of the jth mode and t_N is the

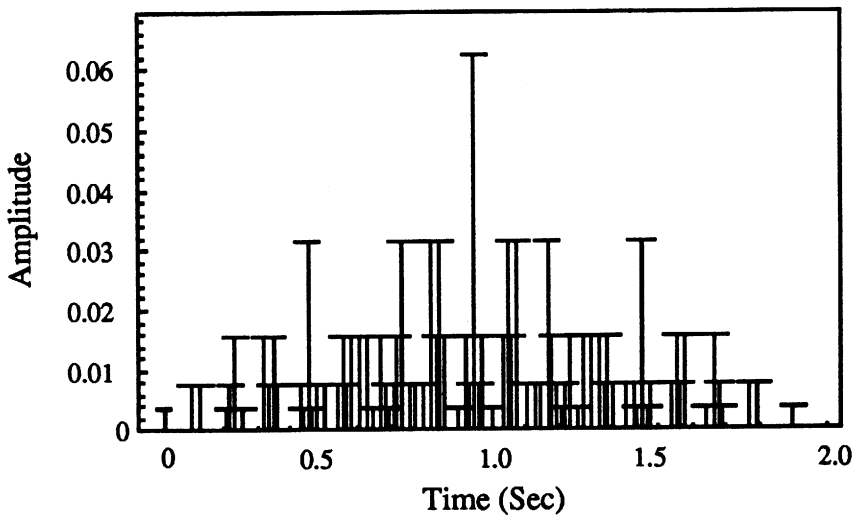

Figure 2-5: Sequence for Four Modes Generated by Convolving Three-Impulse Sequences for 1.0, 2.3, 3.9, and 4.8 Hz.

time of the last impulse. Hyde[10] presents a new method for calculating sequences for multiple-mode systems. He begins with the six basic constraint equations, Eqs. 2-7 - 2-12. He repeats the simple and derivative constraint equations for each mode.

$$\sum_{i=1}^{n} A_i e^{-\zeta_j \omega_j (t - t_i)} \sin\left(t_i \omega_j \sqrt{1-\zeta_j^2}\right) = 0 \tag{2-16}$$

$$\sum_{i=1}^{n} A_i e^{-\zeta_j \omega_j (t - t_i)} \cos\left(t_i \omega_j \sqrt{1-\zeta_j^2}\right) = 0 \tag{2-17}$$

$$\sum_{i=1}^{n} A_i t_i e^{-\zeta_j \omega_j (t - t_i)} \sin\left(t_i \omega_j \sqrt{1-\zeta_j^2}\right) = 0 \tag{2-18}$$

$$\sum_{i=1}^{n} A_i t_i e^{-\zeta_j \omega_j (t - t_i)} \cos\left(t_i \omega_j \sqrt{1-\zeta_j^2}\right) = 0 \tag{2-19}$$

There are now 4 m + 2 equations, where m is the total number of modes to cancel. Hyde's sequences will therefore have

$$N = 2m + 1 \tag{2-20}$$

impulses, thereby avoiding the exponential growth in the number of impulses that Singer noticed. To solve the equations simultaneously, Hyde uses an optimization routine and GAMS [4] and Mathematica [30], two programs with non-linear equation solvers. With this method, he is able to find

sequences for a wide range of multiple-frequency systems. A multiple-mode sequence generated using Hyde's method is shown in Figure 2-6.

Another benefit of direct-solution sequences is their length. Hyde found that the sequences he generated were generally shorter than the comparable convolved sequences Unfortunately, the savings in time is often gained at the expense of insensitivity. Multiple-mode, direct-solution sequences found using Hyde's method are also less robust to errors in modelling and are often difficult to calculate. Problems with low insensitivity are especially pronounced for sequences generated for systems with large frequency ratios. An insensitivity curve for a four-mode solution is shown in Figure 2-7. The insensitivity of the sequence generated by convolution for the same four modes is shown in Figure 2-8. The direct-solution sequence is 30% shorter, but there is a noticeable difference in the insensitivity of the sequence as compared to the convolved sequence. Calculation intensity is another issue with Hyde's method. If sequences are to be generated on-line as a system changes, the optimization method could prevent direct-solution sequences from being implemented.

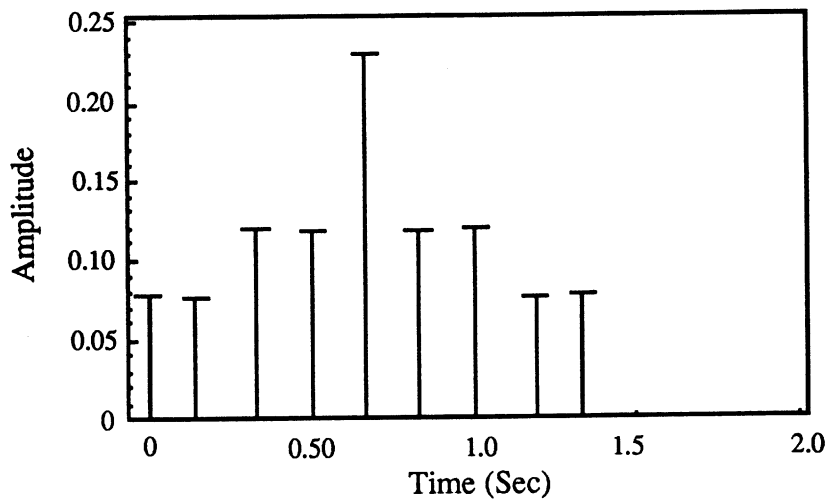

Figure 2-6: Sequence for Four Modes Generated by Direct-Solution of Simple and Derivative Constraints for 1.0, 2.3, 3.9, and 4.8 Hz.

2.4 Conclusions

In this chapter we have presented the current theory of input shaping. Command shaping has been proven to be a simple, robust method of reducing residual vibrations. Implementation on single-mode systems is easy.. Unfortunately, application to systems with many modes of vibration and large variations of frequency over the workspace requires further advances to

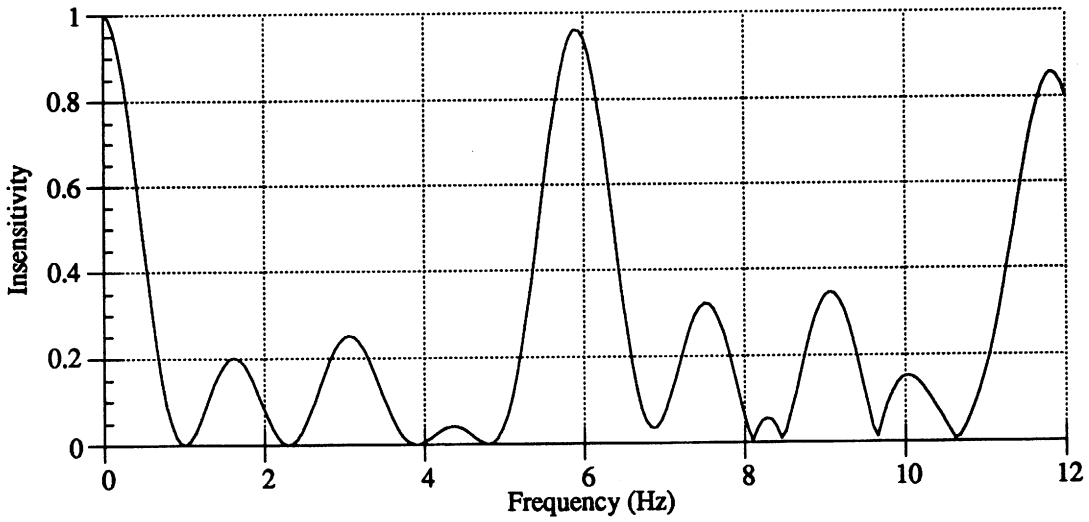

Figure 2-7: Insensitivity of Direct-Solution Sequence Shown in Figure 2-6.

avoid the exponential growth in the number of impulses in Singer's sequences or the intense calculations necessary for Hyde's method of solving the direct-solution problem.

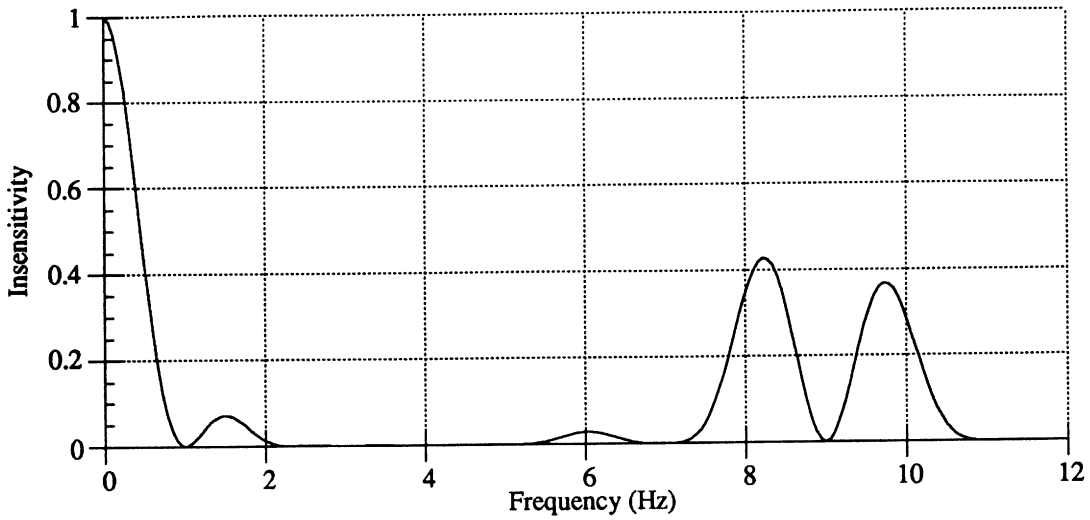

Figure 2-8: Insensitivity of Convolved Sequence Shown in Figure 2-5.

Expansion of Input Shaping Theory

Chapter 3

3.1 Direct Solutions for Multiple Modes

There is a desire for a method of calculating input shaping sequences for systems with multiple frequencies that does not require the optimization routines of Hyde's method[10]. Analytic solutions for multiple-mode sequences would be useful to take advantage of the time savings that direct-solution sequences have over convolved solutions. This chapter describes the development and analysis of a direct solution method found for undamped systems with two frequencies of vibration. It also includes a description of possibilities for finding direct solutions for systems with more vibratory modes and systems with significant damping. An analysis of the similarities between input shaping and some standard data-windowing shapes is included as well.

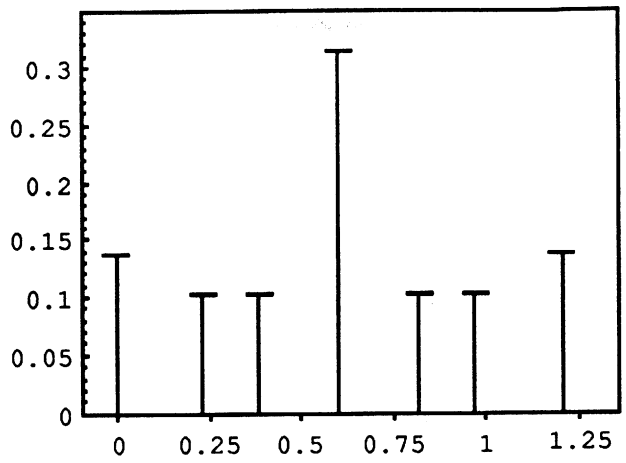

a) Sequence for 1.0, 2.4, and 4.1 Hz., No Damping

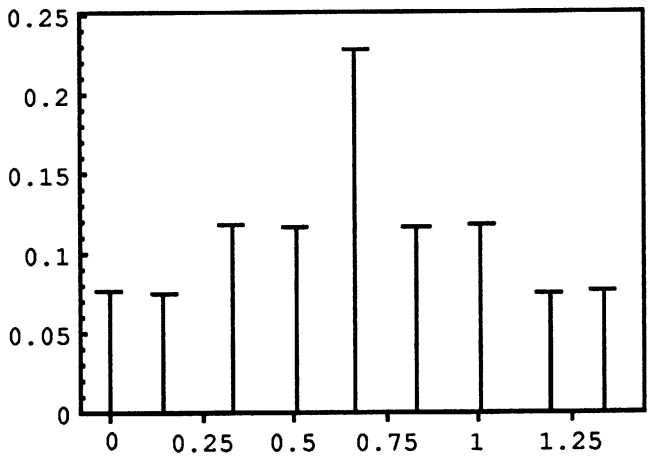

b) Sequence for 1.0, 2.3, 3.9, and 4.8 Hz., No Damping

Figure 3-1: Examples of Sequences found using Hyde's method

3.2 The Two-Mode, Symmetric Solution

In an effort to determine a method for calculating multiple-mode sequences, we examine the solutions generated by Hyde's optimization routines [10]. Observe shows that many of the sequences generated by this method are symmetric (Figure 3-1). The undamped systems have sequences that are symmetric in both time and amplitude, while the systems with damping have sequences that are symmetric only in time. A simple two-mode, zero-damping example is developed to investigate this phenomenon.

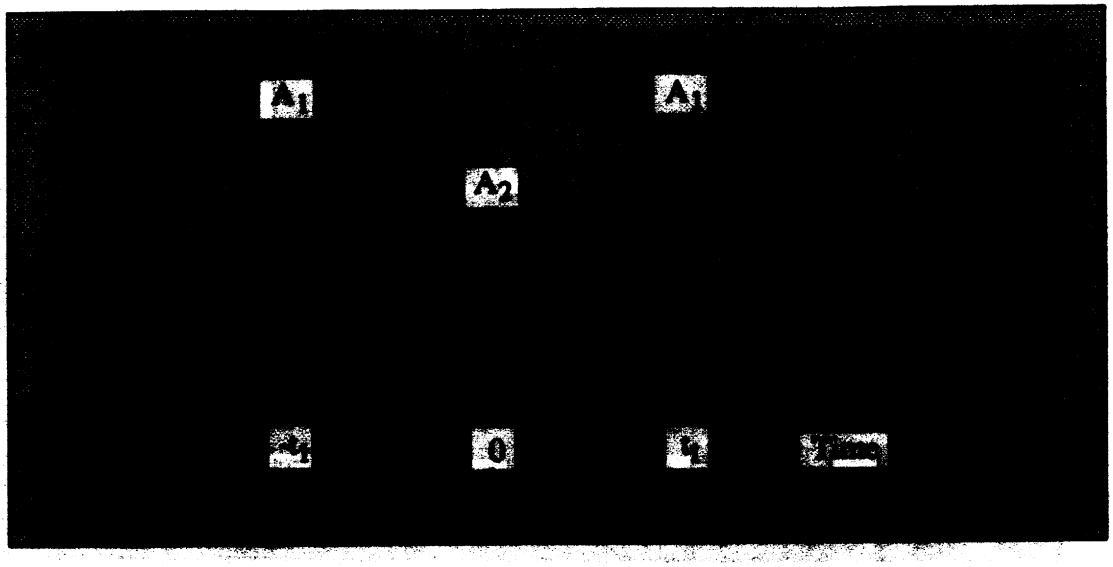

Figure 3-2: Time-Shifted, Symmetric Sequence for Two Modes, Using Simple Constraints

3.2.1 Solution for Simple Constraints

We start with the standard constraint equations for an undamped, two-impulse system, (Eqs. 2-1 - 2-4)

$$\sum_{i=1}^{n} A_i \sin(t_i \omega_j) = 0 \tag{3-1}$$

$$\sum_{i=1}^{n} A_i \cos(t_i \omega_j) = 0 \tag{3-2}$$

$$\sum_{i=1}^{n} A_i = 1 \tag{3-3}$$

$$t_1 = 0 \tag{3-4}$$

where Eqs. 3-1 and 3-2 are repeated for each mode, j = 1,2. These six constraint equations will yield n = 3 impulses. We assume that the sequence will be symmetric in both time and amplitude, and we shift the time origin to the right so that $t_2 = 0$. The time-shifted, symmetric sequence is shown in Figure 3-2. The symmetry assumption reduces the number of unknowns in the problem by making Eq. 3-1 trivial. Using this construct for our sequence, the remaining constraint equations can be simplified. Combining Eq. 3-2 with Eq. 3-3 yields two equations with two unknowns: A_1 and t_1.

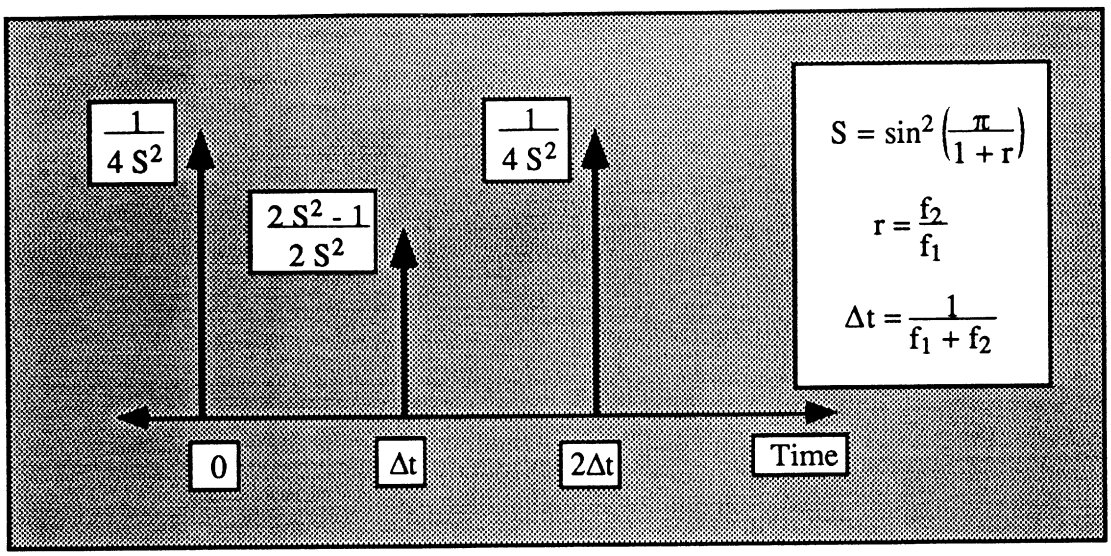

Figure 3-3: Three-Impulse, Direct-Solution Sequence for Two Modes.

$$\frac{1}{4} = A_1 \sin^2\left(\frac{\omega_j t_1}{2}\right), j = 1,2 \tag{3-5}$$

From these two equations we can solve for t_1 as a function of ω_1 and ω_2.

$$t_1 = \frac{2\pi z}{\omega_1 \pm \omega_2}, z \in \{\ldots -1, 0, 1, \ldots\} \tag{3-6}$$

We are searching for the shortest sequences, so we select the smallest positive value of t_1. Simplify by converting from rad/sec to Hz.

$$\omega = 2\pi f \tag{3-7}$$

Using Eqs. 3-3 and 3-5, we calculate the values for the amplitudes. The resulting sequence is shown in Figure 3-3. We now have an analytic solution for two-mode, zero-damping sequences using only the simple constraints. The amplitude equations do not depend upon the actual values of the frequencies, but only upon the ratio of the frequencies, *r*. The formulas for the impulse amplitudes also show that the amplitudes are continuous with variations in frequency ratio--an issue that is important when varying the shaping sequences during a move.

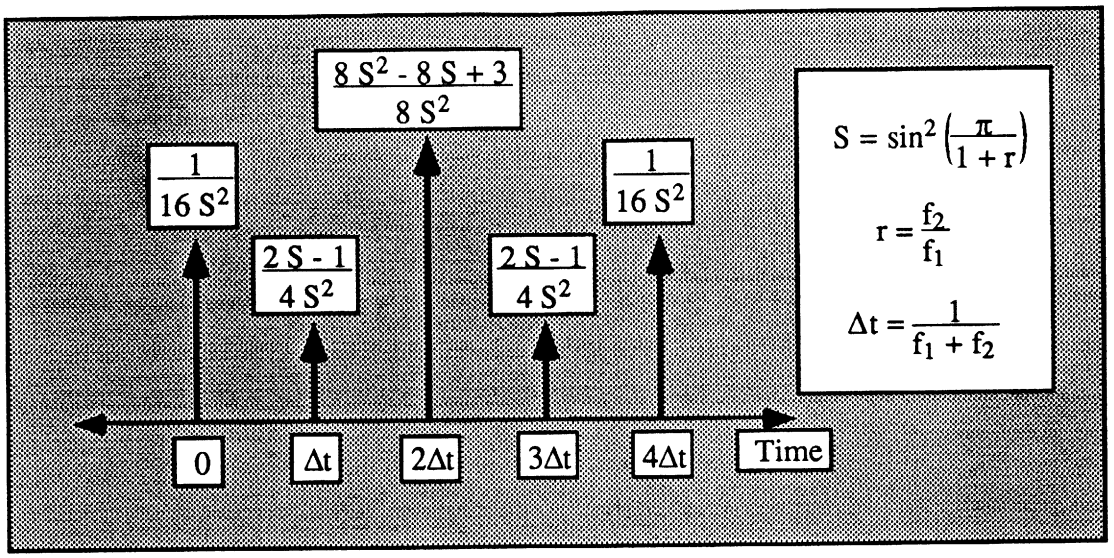

Figure 3-5: Five-Impulse, Direct-Solution Sequence for Two Modes.

$$\frac{1}{4} = A_1 \sin^2\left(\frac{\omega_j t_1}{2}\right) + A_2 \sin^2\left(\frac{\omega_j t_2}{2}\right), j = 1,2 \tag{3-10}$$

The final constraint (Eq 3-8) simplifies to:

$$0 = t_1 A_1 \sin(\omega_j t_1) + t_2 A_2 \sin(\omega_j t_2), j = 1,2 \tag{3-11}$$

Solving the remaining four equations for t_1 and t_2 provides the same impulse spacing as was found in the simple constraint problem.

$$t_i = \frac{2\pi z}{\omega_1 \pm \omega_2}, z \in \{\ldots -1, 0, 1, \ldots\} \tag{3-12}$$

Again, since we are searching for the shortest sequences, so we select the two smallest, positive values for t_1 and t_2: $z = 2$ and $z = 1$, respectively, and convert from rad/sec to Hz.

$$t_1 = \frac{2}{f_1 + f_2} \tag{3-13}$$

$$t_2 = \frac{1}{f_1 + f_2} \tag{3-14}$$

We see that the two-mode sequence with derivative constraints is not only symmetric, but is also evenly spaced. Using these values for the t_i, we can solve for the A_i. and shift the time axis back to the left so that $t_1 = 0$. The resulting sequence is shown in Figure 3-5. We now have a closed-form solution for two-mode, zero-damping systems.

3.3 Analytic Solutions for the Higher-Mode Problem

We have found a method for calculating symmetric sequences for two-mode systems. Although the equations can be expanded to the higher-mode case. solutions to the equations are not easily found. This section presents the general matrix equations for the multiple-mode, zero-damping system. These equations have been solved for the two-mode case, as shown above. They also reduce to Singer's original equations in the single-mode case. Presently, the author has not found analytic solutions for systems with more than two-modes. Some observations on proposed solution methods are noted. The equations presented here satisfy both the simple and derivative constraints for each mode, Eqs. 3-1 - 3-4 and Eqs. 3-8 - 3-9, respectively.

The general form of the solution is

$$\{A\} = [M]^{-1} \{R\} \tag{3-15}$$

where {A} is the vector of impulse amplitudes, {R} is a vector of constants, and [M] is a modally dependent matrix. For a system with number of modes = m, the number of constraint equations will equal $4m + 2$. Therefore our solution will have $n = 2m + 1$ impulses, the same number that Hyde specified Our symmetry assumption specifies the existence of a center impulse, leaving m symmetric impulses. Inspection of the equations developed above, reveals that each additional mode will add a repetition of Eqs. 3-9 and 3-10 for the additional frequency ω_m and an extra term to Eqs. 3-9 and 3-10 for each additional impulse A_m, t_m required by the extra frequency. We can specify the components of Eq. 3-15 as follows. {A} is the vector of symmetric impulse amplitudes:

$$\{A\} = \begin{Bmatrix} A_1 \\ \vdots \\ A_m \end{Bmatrix} \tag{3-16}$$

The matrix [M] is assembled from the coefficients of the $2m$ non-trivial Eqs. 3-9 and 3-10.

$$[M] = \begin{bmatrix} [M_1] \\ \vdots \\ [M_m] \end{bmatrix} \tag{3-17}$$

where

$$[M_j] = \begin{bmatrix} \sin^2(\frac{\omega_j t_1}{2}) & \cdots & \sin^2(\frac{\omega_j t_m}{2}) \\ \\ t_1 \sin(\omega_j t_1) & \cdots & t_1 \sin(\omega_j t_m) \end{bmatrix} \tag{3-18}$$

The vector {R} contains constants--the values from the left side of Eqs. 3-9 and 3-10.

$$\{R\} = \begin{Bmatrix} R_1 \\ \vdots \\ R_m \end{Bmatrix} \tag{3-19}$$

where

$$\{R_j\} = \begin{Bmatrix} \frac{1}{4} \\ 0 \end{Bmatrix} \tag{3-20}$$

The two-mode case is solved by equating the elements of the $[M_j]$ to find the t_i, and then solving the linear matrix equation for the A_i.

$$\{A\} = [M_j]^{-1} \{R_j\}, \; j = 1 \text{ or } 2 \tag{3-21}$$

This solution method fails for systems with more than two modes. The difficulty in solving Eq. 3-21 arises because the equations are a non-linear function of the t_i. Once the t_i are found, the resulting system of equations can be solved. Hyde [10] developed his optimization routine to find approximate values for the t_i and A_i. He then used GAMS[4] and Mathematica[30], two non-linear equation solvers to find the corresponding exact solution. Analysis of Hyde's sequences and the two-mode sequences developed above, suggests that we can approximate the sequence length, t_n.

$$t_n \approx \frac{m^2}{\sum_{j=1}^{m} f_j} \tag{3-22}$$

This formula is exact for the one and two mode cases but only an approximation for higher mode cases. Using the approximate value for t_n, we can calculate values for the t_i in Eq. 3-18 which can be used as starting points for an equation solver such as the FindRoot command in Mathematica[30]. This method of solving the multiple-mode case works for many systems of frequencies. It is not as likely as Hyde's original program to find a solution, but in cases where a solution can be found, it reduces the amount of calculation considerably over Hyde's method.

3.4 Domain of Direct-Solution Sequences

We showed above that we can calculate undamped, two-mode sequences using simple equations. We must consider what range of frequencies will generate sequences that meet all the constraints we have set.

3.4.1 Sequences with Positive Impulses

During the derivation of the two-mode equations, we neglected one of Singer's original constraints:

$$A_i \geq 0 \tag{3-23}$$

This constraint is included to prevent the shaping sequences from exciting higher frequencies--the effect of removing this constraint will be discussed below. This section examines the range of frequencies that yields acceptable sequences.

We begin by examining the formulas for the pulse amplitudes that were developed above. A three-impulse, two-mode sequence will have the following values

$$t_i = \frac{i-1}{f_1 + f_2} \tag{3-24}$$

$$A_1 = A_3 = \frac{1}{4\,S^2} \tag{3-25}$$

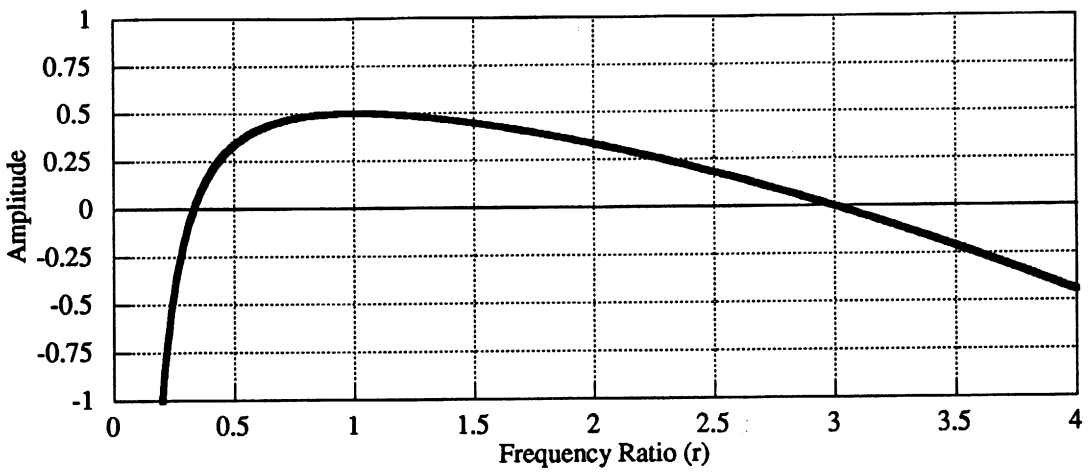

Figure 3-6: Variation of Second Impulse Amplitude with Frequency Ratio: Three-Impulse Sequence

$$A_2 = \frac{4S^2 - 2}{4S^2} \tag{3-26}$$

where

$$S = \sin^2\left(\frac{\pi}{1+r}\right) \tag{3-27}$$

$$r = \frac{f_2}{f_1} \tag{3-28}$$

We see from Eq. 3-25 that A_1 and A_3 are non-negative. Figure 3-6 shows the variation of A_2 with the frequency ratio, r. From the figure we see that A_2 is negative for $r > 3$ and $r < 1/3$. An examination of the sequence length, t_n, shows that the total sequence length becomes shorter than the half-period of the lower frequency at these values of r. This discovery reiterates Singer's statement that the shortest sequence for a frequency with all positive impulses will be as long as the half-period of the frequency [18].

We can similarly examine the variation in pulse amplitude in the two-mode, direct-solution sequences developed with derivative constraints. The five impulses are defined

$$t_i = \frac{i-1}{f_1 + f_2} \tag{3-24}$$

$$A_1 = \frac{1}{16S^2} \tag{3-29}$$

$$A_2 = \frac{2S - 1}{4S^2} \tag{3-30}$$

$$A_3 = \frac{8S^2 - 8S + 3}{8S^2} \tag{3-31}$$

where S is defined in Eq. 3-27. The five-impulse sequence has three impulses that are always positive: A_1, A_3, and A_5. Each of these three has its minimum value at $r = 1$. The remaining two impulses are not always positive. As the five-impulse sequence is exactly twice as long as the three-impulse sequence, we expect the amplitude of A_2 to become zero at the same values of r that we found to be critical for the three-impulse sequence. Our expectation is verified as is seen in Figure 3-7 illustrating the variation of A_2 with r.

Due to the constraint that impulses not be negative, the two-mode, direct-solution appears to be limited to systems with frequency ratios of less than 3. However, we can find direct-solution sequences with all positive impulses for frequency ratios outside these limits. Examining Eq. 3-12, recall that our time step, t_i, results in the shortest possible sequence. We can choose other values for z which will lengthen the sequence and keep the impulse amplitudes positive. This possibility will be discussed completely in section 3.5.

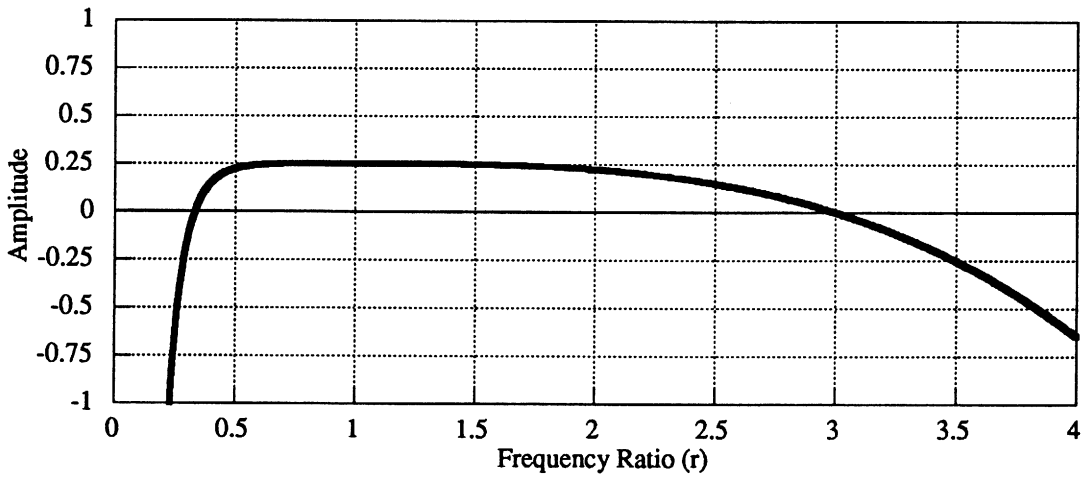

Figure 3-7: Variation of Second Impulse Amplitude with Frequency Ratio: Five-Impulse Sequence

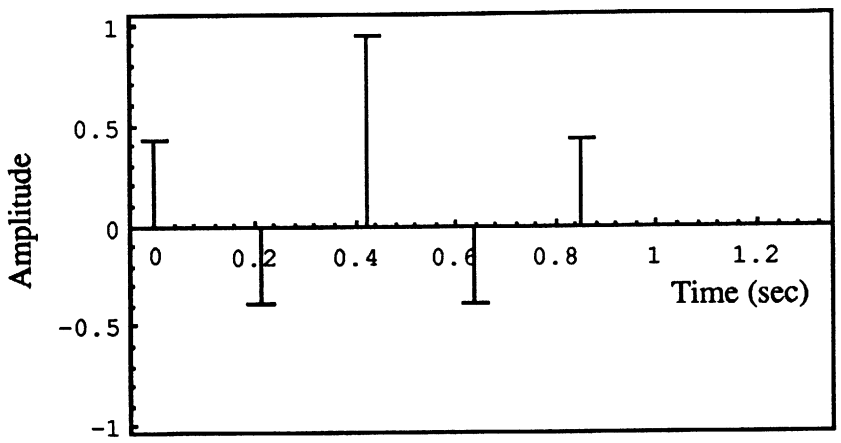

Figure 3-8: Two-Mode Sequence for 1.0 and 3.7 Hz, with Negative Impulses

3.4.2 Sequences with Negative Impulses

Another option to avoid the critical frequency ratio of 3 is to relax Singer's constraint that all impulse amplitudes be positive. The equations developed above for two-modes will generate sequences for frequency ratios larger than 3, however some of the impulse amplitudes will be negative. We can propose a more relaxed constraint that will permit negative impulse amplitudes, but will continue to prevent the shaping filter to amplify the system input. Our new constraint is

$$\left| \sum_{i=1}^{k} A_i \right| \leq 1, \text{ for all } k \in \{1, ..., n\} \tag{3-32}$$

Figures 3-6 and 3-7 show that negative pulses occur naturally for certain frequency ratios. Using the new constraint, we can generate sequences for frequency ratios lower than 3.7668 for a five-impulse sequence and 5 for a three-impulse sequence--the values of r where $A_1 = -A_2$. A benefit of sequences with negative impulses is their length. A sequence with negative impulses for 1.0 and 3.7 Hz will have a time delay of 0.85 sec, compared to the convolved sequence delay of 1.27 sec, a savings of 33%. An example of a

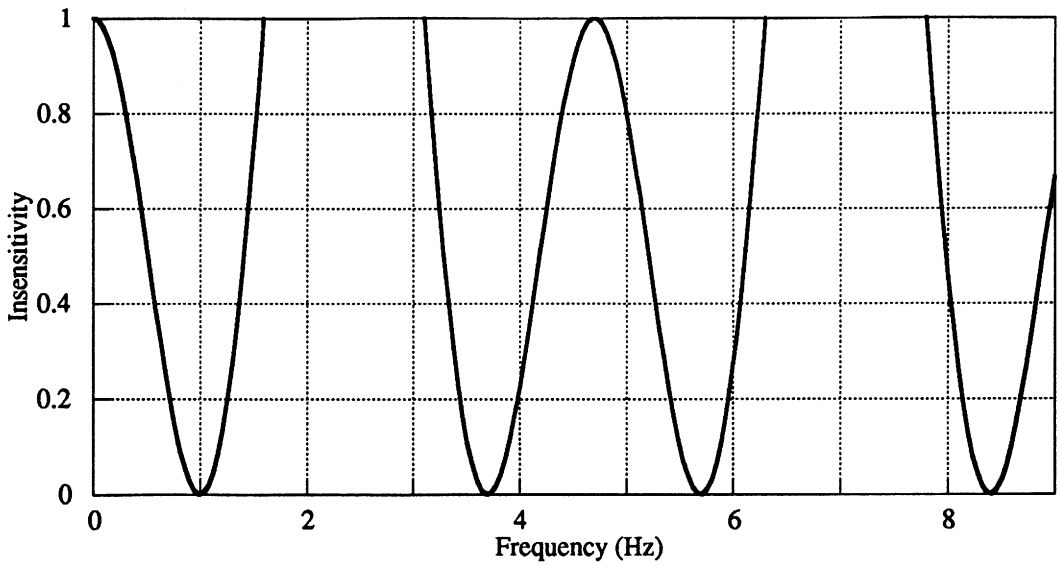

Figure 3-9: Insensitivity of Two-Mode Sequence for 1.0 and 3.7 Hz, with Negative Impulses

negative sequence that satisfies Eq. 3-32 is shown in Figure 3-8. The insensitivity of the negative sequence (Figure 3-9) shows two problems with negative sequences: the sequence is sensitive to modelling errors and there will be excitation of specific frequencies.

From Figure 3-9, we see that the negative sequence shown will keep vibrations below 5% of the unshaped magnitude with up to a 12% error in frequency. A three-impulse, one-mode shaper gives the same results with up to 15% errors in modelling (Figure 2-4). The robustness of the negative sequences continues to decrease as the magnitude of the negative impulses grows and the frequency ratio increases.

The insensitivity curve for the negative sequences shows that higher frequencies can be excited. The even spacing of the impulses in the two-mode, direct-solution sequences causes excitation of the frequencies who are in phase with the impulses. We can solve for the frequencies that will be excited and the amplitude of the excitation.

$$f_c = \frac{(2c+1)(f_1+f_2)}{2}, c \in \{0, 1, \dots\} \quad (3\text{-}33)$$

$$Amp = \sum_{i=1}^{n} |A_i| \quad (3\text{-}34)$$

Amp represents the gain of the shaping sequence at the frequencies f_c. For a truly linear system this excitation should not be problematic as the system will absorb energy from narrow frequency bands only. If we shape for all the vibrational frequencies in a linear system, then no vibration will result. However, in real systems that are not completely linear, the excited-frequency energy could match a previously unknown resonance of the system or be shifted into a mode of the system, thereby deteriorating the benefits of the input shaping.

3.5 Time Delay of Direct-Solution Sequences

3.5.1 Comparison of Direct-Solution and Convolved Sequences

One of the benefits of the direct-solution shapers is their shorter time delays as compared to convolved sequences. Hyde found that direct-solution sequences can be up to 25% shorter than convolved sequences, however, he was not able to predict what the time savings would be for a given set of frequencies. Using the two-mode, zero-damping solution, we can calculate the sequence length for any pair of frequencies and determine the time savings.

A multiple-mode sequence generated by convolving together two single-mode two-impulse shapers has a known length.

$$t_n = \frac{1}{2f_1} + \frac{1}{2f_2} \quad (3.35)$$

A sequence generated for two modes using the direct-solution method described above also has a known length.

$$t_n = \frac{2}{f_1 + f_2} \tag{3-36}$$

Comparing the values of t_n we see that the direct solution is shorter than the convolved solution except for the case $r = 1$, where the time delays are equal. Figure 3-10 shows the time savings of the direct-solution as a function of frequency ratio, r. When $r = 3$ or $r = 1/3$, the direct-solution sequence will provide the greatest time savings of 25% for sequences with strictly positive impulses. At these values of r, the direct-solution sequence will be exactly the same as a single-mode sequence for the lower-frequency mode. The insensitivity curve illustrates why the direct-solution sequence generates this solution. Figure 3-11 shows the insensitivity for a three-impulse shaper. The insensitivity drops to zero at every odd multiple of the original frequency.

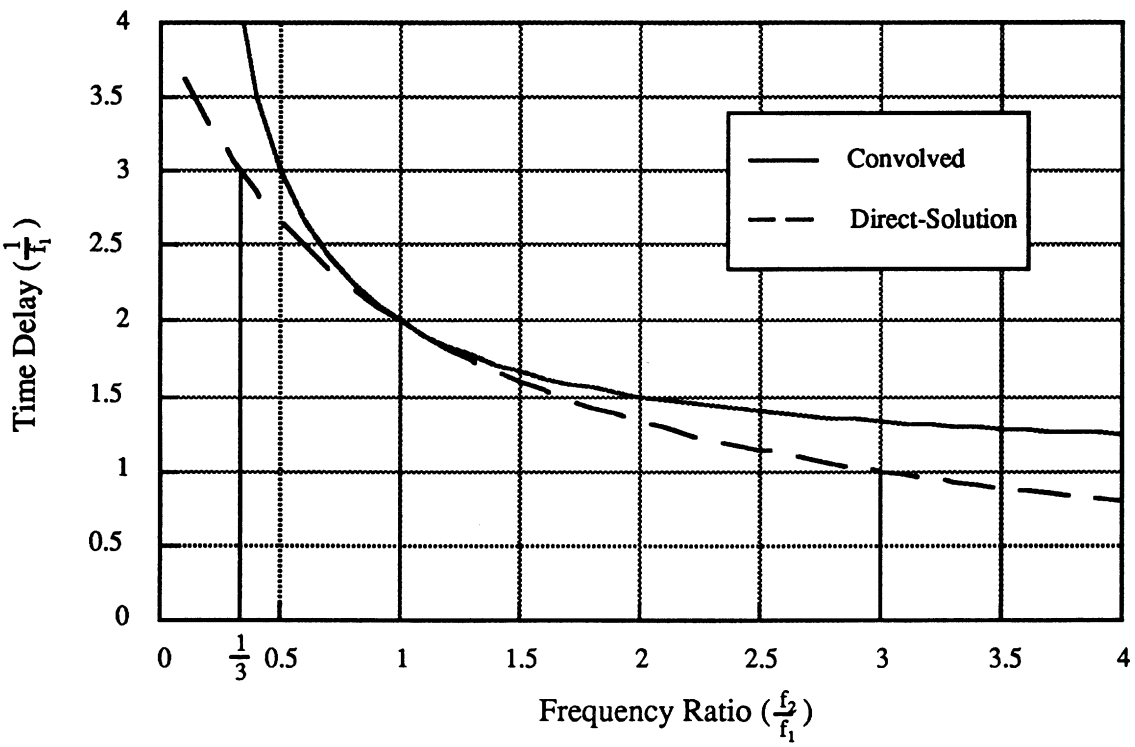

Figure 3-10: Comparison of Time Delay Caused by Convolved and Direct-Solution Shapers--Generated with both Simple and Derivative Constraints

The direct-solution method uses this fact in its sequences for the critical values of $r = 3$ and $r = 1/3$.

3.5.2 Lengthening Sequences to Keep Positive Impulses

As mentioned above, we can lengthen the sequences by changing the factor z in Eq. 3-12 for frequency ratios greater than 3. For any pair of frequencies, a value of z exists that will keep all the pulse amplitudes positive. However, we cannot guarantee a time savings when other values of z are used, in fact, most direct-solution sequences are longer than the convolved sequences for frequency ratios greater than three. Figure 3-12 shows how the factor z affects sequence length as a function of r.

If we plot the insensitivity curves for sequence generated using alternative values for z, we see an interesting result: the selection of z determines which of the zeros of the insensitivity curve matches the desired frequency. For example, the insensitivity curve for a sequence generated for 1.0 Hz and 2.5 Hz with z =1 and z = 2, is shown in Figure 3-13. If we change the values of z to 1 and 3 and calculate a sequence for 1.0 Hz and 4.5 Hz, we

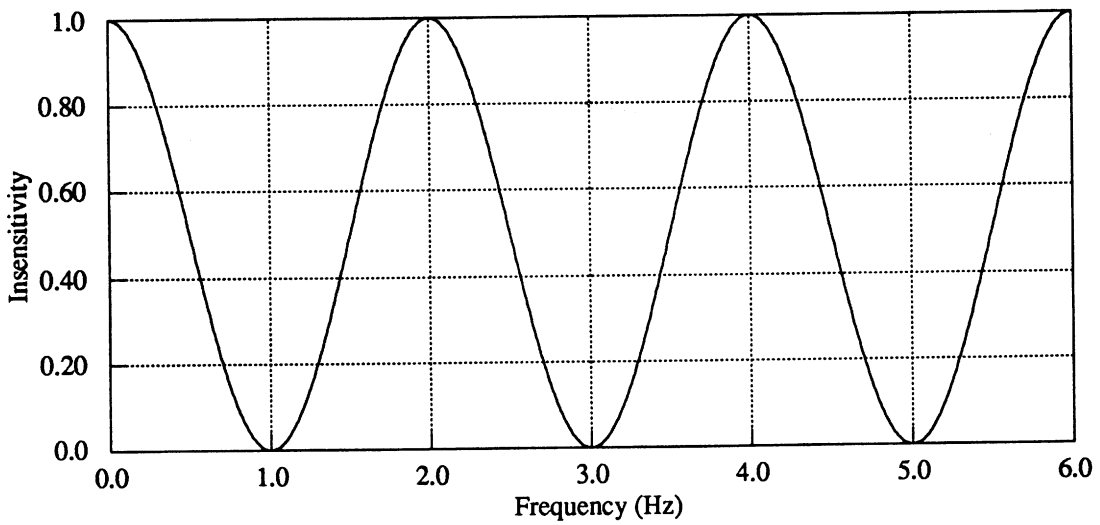

Figure 3-11: Insensitivity of a Three-Impulse Shaper: The Insensitivity is Zero at Odd Multiples of the Sequence Frequency

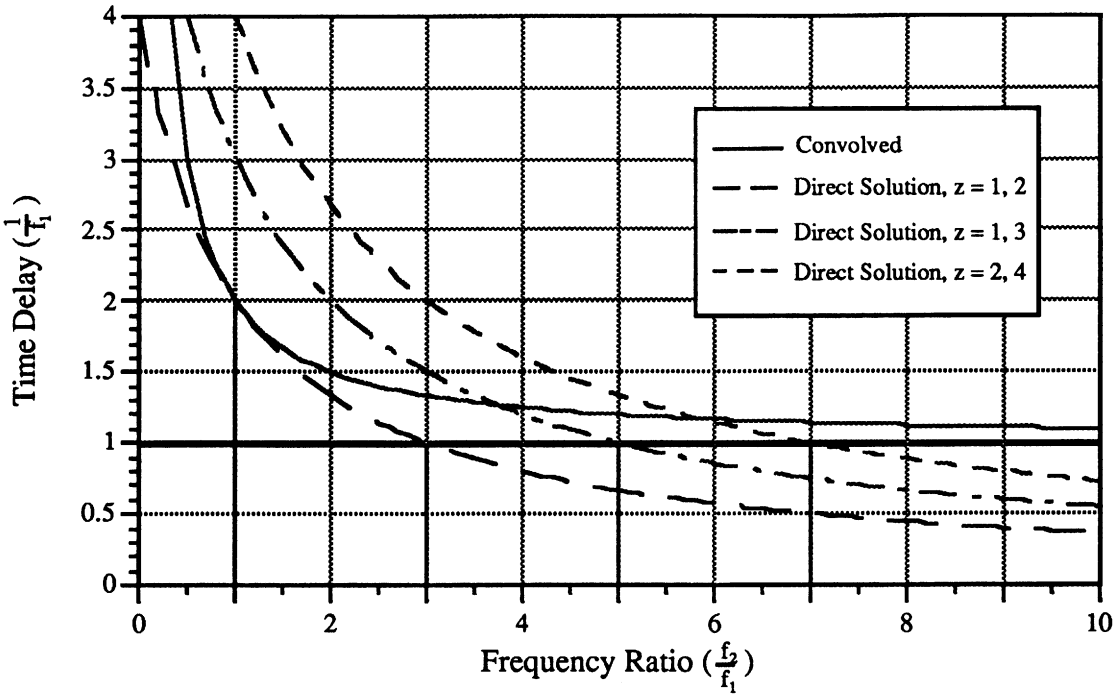

Figure 3-12: Variation of Time Delay with Choice of *Z*.
Time Delay < 1 Yields Negative Impulses

get an interesting result: the two sequences are identical. By changing the value of *z* we merely change the choice of zeros of the insensitivity curve. The shortest sequences using *z* = 1 and *z* = 2 select the first two zeros of the insensitivity curve. Other values for *z* correspond to the other frequencies where the insensitivity is also zero.

This phenomenon can explain the lack of insensitivity that Hyde noticed in his sequences for systems with large frequency ratios. In Figure 3-13, we see that the insensitivity curve of the two-mode case repeats itself every f_1 + f_2 Hz. Around f_1 we will have +/- 15 % insensitivity for this sequence with simple and derivative constraints. As we move to the higher zeros of the insensitivity curve, the shape of the curve that permits frequency errors of +/- 15% at the low frequency only allows +/- 7% error at the next zero of 2.5 Hz

and +/- 4% at 4.5 Hz. The percent insensitivity will continue to decrease as we move to higher zeros.

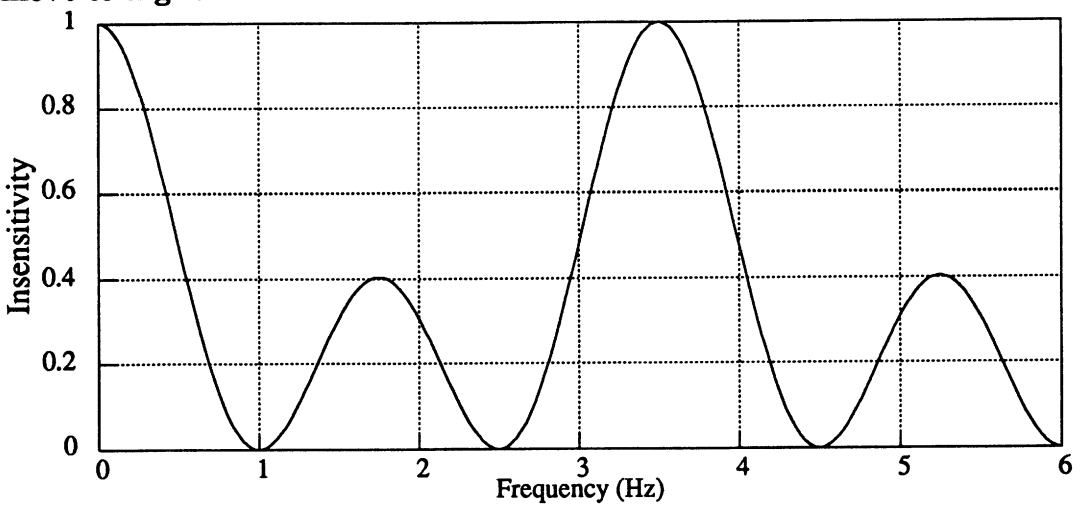

Figure 3-13: Insensitivity Curve for Five-Impulse Sequence for 1.0 and 2.5 Hz.

We can use the knowledge that the insensitivity curve repeats itself every $f_1 + f_2$ Hz to derive an expression for all the locations on the curve that will have zero insensitivity. Rearranging Eq. 3-12 to solve for all the ω_2 that will result in the same impulse spacing as a function of z, we find

$$f(z) = z(f_1 + f_2) - f_1, \text{ or}$$

$$f(z) = z(f_1 + f_2) - f_2 \,, z \in \{1, 2, \cdots\}. \tag{3-37}$$

This equation allows us to calculate all the frequencies at which our sequence should eliminate residual vibrations. Using a sequence generated for low frequencies to cancel higher-frequency vibrations may not provide the shortest possible sequence, nor will it have as good insensitivity as at the low frequency, but it can be effective in reducing the vibration of the higher-mode.

Previous research by Hyde [10] has noticed that direct-solution sequences do not have good insensitivity at the higher frequencies. Concurrent research by Chang[5] has also shown that direct-solution sequences have poor insensitivity when the frequency ratios are large. Convolution may prove to

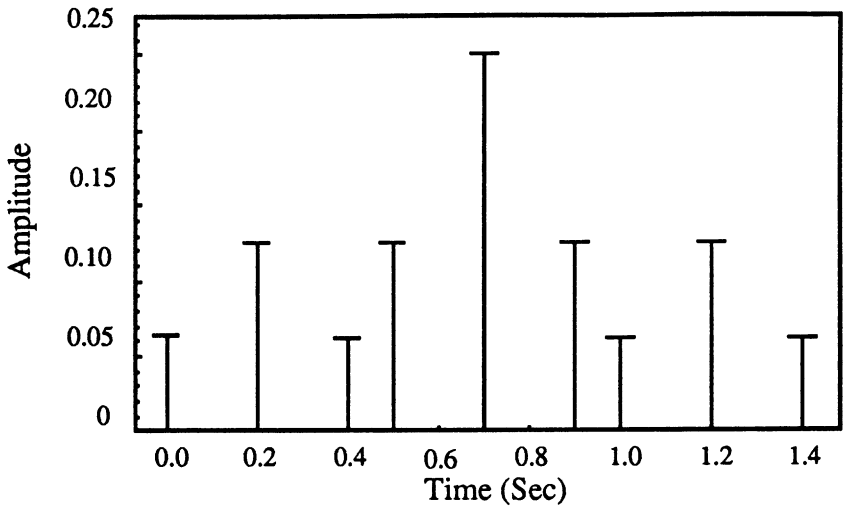

Figure 3-14: Two-Mode Convolved Sequence, 1.0 and 2.5 Hz.

be the best method of shaping for systems with large frequency ratios and for systems with many frequencies. The sequences are often shorter than the direct-solution sequences and they generally have better insensitivity. Figure 3-14 shows a nine-impulse sequence, found by convolution, generated for 1.0 and 2.5 Hz. Figure 3-15 shows a direct-solution sequence for the same frequencies.

The insensitivity of each of these two sequences are shown in Figures 3-16

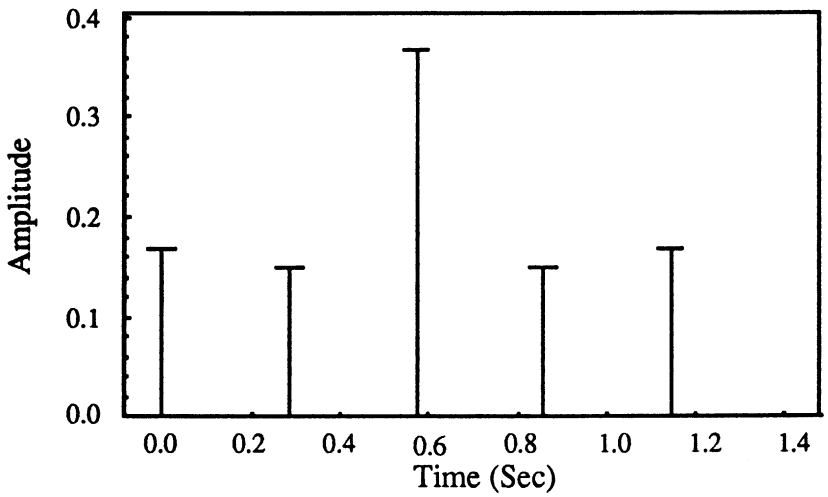

Figure 3-15: Two-Mode Direct-Solution Sequence, 1.0 and 2.5 Hz.

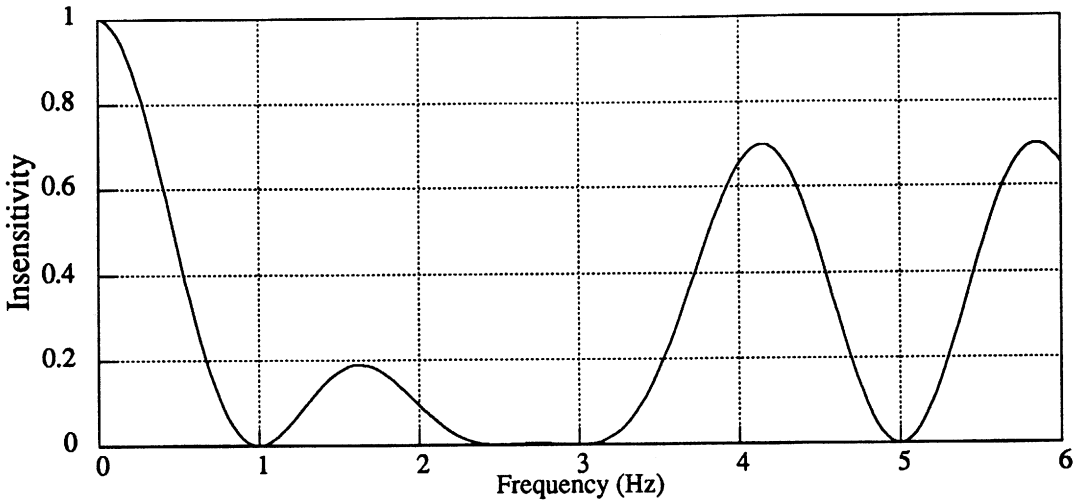

Figure 3-16: Insensitivity of Convolved Sequence for 1.0 and 2.5 Hz, from Figure 3-14.

and 3-13, respectively. For this set of frequencies, with r = 2.5, the two sequences have similar insensitivity around the first frequency, but the convolved sequence has better insensitivity around the 2.5 Hz frequency than the direct-solution.

We can use the increased insensitivity of convolved solutions to our advantage when generating sequences for multiple-mode systems. Using the two-mode solution developed above, we can convolve together two-mode equations to shape for any number of modes. The number of impulses will increase exponentially as Singer noticed [18] but more slowly than the single-mode convolved sequence. Figure 3-17 shows a sequence generated by convolving together two symmetric, two-mode sequences for the same four modes as in the sequences in Figures 2-5 to 2-8. Compare the insensitivity of this convolved sequence, shown in Figure 3-18, with the direct-solution sequence in Figure 2-8. The time delay of the convolved, symmetric sequence is 1.672 sec, compared with 1.336 for the direct solution in Figure 2-6 and 1.900 for the convolved sequence in Figure 2-5. We can gain some of the time

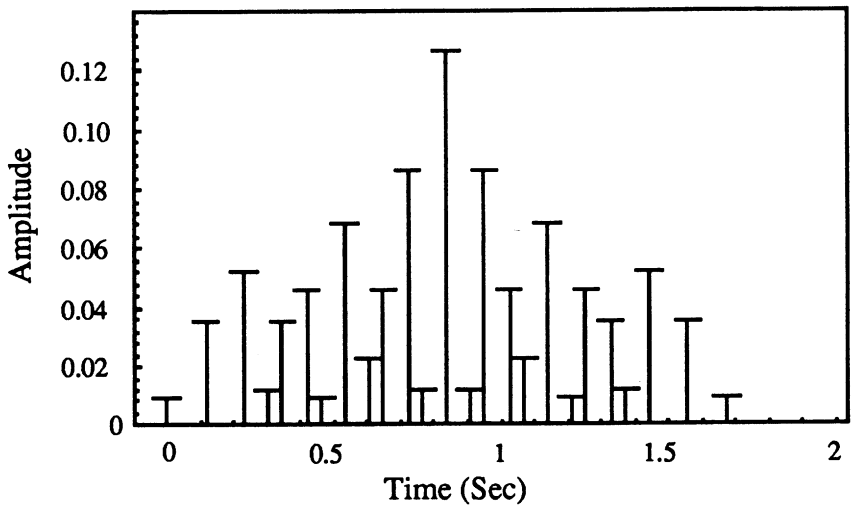

Figure 3-17: Sequence Generated by Convolving Two-Mode, Symmetric Solutions for 1.0 and 2.3 Hz and 3.9 and 4.8 Hz.

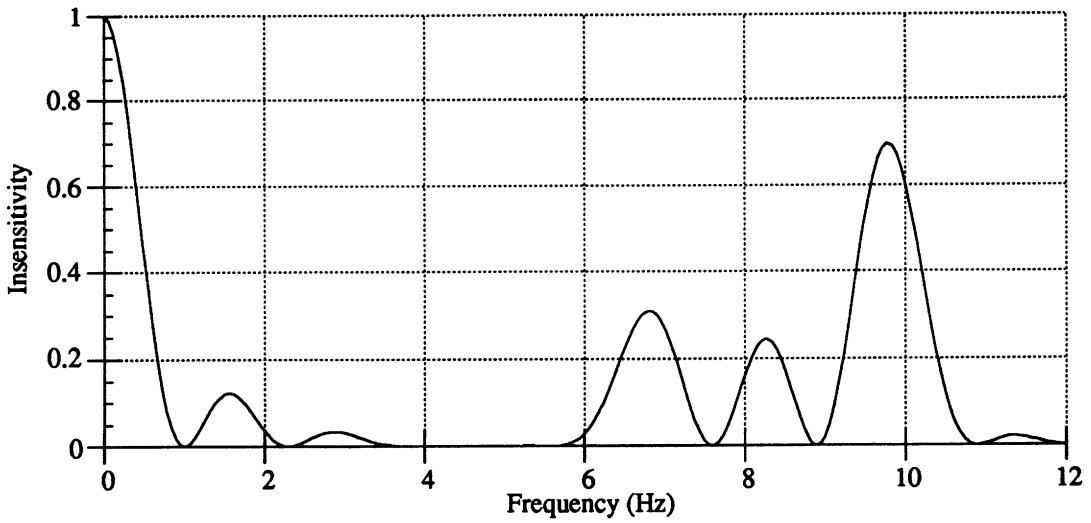

Figure 3-18: Insensitivity of Sequence in Figure 3-17.

savings of the direct-solution method, while keeping the high robustness to modelling errors by convolving two-mode sequences.

3.6 Approximate, Damped Solution

Above, we derived the direct-solution method for two-modes without damping. Unfortunately, when damping is included, the constraint equations become intractable. Using an empirical analysis of the effect of damping on Singer's single-frequency solution, we can develop an approximate sequence for the two-mode system with damping.

We start with a two-impulse sequence generated for one mode with zero damping.

$$A_1 = A_2 = \frac{1}{2} \tag{3-38}$$

$$t_0 = 0,\ t_1 = \frac{\pi}{\omega} \tag{3-39}$$

We can add damping to the sequence by overlaying a decaying exponential curve on the undamped sequence. The exponential curve is generated from Eq. 3-1.

$$y(t_i) = e^{-\zeta \omega t_i} \tag{3-40}$$

If we increase the time step between impulses to correspond to the damped time step

$$t_1 = \frac{\pi}{\omega\sqrt{1-\zeta^2}}, \tag{3-41}$$

multiply the amplitude of each pulse, A_i, by the corresponding value of $y(t_i)$, and normalize the amplitudes so that $\sum_{i=1}^{n} A_i = 1$, the result is exactly the same as Singer's sequence for a single, damped frequency.

$$A_1 = \frac{1}{D},\quad A_2 = \frac{K}{D} \tag{3-42}$$

$$K = e^{\frac{-\zeta\pi}{\sqrt{1-\zeta^2}}},\quad D = 1 + K \tag{3-43}$$

Performing the same sequence of operations on the three-impulse sequence yields the same result--adding the damping to the sequence has the same effect as calculating the sequence with the damping ratio known. We can

attempt to expand this method of calculating sequences for damped systems to the two-mode case. Mathematically, the solution method is not exact for two-modes. The results we will show are individual cases, where the damping has been added to a known sequence. We can find the solution using a non-linear equation solver as described above We will judge the damped sequences based on their insensitivity curves.

Adding damping to a two-mode solution has several effects. First, the pulse amplitudes and times change. The method outlined above approximates these changes in amplitude and time. When derivative constraints are included, the time spacing in the exact solution is no longer even. Impulses 2 and 4 move away from the center impulse. This phenomenon is not accounted for in the approximation. Adding damping to a multi-mode sequence requires the selection of an effective damping and an effective frequency, two values that do not exist. After some experimentation we can determine that the average damping ratio should be used as well as the average frequency in implementing Eq 3-40.

We start with the undamped, five-impulse sequence for 1.0 Hz and 2.5 Hz shown in Table 3-1. Add a damping ratio of 0.1 to the 1.0 Hz mode and 0.05 to the 2.5 Hz mode to our system. The insensitivity of the undamped sequence to the damped system is shown in Figure 3-19, and the insensitivity of the exact sequence is in Figure 3-21 We now calculate the approximate damped sequence using the method outlined above--with effective damping = 0.05 and effective frequency = 1.0 Hz. The resulting sequence is shown in Table 3-2. The exact solution for the damped system is shown in Table 3-3. Comparing the insensitivity of the approximate sequence (Figure 3-19) and the undamped sequence (Figure 3-20), we see that the approximation is closer to the exact than the undamped sequence (Figure 3-21).

Table 3-1: Direct-Solution, Five-Impulse Sequence for 1.0 Hz, 2.5 Hz, Zero-Damping

Impulse	Time	Amplitude
1	0.0000	0.1672
2	0.2857	0.1489
3	0.5714	0.3677
4	0.8671	0.1489
5	1.1428	0.1672

Table 3-2: Approximate, Five-Impulse Sequence for 1.0 Hz, 0.10 damping and 2.5 Hz, 0.05 damping

Impulse	Time	Amplitude
1	0.0000	0.2564
2	0.2865	0.1802
3	0.5730	0.3514
4	0.8596	0.1123
5	1.1461	0.0997

Table 3-3: Exact, Five-Impulse Sequence for 1.0 Hz, 0.10 damping and 2.5 Hz, 0.05 damping

Impulse	Time	Amplitude
1	0.0000	0.2407
2	0.2958	0.1727
3	0.5745	0.3577
4	0.8683	0.1175
5	1.1458	0.1131

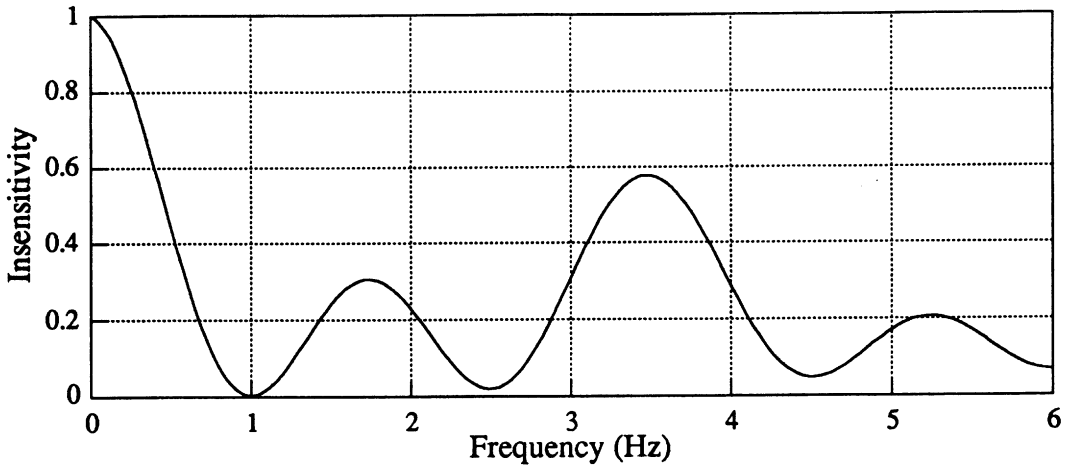

Figure 3-19: Insensitivity of Undamped Sequence from Table 3-1.

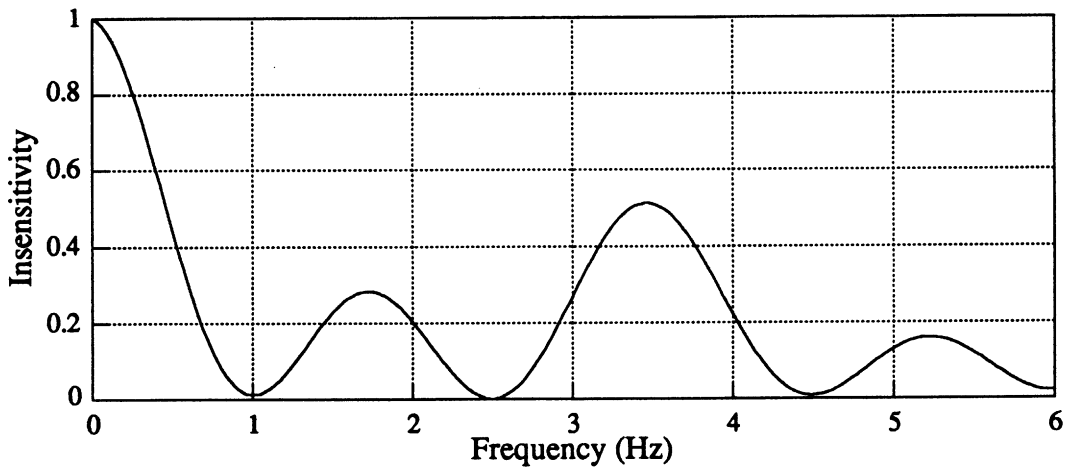

Figure 3-20: Insensitivity of Approximate, Damped Sequence from Table 3-2.

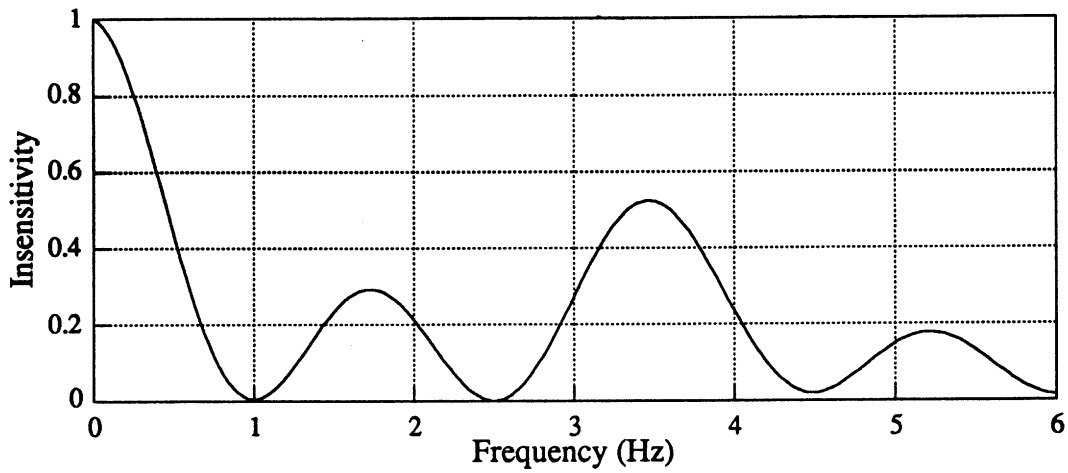

Figure 3-21: Insensitivity of Exact, Damped Sequence from Table 3-3.

3.7 Similarities of Input Shaping and Windowing

As command input shaping becomes a widely accepted method of reducing residual vibration, we must investigate how this new method compares to old, accepted filtering methods. This section investigates the similarities between command shaping sequences and the shape of the windows used in standard data-windowing techniques. If the standard windows can reduce frequency aliasing of data, the shapes that are used might be useful in minimizing vibrations. Two windows that are often used are the square window and the Parzen window, both of which are shown in Figure 3-22 [17].

The two-impulse and three-impulse, single-mode sequences have the same general form as the standard windows. We can increase the similarity by convolving sequences for higher frequencies. We select the higher frequencies based upon the insensitivity curves. Figure 3-11, above, shows the insensitivity curve for a three-impulse, one-mode sequence, for a frequency f_1. The lowest frequency that does not benefit from this sequence is $2f_1$. If we convolve two sequences--one for f_1 and the second for $2f_1$, we see

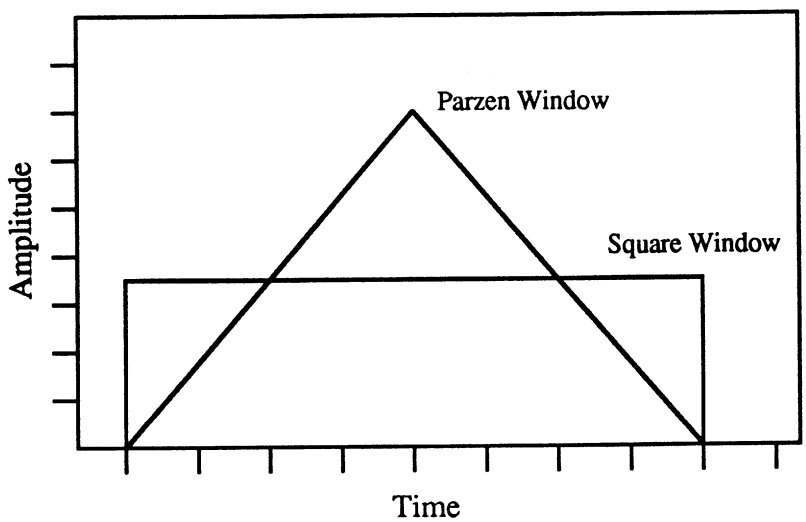

Figure 3-22: Parzen and Square Windows

that 4 f_1 is now the lowest frequency with an insensitivity of 1.0. By convolving together sequences for all the frequencies that are powers of two times the lowest frequency, we can shape for a wide range of frequencies. Mathematically, if we convolve N sequences for all the f_n,

$$f_n = 2^n f_0 \, , n \in \{0, 1, ...N \} \tag{3-44}$$

we will eliminate vibration for all the system frequencies, f_s.

$$f_0 < f_s < 2^{N+1} - f_0 \tag{3-45}$$

The sequences generated using this method approach the form of the continuous windows mentioned above. Figure 3-23 shows a three-impulse convolved sequence where $N = 4$, and Figure 3-24 shows a two-impulse convolved sequence for $N = 4$. The insensitivity curves for these two sequences are shown in Figure 3-25 and 3-26 respectively.

When convolved in this manner, the two-impulse convolved sequence approximates a square window. Its insensitivity does not stay below the 5% threshold for all the frequencies in the range f_s. The time delay caused by this sequence will be less than twice the length of the original sequence. The three-impulse, convolved sequence gives much better results. It approximates a Parzen, or triangular, window. For the entire range of f_s, the insensitivity of the sequence remains below 5%. The time delay of this sequence is 1.875 sec, for a sequence that eliminates all frequencies between 1 and 15 Hz. This result suggests that for the shortest sequences, we should not convolve together sequences for frequencies that are closer than a ratio of two.

If we increase N until the time step between the impulses reaches the servo frequency of our system, we should be able to eliminate vibration in all frequencies up to the Nyquist frequency of the system. Implementing the

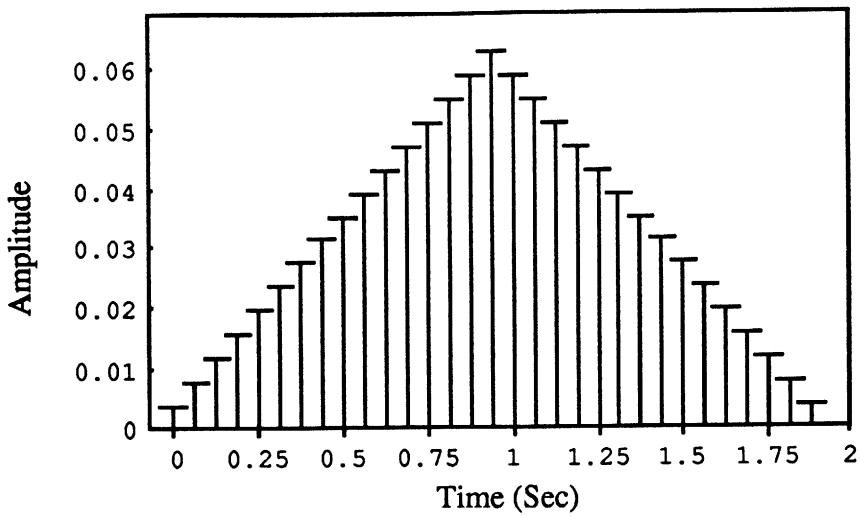

Figure 3-23: Three-Impulse Convolved Sequences for 1.0, 2.0, 4.0, and 8.0 Hz.

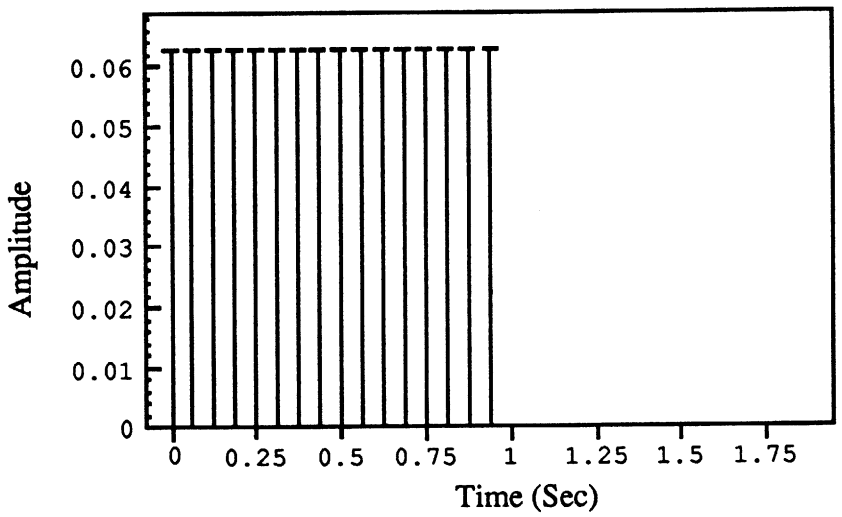

Figure 3-24: Two-Impulse Convolved Sequences for 1.0, 2.0, 4.0, and 8.0 Hz

Parzen window in this fashion allows for simple algorithms to generate the filtered output.

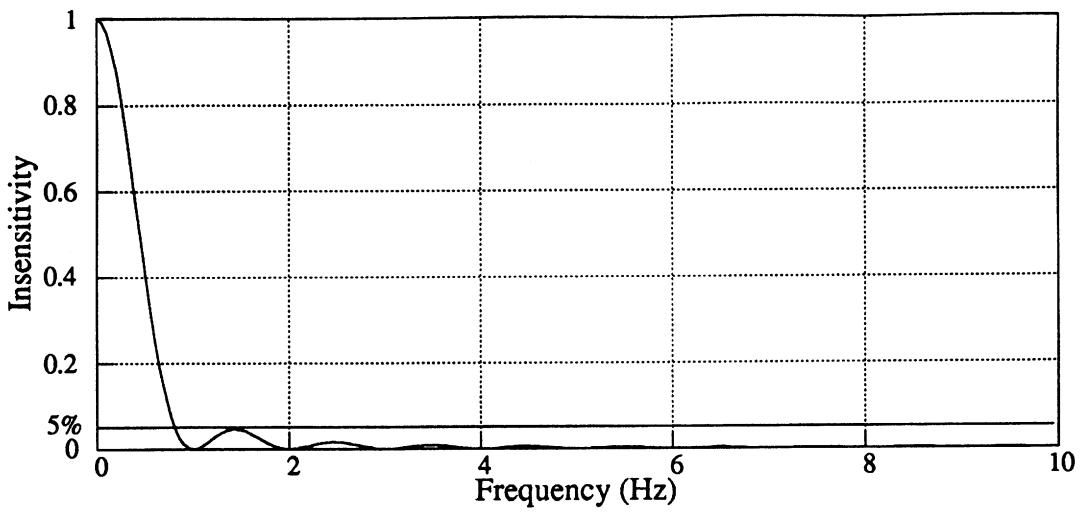

Figure 3-25: Insensitivity of Three-Impulse, Convolved Sequences Shown in Figure 3-23

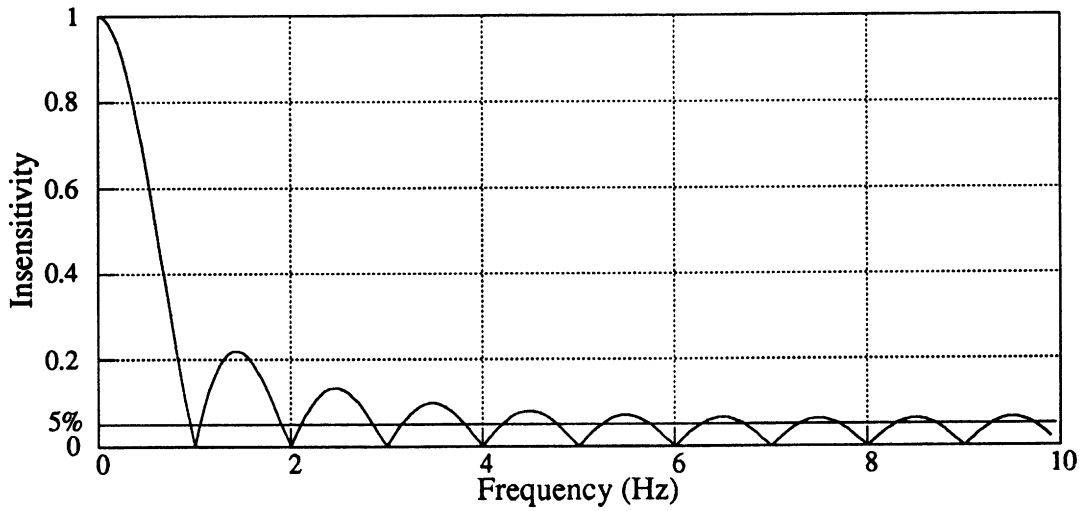

Figure 3-26: Insensitivity of Two-Impulse, Convolved Sequences, Shown in Figure 3-24

Figure 3-25: Transmissivity of Three-Impulse, Convolved Sequences Shown in Figure 3-23

Figure 3-26: Transmissivity of Two-Impulse, Convolved Sequences, Shown in Figure 3-24

Implementation on a Real System

Chapter 4

4.1 Introduction

The previous chapters presented a description of input command shaping as a method of minimizing residual vibrations. With the mathematic machinery in hand, we will now discuss the experimental setup used to test the vibration reducing ability of the new command shaping techniques and issues involving implementation of the theory. We selected the Flexbot, a three-degree-of-freedom, flexible system, as the test bed for the new shaping theories. This chapter presents an overview of the Flexbot, including issues of control and vibration characterization. The sharp variation of vibrational frequency with joint angle requires some additional modifications to the input shaping technique. A frequency mapping of the Flexbot workspace is completed, and discretization effects are discussed.

4.2 Selection of a Flexible System

Much of the prior research in input shaping theory focused on simulation. The research has as one of its long-term goals, application of the shaping techniques to the Space Shuttle Remote Manipulator System (RMS). The RMS is a fifty-foot long, fifteen-inch diameter arm. It is designed exclusively for use in space, as it cannot lift itself against the force of gravity. The RMS suffers from extreme vibration problems due to the long, lightweight design. Typically, 30% of the arm's running time is spent waiting for vibrations to dissipate [33]. The cost of many thousands of dollars per hour to maintain the Space Shuttle in orbit motivates NASA to eliminate time spent waiting for the arm to stop vibrating.

Unfortunately, the RMS is not an accessible test facility. The Flexbot provides a flexible structure that closely resembles the first three joints of the RMS. It was designed and built by Christian[6] for the purpose of providing a system for studying vibration control methods. The Flexbot has similar variations in frequency as the RMS[32], although the frequencies are not as low as the Shuttle Arm.

4.3 The Flexbot as a Flexible System

This section describes the changes in computer hardware and software that were completed during my research. The authoritative document on the Flexbot remains Christian's thesis[6].

4.3.1 Hardware Changes:

The computer control has changed quite a bit from the original design. The Condor system[16] Christian describes has been replaced by a VXworks system. VXworks provides a low level operating system for interfacing with

the robot [28, 29]. We are using three parallel processing boards to control the system. The processing boards are housed in a VMEbus expansion bus. The expansion bus contains three processing boards, a digital to analog converter, an analog to digital converter, two optical encoder cards, and a digital I/O card. A description of the boards in the VMEbus is found in Table 4-1. The processing boards are accessed directly from a Sun SPARCstation, a UNIX based workstation. Wiring the front plane of the new mounting rack for the Flexbot was one of my tasks. Most of the computer control changes are not visible to the user, and the operation of the Flexbot remains consistent with [6].

4.3.2 Software Changes:

Many aspects of the software have remained unchanged through my reconfiguration. The change to VXworks required many low level changes in the code, but did not dramatically affect the front-end of the program. I have chosen to keep the basic structure of the control program the same as it was. A schematic of the computer control is shown in Figure 4-2. The first processor board, Aruba, controls the interface with the user. The user specifies the type of prefilter to use, the velocity limits, the desired positions, and the choice of joint or Cartesian control through the keyboard or the joystick. The control program is completely menu driven off of Aruba. During most operations, Aruba runs on a 125 Hz timing loop. The position commands entered by the user are translated into acceptable commands based upon the current velocity limit and passed to the second processor board, Bahamas. The joystick signals are also processed at 125 Hz.

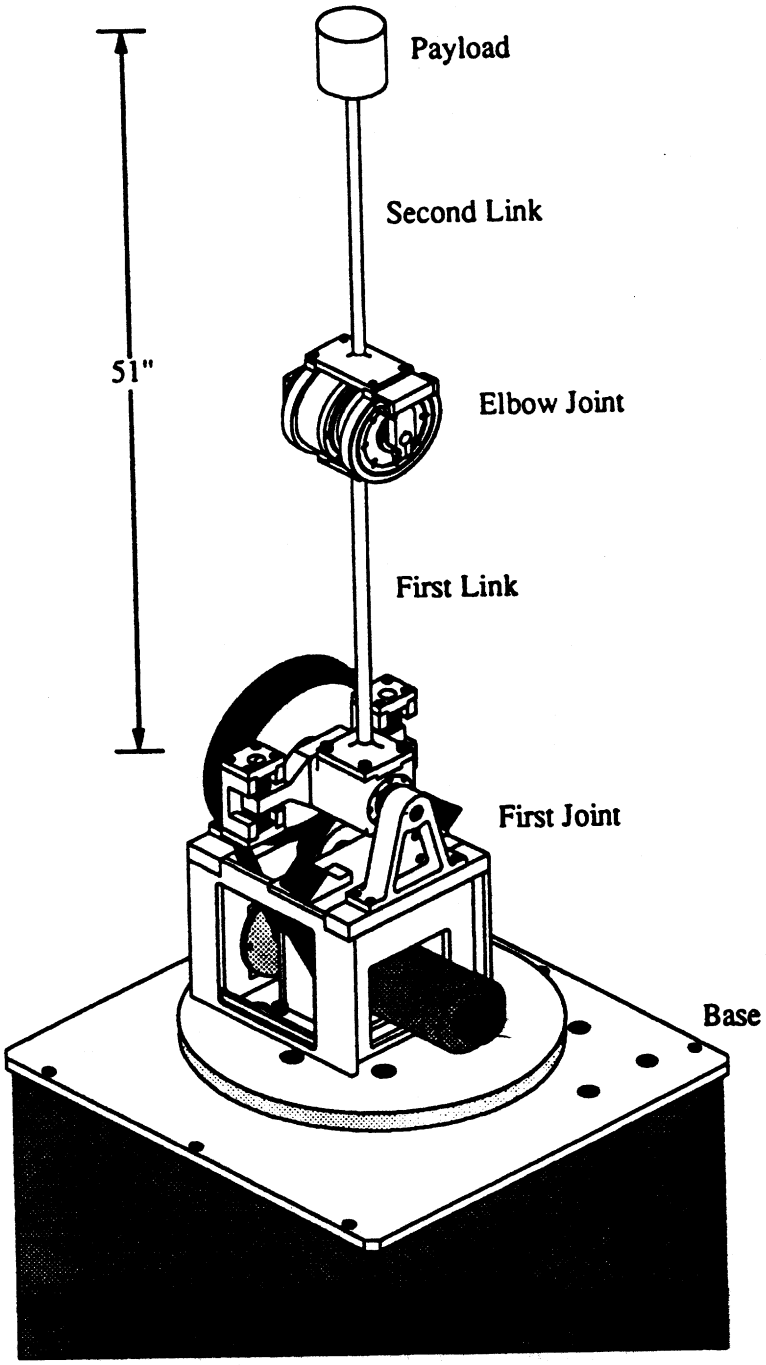

Figure 4-1: The Flexbot.
Taken from [6].

Table 4-1: Description of Boards in VMEbus.
[15, 25, 26, 27]

Board	Function	Quantity
MVME 147	Processor Board	4
DT1402	8 A/D, 2 D/A, 16DIO	1
DT1406	8 D/A	1
Whedco 3570	2 Encoder Channels	2
MPP	80 DIO	1

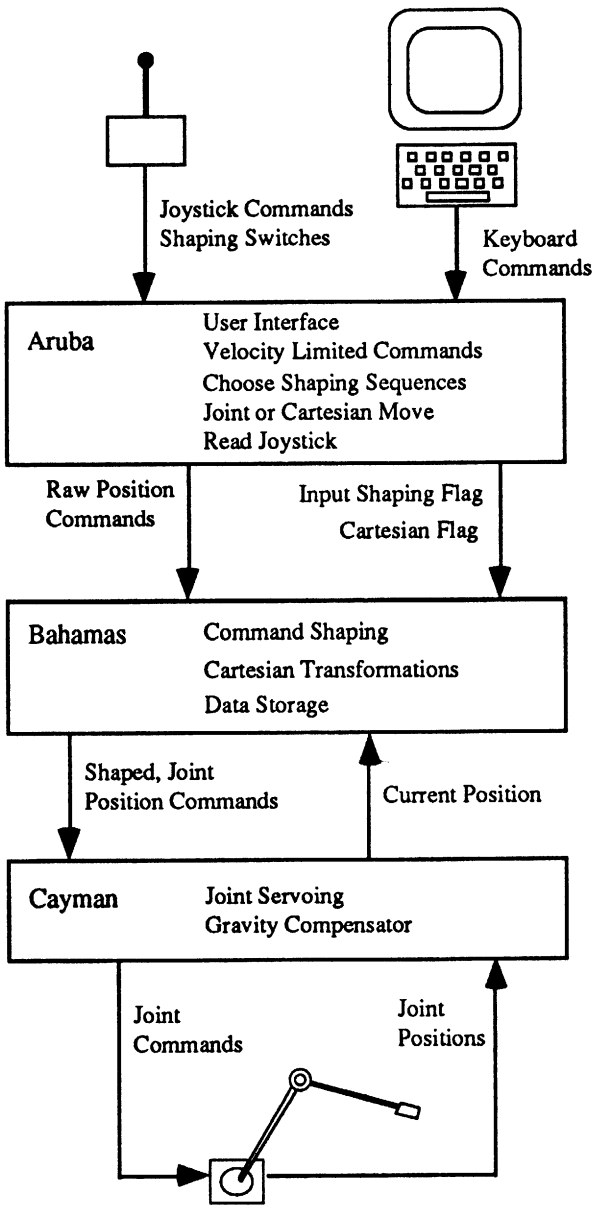

Figure 4-2: Interaction of Boards in VMEbus

Bahamas performs three tasks: Cartesian transformations, input command shaping, and data storage. It typically runs on a 125 Hz timing loop, processing each command from Aruba. The Cartesian transformation and data storage have remained unchanged from the original code. The new implementation of command input shaping will be described completely in section 4.4. The third processor board, Cayman, does the actual servoing of the three joints. It runs a 500 Hz servo loop that takes the commands from Bahamas as input to a PD servo with estimated velocities. The controllers are based upon those used by Christian [6]. However, the reduced servo rate, caused due to the overhead of the VXworks operating system, necessitated recalculating the gains. During each servo cycle, Cayman reads the encoder position of each joint, reads the desired position from Bahamas, calculates the observer position and velocity, adds a gravity compensation factor, and sends commands to the joints.

The gravity compensation attempts to offset any joint position error due to gravitational forces. It does not account for flexing of the links due to gravity. The compensator values were found experimentally by measuring the output to the amplifier that was necessary to hold a given position. The equations used are

$$G_1 = -\left[W_1 + W_2 \cos\left(\Theta_2\right)\right] \sin\left(\Theta_1\right) \tag{4-1}$$

$$G_2 = - W_2 \sin\left(\Theta_1 + \Theta_2\right) \tag{4-2}$$

where the Θ_i are defined as in Figure 4-3, and W_1 and W_2 are the current commands necessary to support the elbow-joint and the payload, respectively. The gravity compensator terms are added directly to the PD terms

$$\text{Voltage Out} = K_p\left(\Theta_{des} - \Theta_{act}\right) + K_d\left(\dot{\Theta}_{des} - \dot{\Theta}_{act}\right) - G \tag{4-3}$$

An instability due to a 38 Hz mode of the base joint caused problems with the controller. The low damping of the joint and the slow servo rate caused

the joint to limit cycle. This problem was solved by moving the poles of the observer for the base joint and slowing the controller. However, the joint still limit cycles--it does not cause stability problems in the system, however, it may have an effect on the vibration reduction of the inputs shaping scheme. Concurrent research by Avery[3] explains the problem of this type of limit cycle in terms of quantization error due to the encoders and time delays due to the digital nature of the control.

4.4 Analysis of Vibrational Workspace

Christian [6] showed that there is considerable variation in the vibrational frequencies as the Flexbot moves about its workspace. A variation of +/- 25% was found for each of the first three modes. In hopes of improving the effect of command input shaping, a method was developed to account for known frequency variations with the workspace. The method requires a knowledge of the frequency variation as a function of position. The first four frequencies

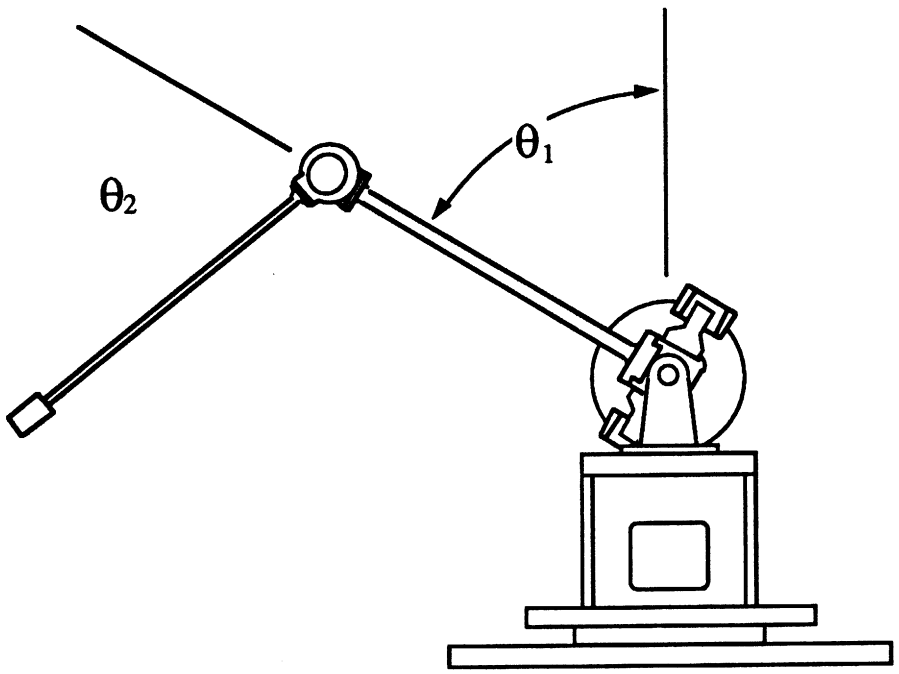

Figure 4-3: Definition of Flexbot Joint Angles
Taken from [6].

of the Flexbot were mapped throughout the workspace of the robot. Moving about the workspace in 20 degree increments, two symmetries appeared. First, the base angle does not affect the vibrational frequencies. Second, the system is symmetric about the vertical position. The reduced workspace was mapped, using knowledge of these symmetries.

To measure the vibrational frequencies, all three joints were excited using pseudo-white noise. The noise was generated using ran2(), a random-number generator algorithm from Numerical Recipes in C [17]. The random number generator provided position commands and were sent to the servo loop. To measure the vibrations produced by the white noise, two accelerometers were attached to the elbow joint of the Flexbot--one in-plane with the shoulder and elbow motors and one out-of-plane. Bruel & Kjaer Type 4371 Accelerometers were connected to Bruel & Kjaer Type 2651 Charge Amplifiers. The amplified signal was fed to a Hewlett-Packard 3563A Control Systems Analyzer [9]. The analyzer sampled the signal at 9.77 ms intervals for 100 seconds. The resulting time sample was processed and displayed as a frequency response.

Figures 4-4 - 4-7 show the results of the mapping exercise. The first and third frequencies are characterized as being in-plane with the shoulder and elbow joints. These two frequencies have significant damping from the motor servos and the backlash in the elbow joint. They are primarily a function of elbow position as the elbow position changes the inertia seen by the shoulder joint. The first frequency varies from 2.05 Hz when the robot is pointing straight up to 3.15 Hz down near the base. The third frequency has its minimum, 4.70 Hz, near the bottom of the workspace and its maximum, 6.45 Hz, at the top. The second and fourth frequencies are primarily out-of-plane with the joints. They are almost completely undamped and vary with both

elbow and shoulder position. The second frequency is 2.85 Hz when the robot is vertical, compared to 3.85 at the bottom. The fourth frequency changes from a minimum 5.80 Hz near the base to a maximum 7.95 Hz when the robot points straight up. The frequency map was consolidated into a 14 x 14 grid, covering the whole workspace. When the system is used, the resulting array of frequencies is loaded into the Flexbot control program so the frequencies can be accessed constantly while running the system.

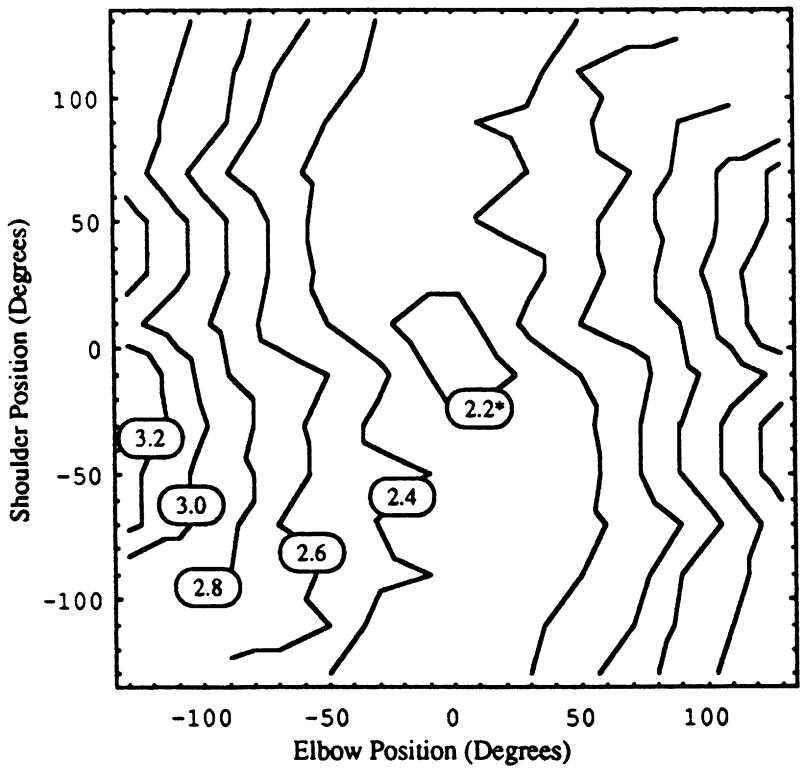

Figure 4-4: Frequency Variation of First Mode

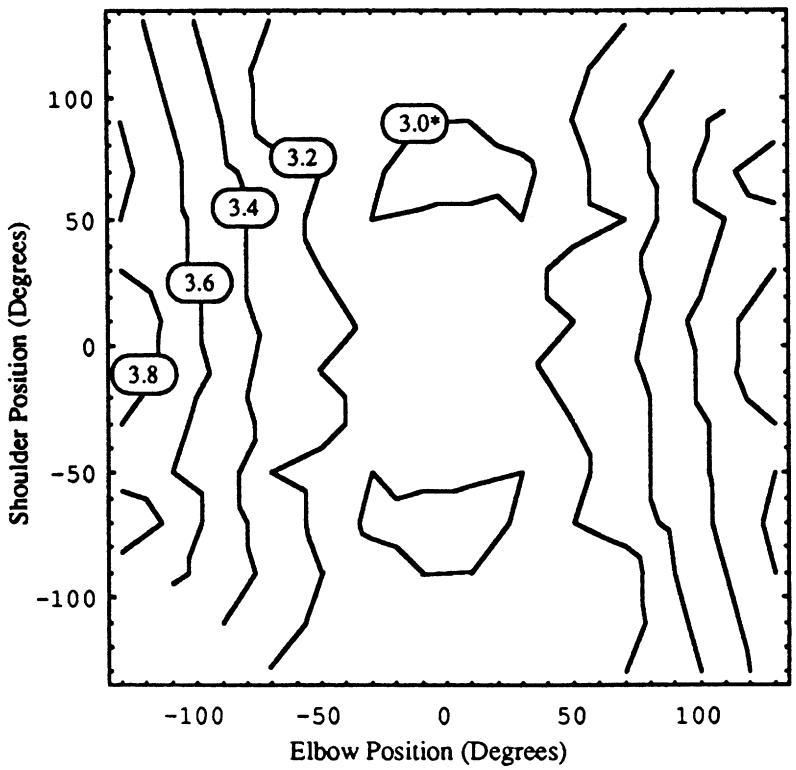

Figure 4-5: Frequency Variation of Second Mode

* All Frequencies are in Hz

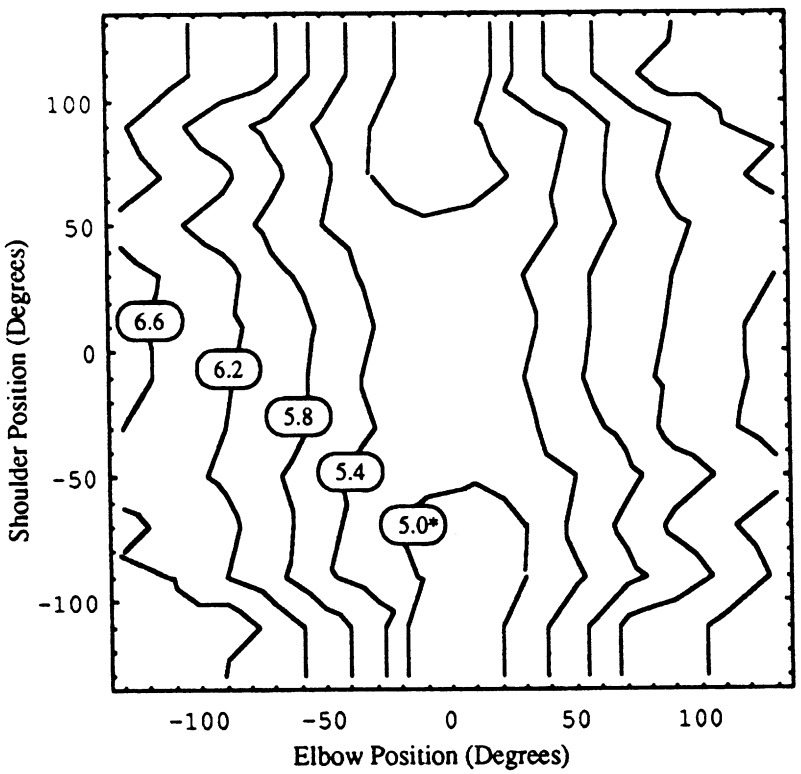

Figure 4-6: Frequency Variation of Third Mode

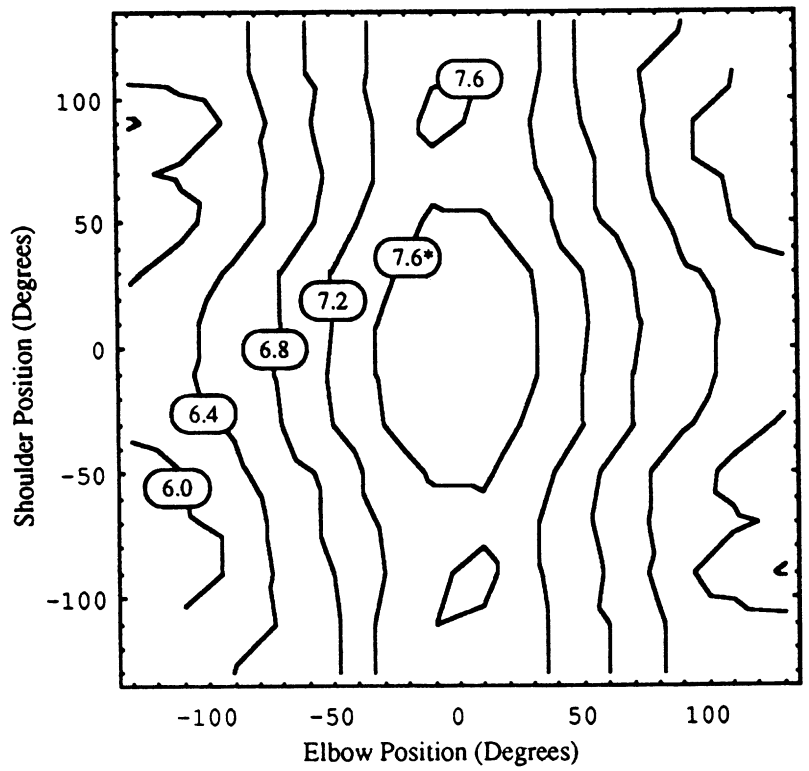

Figure 4-7: Frequency Variation of Fourth Mode

* All Frequencies are in Hz

4.5 Implementation of Command Shaping Techniques

4.5.1 Varying Frequencies

Unfortunately, the implementation of an adaptive-preshaping technique is not simple. There are many of issues to consider when designing the system controller. The frequency map illustrates that the Flexbot vibrational frequencies vary considerably around the workspace. The insensitivity plots presented in Section 2.3, show that input shaping should be robust to modelling errors of 15% for simple and derivative constraint sequences. All four of the Flexbot frequencies vary as much as 20% over the workspace. (see Figures 4-4 -- 4-7). In the adaptive-shaping scheme, the sequences will be calculated at each time step, based upon the system configuration. At each time step, we must determine the frequencies , calculate the sequences for those frequencies, and convolve the current command with the new sequence. We chose to vary the sequences at each time step, instead of changing at specific intervals, to reduce any possibility of inducing vibration in the system due to abrupt changes in the sequences.

4.5.2 Accessing Frequency Data

The method of accessing the frequency data is simple. The frequency map is loaded into an array on Bahamas when the control program is started. The array contains the four frequencies as a function of the elbow and shoulder positions. At each time step, the processor board reads the actual positions from the servo board, and performs a two-degree linear interpolation of each frequency. The four frequencies are then used to calculate new sequences for the current command.

4.5.3 Discretization Problems

The discrete nature of the control systems can cause problems from instability of the system to inducing vibration due to timing errors of the shaping sequences. Although the Bahamas timing loop runs at 125 Hz, errors in timing due to the discrete nature adversely affect the vibration reduction scheme. This problem is especially troublesome when we adapt to frequency changes continuously.

If we ignore the discretization issue and place the impulses of the sequence in the nearest discrete time step, a discontinuity in the shaper output occurs when the frequency changes enough to switch the last impulse from one time step to another. Two sequences discretized using this "Nearest Neighbor" approach are shown in Figures 4-8 and 4-9--a 0.001 Hz difference in frequency causes the third impulse to move from the 17th cycle to the 16th. Figure 4-10 shows the shaped commands for a step input where the sequence is changed from the one in Fig. 4-8 to the one in Fig 4-9 after 1.0 Sec. Magee[11] also noticed that changing frequencies causes problems. He describes a method of adding or subtracting impulses, depending on the sign of the variation, to attempt to compensate for the vibration induced by the

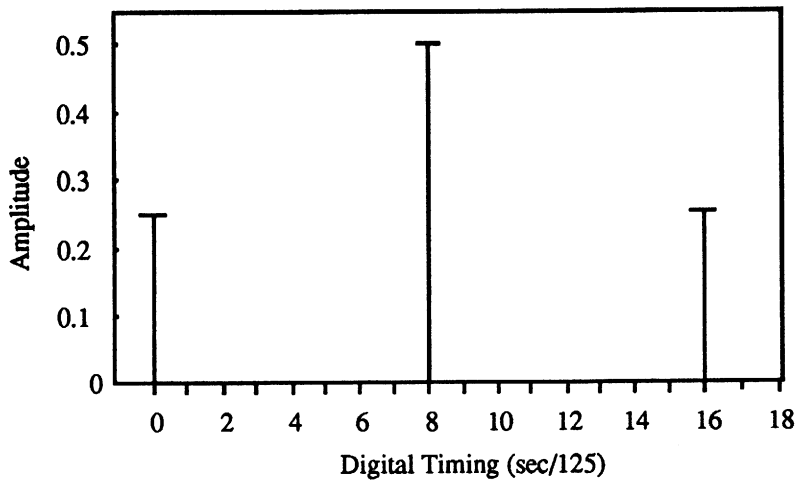

Figure 4-8: Sequence for 7.576 Hz Discretized to 125 Hz Timing Loop

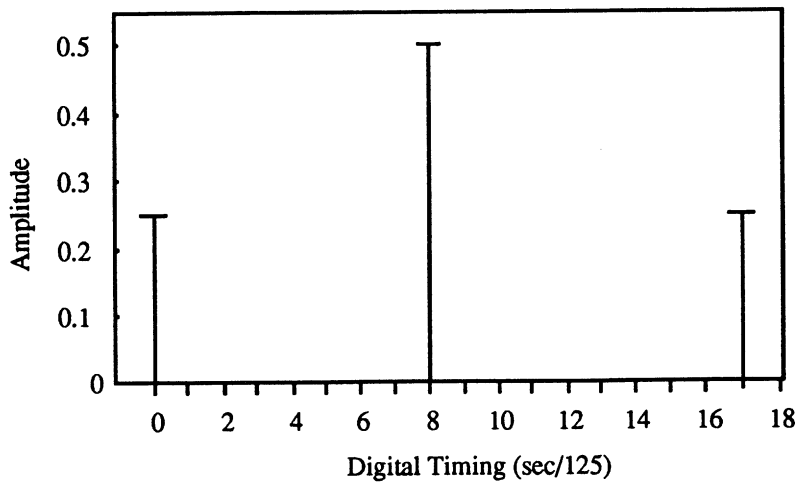

Figure 4-9: Sequence for 7.575 Hz Discretized to 125 Hz Timing Loop

switching of sequences.

We can eliminate the discontinuity caused by changing shaping sequences if we can continuously vary the shapers from one time step to the next. By using a linear extrapolation on the continuous sequence, splitting each impulse into two impulses placed in the two nearest neighbors, we will create sequences that vary continuously with changes in frequency. The discrete pulse amplitudes are calculated as follows. The extrapolation method is shown in Figure 4-11. The amplitude of the new impulses is calculated using a linear weighting of the time offset of the discrete time from the continuous impulse. Figure 4-12 shows a continuous sequence for 7.575 Hz--the highest Flexbot frequency. Figure 4-13 shows the extrapolated version of the same sequence onto a 125 Hz time step. The respective insensitivity curves are shown in Figures 4-14 and 4-15. The two insensitivity curves are virtually identical for the continuous and extrapolated sequences. The extrapolated sequence is limited in its ability to cancel the higher frequencies that the continuous sequence will cancel. Discretization reduces the vibration reduction effect on the higher frequencies by changing the timing of the

pulses. The timing change may be effective at the low frequency, but the same change in time at the low frequency causes a greater phase shift at the higher frequencies.

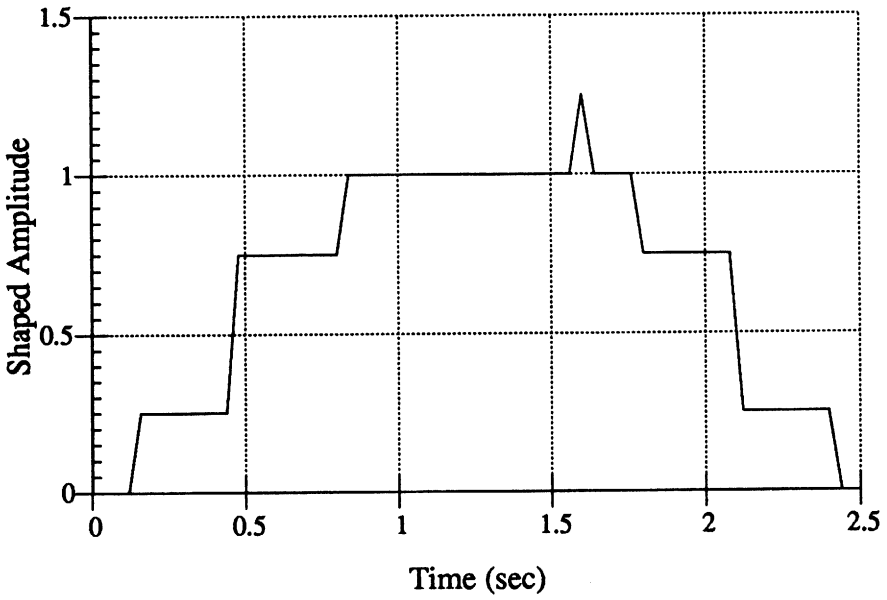

Figure 4-10: Shaped Command With Varying Sequences--
The Wrong Way

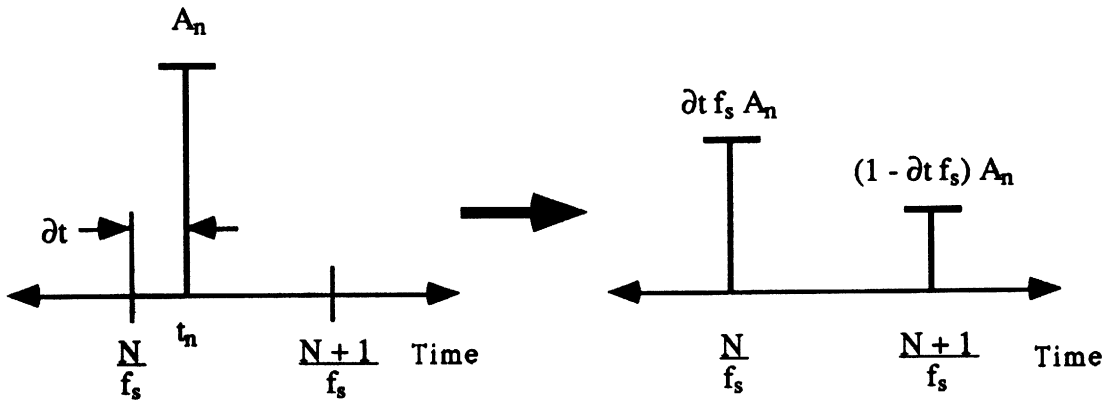

Figure 4-11: Method of Extrapolating Sequences.
f_S is the Servo Frequency, and N is an Integer.

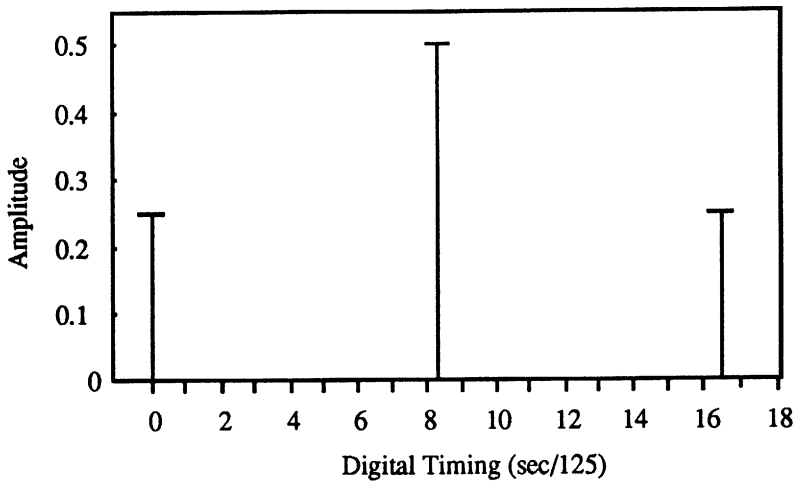

Figure 4-12: Continuous Time Sequence, 7.575 Hz, 125 Hz Timing Loop

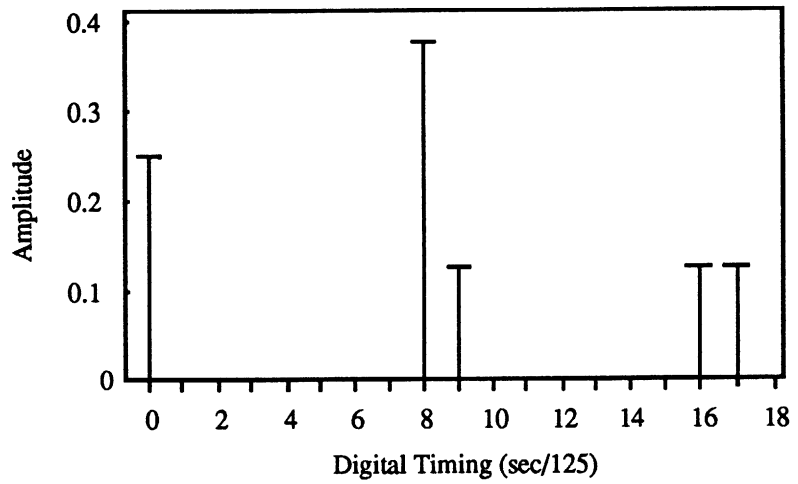

Figure 4-13: Extrapolated Sequence for 7.575 Hz, 125 Hz Timing Loop

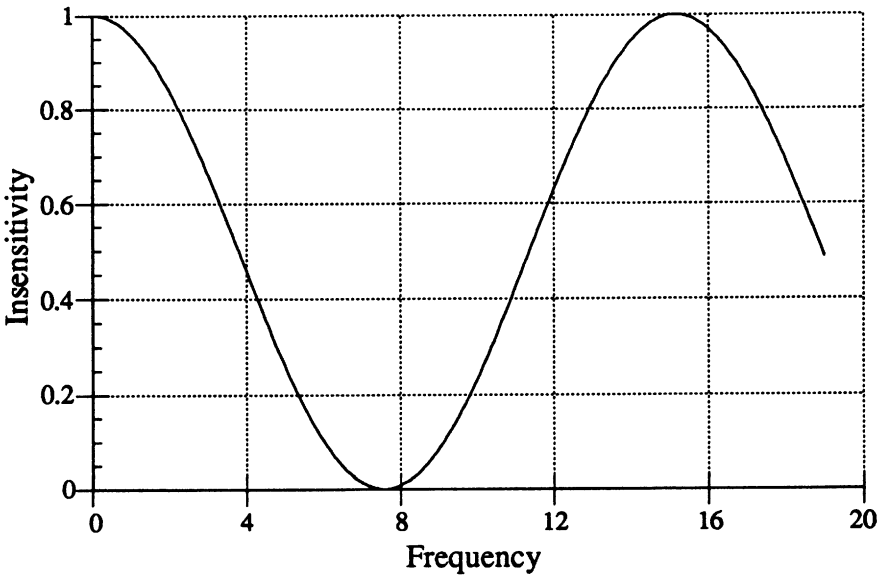

Figure 4-14: Insensitivity Curve for 7.575 Hz Continuous Sequence, from Fig. 4-12

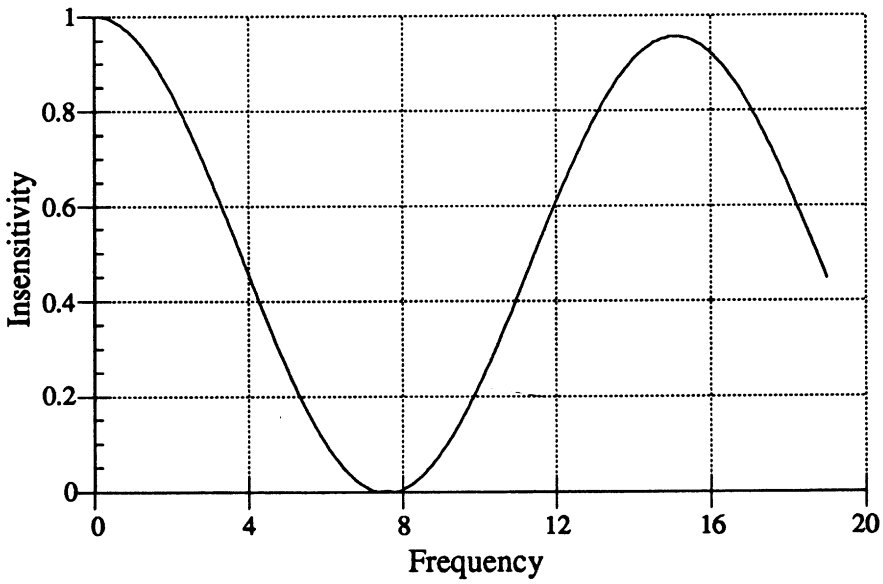

Figure 4-15: Insensitivity Curve for 7.575 Hz Sequence Extrapolated to 125 Hz Timing Loop, from Fig. 4-13

The insensitivity curves for the two sequences found by the "Nearest Neighbor" approach are shown in Figure 4-16. One of the sequences, from Figure 4-8, shows good insensitivity, although the frequency of the sequence

is not the desired frequency. The "Nearest Neighbor" technique will shift the actual frequency, in this case from 7.575 Hz to 7.813 Hz. The second "Nearest Neighbor" sequences shows very poor insensitivity. The low ratio of timing loop frequency to sequence frequency degrades the performance of this shaper. Since the direct-solution method derived above generates impulse amplitudes that are continuous with variations in frequency, the shaped-commands generated from our continuously varying shaper will be smooth.

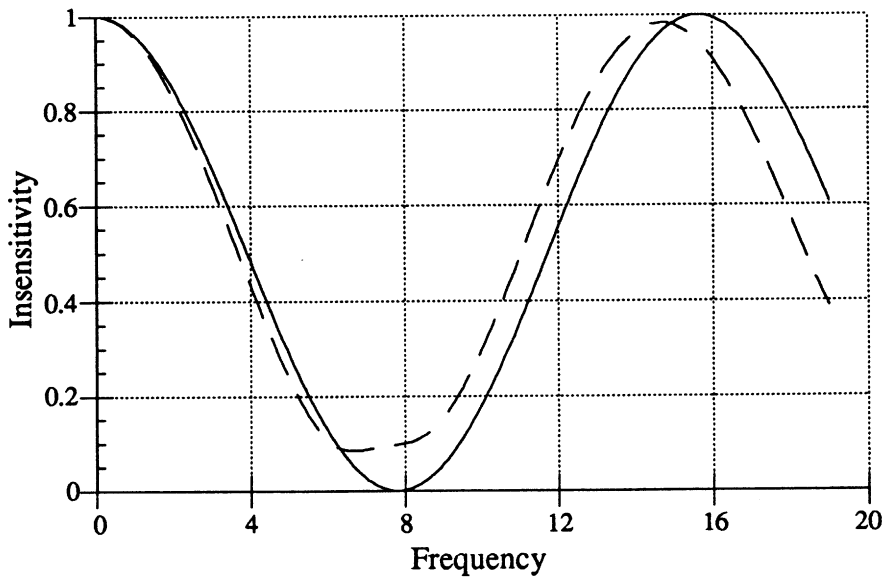

Figure 4-16: Insensitivity Curves for 7.575 and 7.576 Hz Sequence Moved to Closest Time Step, 125 Hz Timing Loop

4.5.4 Buffering Method

To minimize the number of calculations per time step, a new buffering technique was developed for storing the shaped commands. Instead of convolving each sequence together, thereby multiplying the number of impulses, we choose to run our sequences in series, only sending the current impulse from the first shaper to the second shaper. Using this method, we can effectively add the number of impulses in all the shapers being used to

find the number of calculations per time step. Figure 4-16 shows the buffering technique. At each time step, a raw command enters the shaper. It is convolved with the first sequence, and the resulting 'partial-shaped commands are stored in the first buffer. The first buffer contains partial commands for a small amount of time into the future. At the next time step, the buffer will shift down one step and the new command will be entered. When a partial-shaped command reaches the bottom level, is the output for the first shaper for the current time step. It is then sent to the next buffer where the process is repeated. The number of calculations required by the new buffering scheme is roughly 1/5 the number for a convolved sequence for four modes.

4.6 Conclusions

There are many important issues to confront when implementing command input shaping on a real system. The Flexbot is a complex piece of hardware that is well suited to input shaping. Its three-degree-of-freedom

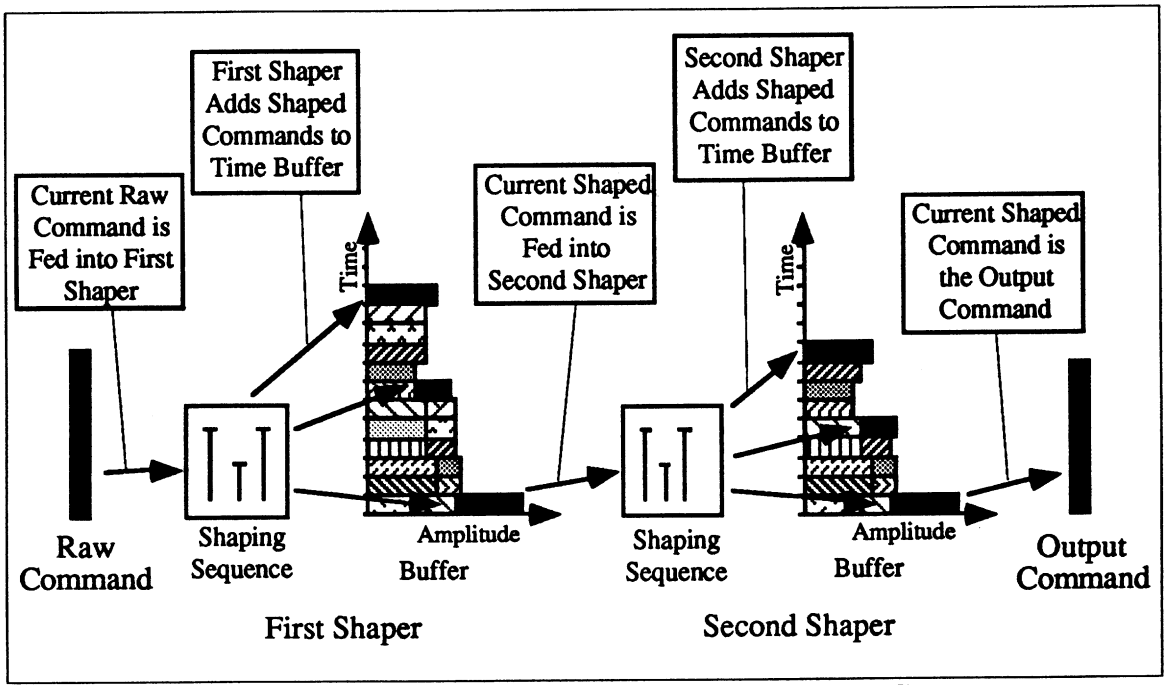

Figure 4-16: Buffering Technique used for Multiple Sequences

design generates complex mode shapes not found in planar manipulators. The Flexbot also has vibration characteristics somewhat similar to the Shuttle RMS and other space structures. The issues of large frequency variation over the workspace and discretization will arise in other systems when input shaping is applied. The methods derived in this chapter will allow us to implement a smooth and continuous input shaping scheme that will allow us to compensate and adapt to the changes in frequency over the workspace.

Experimentation and Results

Chapter 5

5.1 Introduction

In the previous chapters we developed a new method for implementing command input shaping techniques. The new method is designed to effectively use shaping techniques on a system with large frequency variations over its work space. The symmetric, two-mode solution developed above allows us to take advantage of the time savings of direct-solution sequences in an application that requires on-line calculation of sequences. This chapter presents the results of experiments performed on the Flexbot. Tests were run comparing the new, direct-solution technique with previous methods of calculating sequences. Experiments in which shaping sequences are calculated on-line, adapting to the frequencies of the current position, were also completed and this new method of command input shaping is compared with the constant valued shaping tests.

5.2 Experimental Set Up

For an accurate comparison of the various command input shaping methods, consistency in data collection is important. All of the tests were performed with the apparatus shown in Figure 5-1. Two accelerometers were positioned on the Flexbot in the same manner as described in Section 4.3. The Bruel & Kjaer Type 4371 Accelerometers were connected to Bruel & Kjaer Type 2651 Charge Amplifiers. The amplified signal was fed to a Hewlett-Packard 3563A Control Systems Analyzer. The analyzer sampled the signal at 9.77 ms intervals and recorded the acceleration trace for 20 seconds. A software triggering method was used to synchronize the timing of the analyzer's collection with the VXworks program--the analyzer was triggered as the computer began sending commands to the robot. Two sets of data were collected for each test. The first set comes from the computer and consists of the desired position command, shaped position command, actual position, and voltage signal for each joint. The second set of data is the acceleration signals from the analyzer.

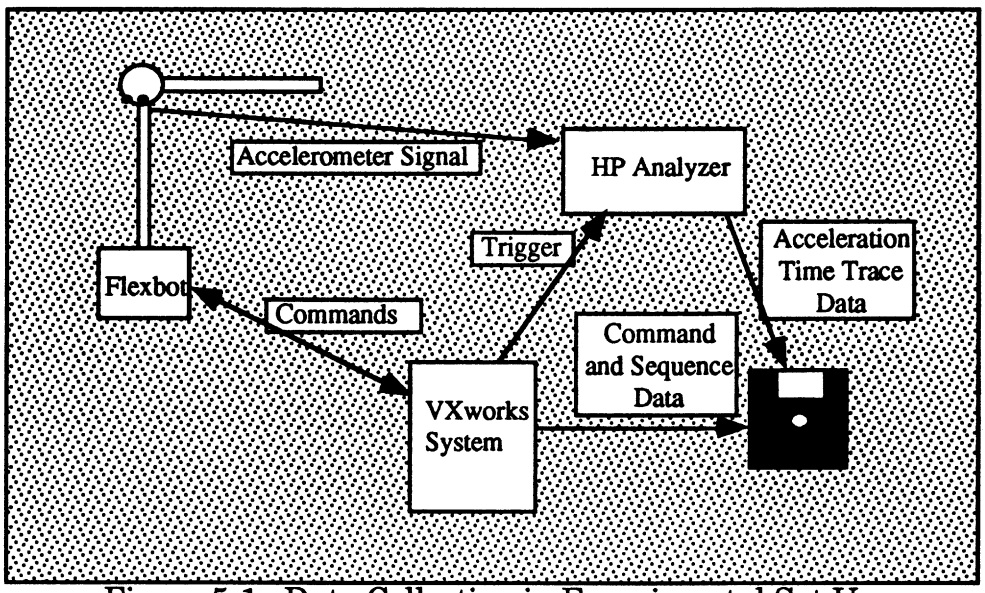

Figure 5-1: Data Collection in Experimental Set Up

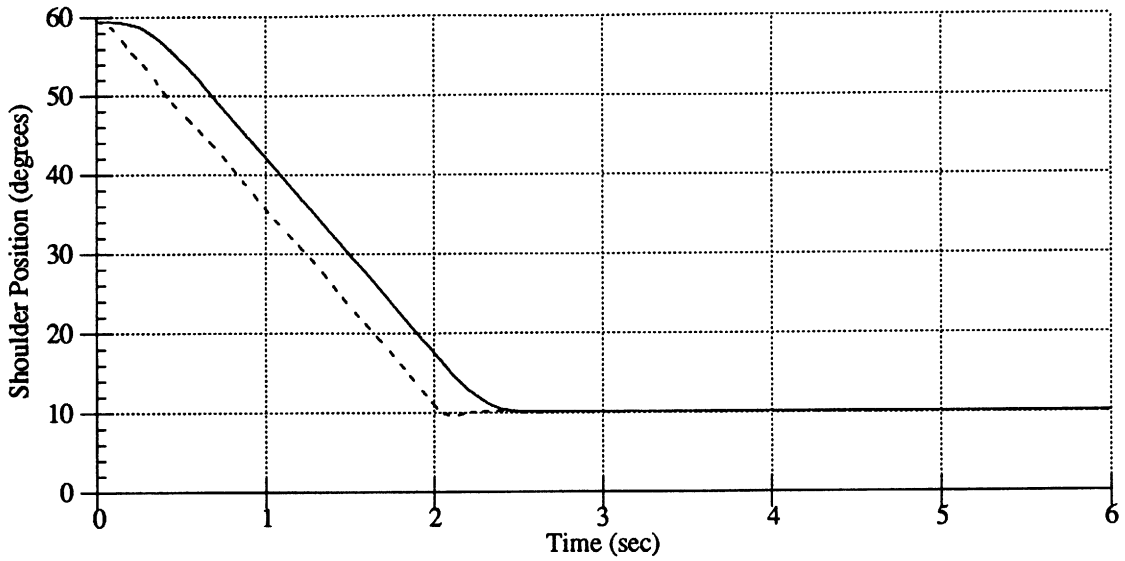

Figure 5-2: Joint Position Data: Note Lack of Position Resolution

The computer data allows us to see the time delay introduced by the input shaping and the vibration left in the joints at the end of a move. Due to the PD controller's high damping, relatively little vibration is left in the joints after a move. Figure 5-2 shows the position of the shoulder joint during a shaped and an unshaped test. The time delay is noticeable in the figure, but the vibration amplitude is very small. Most of the residual vibration resides in the flexing of the links. The flexing causes vibrations at the joints, but, typically, these vibrations are on the order of the encoder resolution. During tests with adaptive sequences, the variations in the sequences are recorded.

We also collect acceleration data, which is useful for two reasons. The first is to compare the time-traces of the acceleration for different sequences. The second is for calculating the Fast Fourier Transform (FFT) [17]. The magnitude of the FFT shows the amplitude of the acceleration at a specific frequency. In a linear system, the acceleration amplitude is a constant multiple of the position amplitude. Comparing the magnitude of the FFT of an unshaped response to a shaped system response allows us to gauge what

percent of the vibration amplitude was eliminated by the shaping procedure. Since command shaping attempts only to reduce the level of residual vibration in a system, we want to calculate the FFT only for the data collected after the end of the move. Therefore the data is processed as follows: the DC bias of the charge amplifiers from the acceleration signal is removed (about 0.02 m/s^2), the first 1024 data points after the completion of the move are selected, and the FFT is calculated. The resulting FFT yields frequency data for 0 to 40 Hz at 0.10 Hz increments. Figure 5-3 shows what portion of a typical acceleration profile is being used for the FFT.

To accurately compare the different methods of command shaping, several tests were performed. The first tests involve maneuvers along lines of constant frequency. We compare the two-mode, direct solution sequences with the convolved sequences based on the results of these tests. Second, we performed several non-constant frequency tests. These tests will allow comparison of the new method of adapting to frequency changes to the current method of constant-valued sequences.

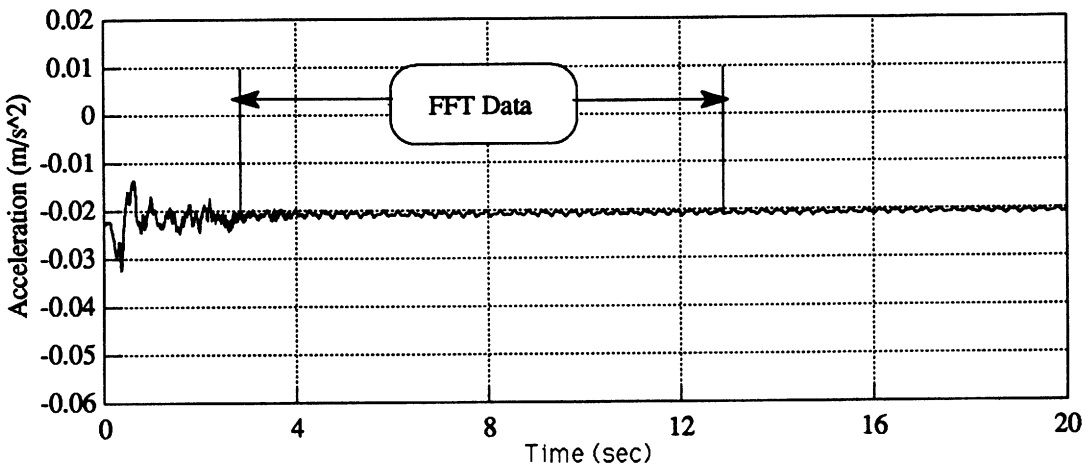

Figure 5-3: Data Used for FFT Calculation

Five different shaping sequences were compared in these tests. The different types are described in Table 5-1. I will refer to the different sequences by the abbreviations listed in Table 5-1. Each constant-valued shaper is generated for the four frequencies when the shoulder and elbow are both at 30°. These frequencies are 2.35, 3.15, 5.80, and 7.60 Hz, all with zero damping. The four frequencies represent the first four modes of the Flexbot. In different configurations, the system frequency values will change, but the constant-valued shapers will always be calculated for these values. The adaptive shapers will be continuously updated based upon current position. The time-delay of the adaptive shapers will depend upon the final configuration of the system but will be close to the approximate value listed in the table.

When comparing the different sequences, two values are checked: the time delay of the sequence and the magnitude of the peaks of the acceleration FFT. The very low damping of the two out-of-plane modes is a cause for concern, since any disturbance will remain in the system for an extended period of time. Command shaping does not presume to eliminate existing vibrations in a system, so the amount of residual vibration depends upon the vibration that exists in the system at the beginning of the move and the vibration caused by forces other than the actuators. For the most part these exogenous disturbances are small, but they can influence the data.

To show the affect of noise on the data, Figures 5-4 to 5-6 show details of the acceleration signal measured during three tests. The first two are immediately following slews with shaping; the final one is from the idle robot, after an extended period of time with no commanded motion. The residual vibration present after the adaptive shaping move is virtually indistinguishable from the idle noise. Much of this noise is due to the limit

cycle described in Section 4.3.2, as the 38 Hz signal can be seen in the acceleration data. The noise level in Figure 5-6 will be the base for all vibration measurements. The percent residual vibration is included in the results. This value is calculated from the FFT magnitude. Typically, the idle values are close to 5.0% of the unshaped values for the tests. Any shaped response that is close to this value has eliminated as much vibration as is possible.

5.3 Constant-Frequency Moves

One objective of the tests is to compare the new, two-mode sequences with single-mode sequences. Two constant-frequency moves were performed using a variety of different shaping sequences. As mentioned above, the base angle does not affect the vibrational frequencies of the system, so the test motions were movements of the base joint alone. The vibration reduction ability of each is noted. The first test was performed with sequences tuned to the robot configuration. For the second test, the Flexbot was configured so that the sequences that were tuned to the system vibrational characteristics in the first experiment were no longer accurate. The system frequencies are between 17% and 34% different from the sequence frequencies in the second test. In both tests, the shapers are also compared to the varying-mode sequences which are constantly tuned to the system position.

5.3.1 Move with Tuned Shapers

The first set of tests consisted of a slew along a line of constant frequency. The shoulder and elbow joints were both set to 30°, and the base joint was moved from 30° to -30°. The velocity limit was set to 15°/sec. We selected a low velocity limit to minimize the inertial forces on the system. This move primarily excites the two out-of-plane vibratory modes, so data was collected

Table 5-1: Types of Shaping Sequences Used in Tests

Type of Sequence	**Total Impulses**	**Time Delay**	**Abbreviation**
Four Single-Mode, Three-Impulse Sequences for 2.35, 3.15, 5.80, and 7.60 Hz	81	1.048 sec	1M3
Two Three-Impulse, Two-Mode Sequences. First for 2.35 and 5.80 Hz, Second for 3.15 and 7.60 Hz	9	0.440 sec	Short-2M3
Two Three-Impulse, Two-Mode Sequences First for 2.35 and 3.15 Hz, Second for 5.80 and 7.60 Hz	9	0.528 sec	Long-2M3
Two Five-Impulse, Two-Mode Sequences First for 2.35 and 5.80 Hz, Second for 3.15 and 7.60 Hz	25	0.872 sec	Short-2M5
Two Five-Impulse, Two-Mode Sequences First for 2.35 and 3.15 Hz, Second for 5.80 and 7.60 Hz	25	1.016 sec	Long-2M5
One Four-Mode, Nine-Impulse Sequence for 2.35, 3.15, 5.80 and 7.60 Hz	9	0.848 sec	4M9

from the out-of-plane accelerometer. Figures 5-7 and 5-8 show acceleration time-traces for the unshaped move and one shaped slew.

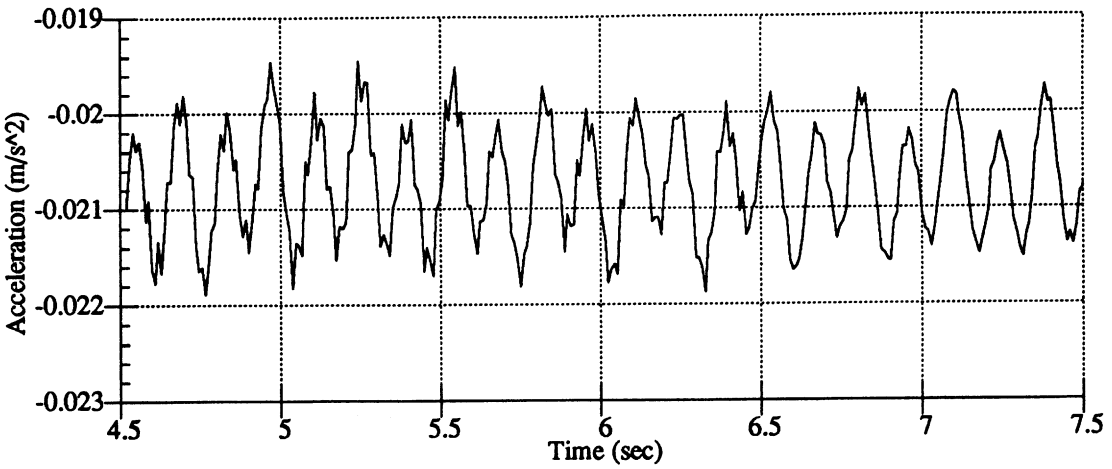

Figure 5-4: Detail of ResidualAcceleration for Shaped, 15°/sec Slew, Using Long-2M3 Sequence, from {30,60,10} to {-30,10,60}.

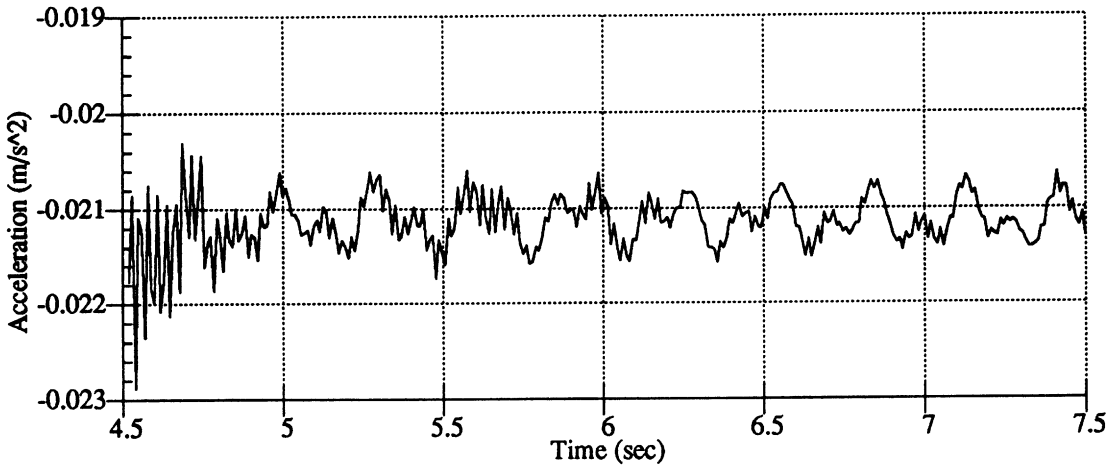

Figure 5-5: Detail of Residual Acceleration for Shaped, 15°/sec Slew, Using Adaptive Long-2M3 Sequence, from {30,60,10} to {-30,10,60}.

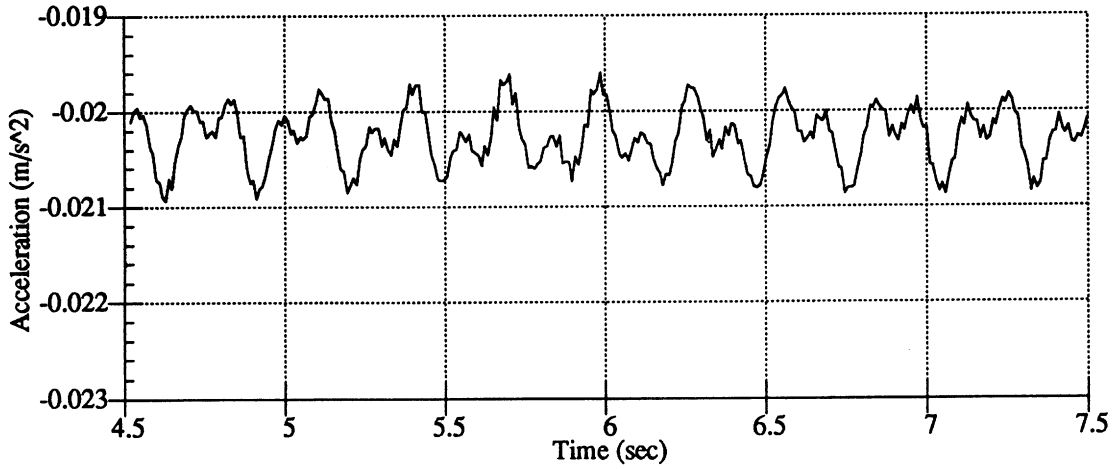

Figure 5-6: Detail of Residual Acceleration of Idle Robot. Recorded Two Minutes After Last Commanded Motion.

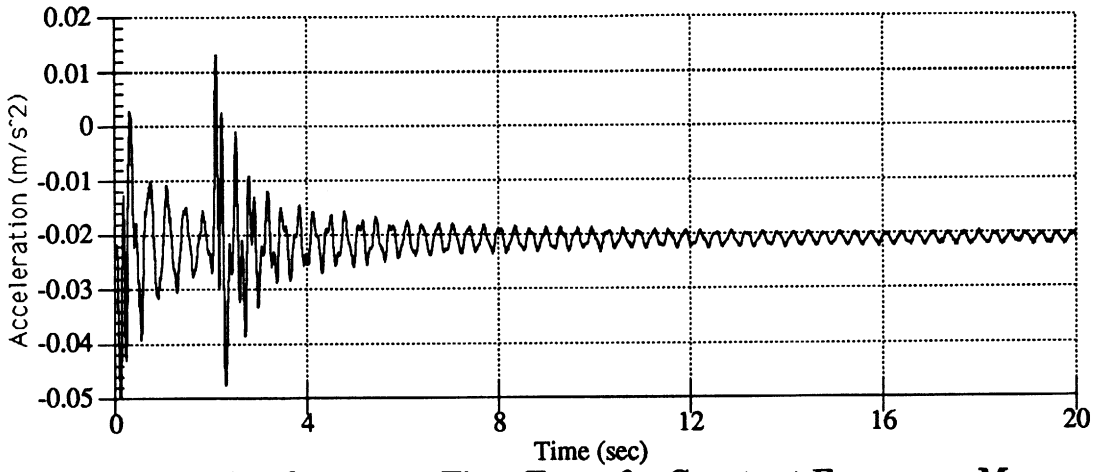

Figure 5-7: Accelerometer Time Trace for Constant Frequency Move, No Shaping.

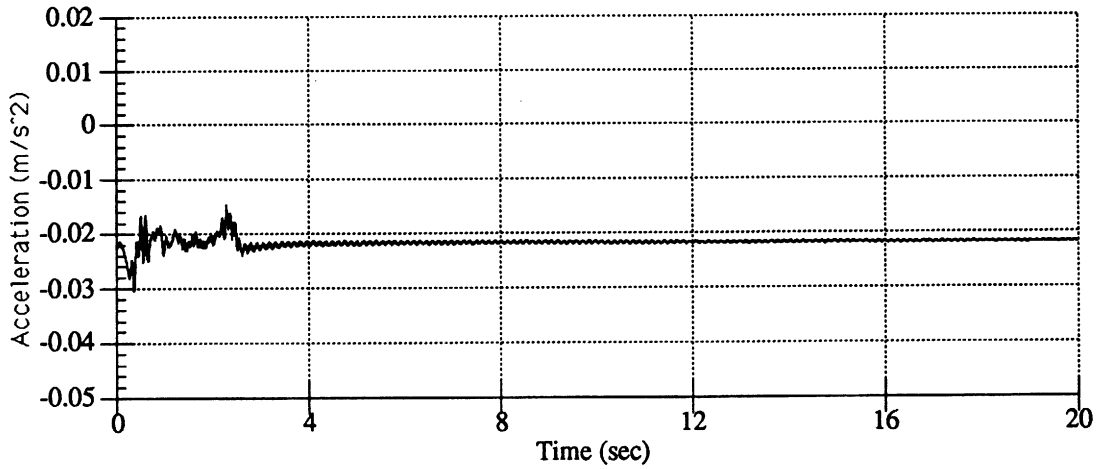

Figure 5-8: Accelerometer Time Trace for Constant Frequency Move, Long-2M3 Sequence.

Figures 5-9 and 5-10 show the FFT data for the same sequences. The rest of the data are presented in Table 5-2. The data show that one of the shortest sequences, the Long-2M3, gives the best vibration reduction. However all the sequences bring the vibration close to the idle level. Since the longer sequences are more robust to modelling errors, we might expect them to result in less vibration. However, the sequences used during this test were tuned to the frequencies of the test configuration. The sequences were calculated using out-of-plane frequencies of 3.15 and 7.60 Hz. From the FFT

magnitude data collected, we see that the actual frequencies were 3.10 and 7.50 Hz, within 1.6%. This accuracy in frequency modelling should yield comparable results for all the different sequences.

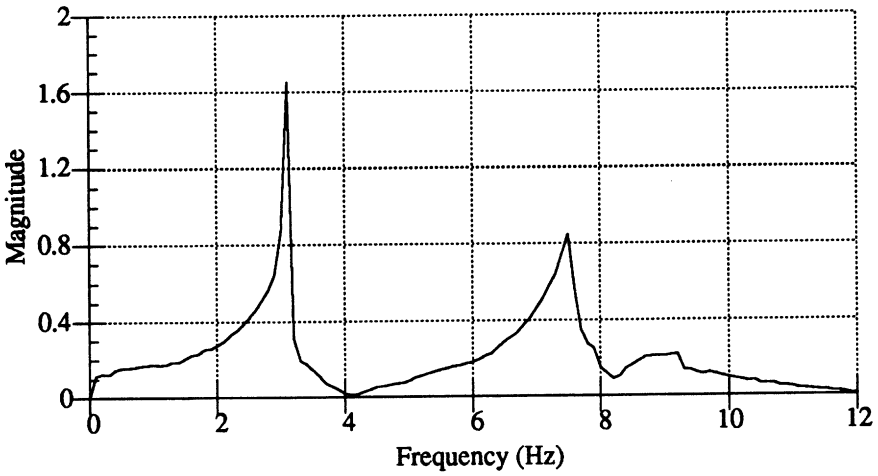

Figure 5-9: FFT Magnitude of Unshaped, Constant Frequency Move

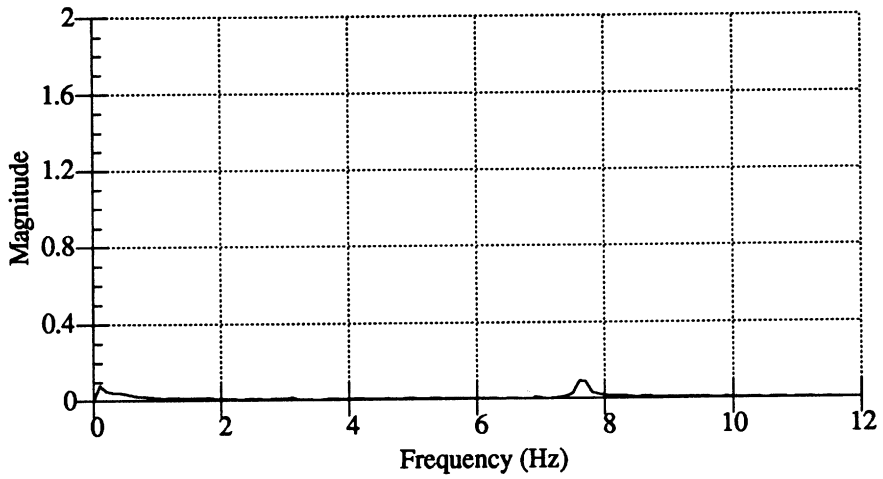

Figure 5-10: FFT Magnitude of Constant Frequency Move Using Long-2M3 Sequence.

The low insensitivity of the Short-2M3 sequence to the higher frequency, as discussed in Section 3.5, can be seen in the data. Comparing the new method of calculating direct-solution sequences to Singer's method [18], we see, from Table 5-2, that the direct-solution sequences yield better results. The three-impulse single-mode shaper gives slightly poorer results than the

five-impulse, two-mode shapers. Chang [5] noticed in his work on the Mid-deck Active Control Experiment, that short sequences with a small number of impulses often work better than long sequences. This helps explain the good performance of the Long-2M3 sequence and the relatively poor performance of the 1M4--convolved Singer-- sequence. The data from tests done with the adaptive sequences is also included in Table 5-2. Although the frequency should not change during this move, the varying sequences result in slightly larger residual vibrations than do the constant-valued sequences.

5.3.2 Constant-Frequency Move with Poorly Tuned Sequences

We have seen how well the new, direct-solution sequences perform when they are properly tuned. The next test is a constant-frequency maneuver in a position where the sequences are not tuned. For the new test, the shoulder and elbow joints are both set at 80°, and the base is moved from 30° to -30°. This configuration is far enough from the tuned-frequency-position that the actual system frequencies will differ significantly from the constant-valued sequence frequencies. We will be able to discern from this test how robust the different sequences are to errors in frequency modelling. The speed limit will be set to 50°/sec for this test. Again, we run the test twice for each of the five different shaping sequences as well as unshaped. The results of the test are shown in Table 5-3. All the shapers keep the vibration close to the idle limits. Within this limit, this test shows that the robustness of the longer sequences helps when the modelling error of the frequencies is large. The sequences are the same as above--generated for 2.35, 3.15, 5.80, and 7.60 Hz. However, the system frequencies have changed significantly. From the unshaped FFT, Figure 5-11, we see that the two out-of-plane frequencies are now 2.7 and 4.9 Hz. These measured frequencies differ from those found in

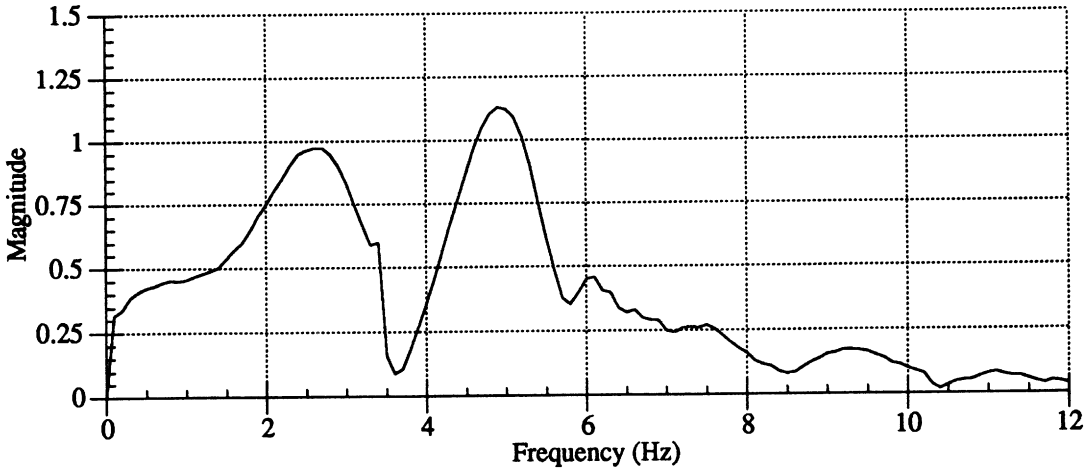

Figure 5-11: FFT Magnitude of Unshaped Slew from {30,80,80} to {-30,80,80} at 50°/sec

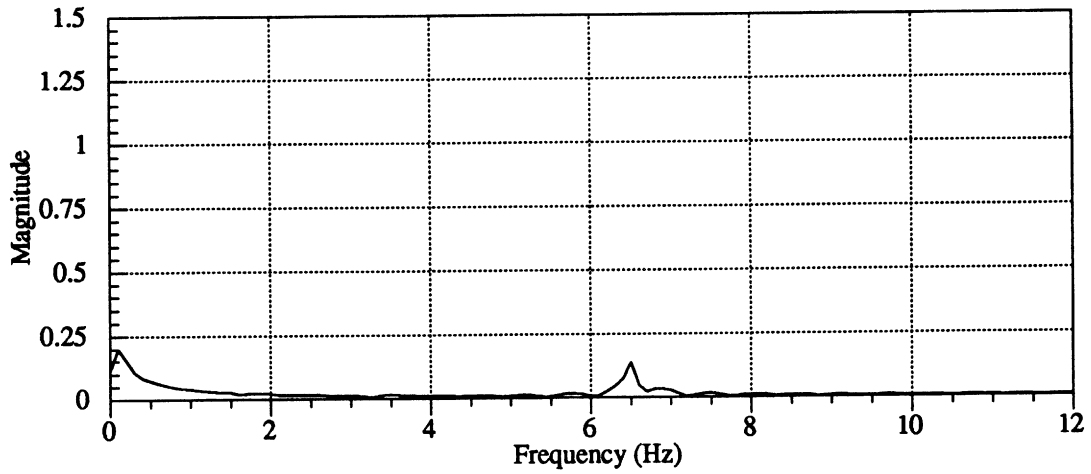

Figure 5-12: FFT Magnitude of Long-2M5 Slew from {30,80,80} to {-30,80,80} at 50°/sec.

the white-noise tests discussed in Section 4.4. The data supports the theory that sequences with derivative constraints are better at reducing the vibration when the frequency modelling error is large than are the sequences generated from simple constraints alone.

The varying-sequence data is also included in Table 5-3. In this case the varying shapers appear to minimize vibrations below the constant-shaper values, even in a constant frequency move. Since the varying-shapers will be

Table 5-2: Vibration Reduction in Constant Frequency Move, {30,30,30} to {-30,30,30} at 15°/sec.

Type of Shaper	Time Delay (sec)	3.3 Hz Residual Vibration (%)	7.0 Hz Residual Vibration (%)
Unshaped	0.00	100	100
Short-2M3	0.440	1.81	15.29
Long-2M3	0.528	0.87	3.28
Short-2M5	0.872	2.82	4.75
Long-2M5	1.016	2.67	4.32
1M3	1.048	1.92	10.73
Short-2M3, Varying	0.44 approx	4.47	14.26
Long-2M3, Varying	0.52 approx	1.78	6.37
Short-2M5, Varying	0.87 approx	8.39	3.49
Long-2M5, Varying	1.02 approx	5.96	10.44

calculated for frequencies closer to the actual frequencies than the constant sequences, the adaptive-sequences are more successful in reducing residual vibrations.

Table 5-3: Vibration Reduction in Constant Frequency Move, {30,80,80} to {-30,80,80} at 50°/sec

Type of Shaper	Time Delay (sec)	3.3 Hz Residual Vibration (%)	7.0 Hz Residual Vibration (%)
Unshaped	0.00	100	100
Short-2M3	0.440	5.04	9.67
Long-2M3	0.528	3.02	5.50
Short-2M5	0.872	1.14	1.81
Long-2M5	1.016	1.50	0.75
Short-2M3, Varying	0.44 approx	6.83	4.70
Long-2M3, Varying	0.53 approx	2.70	2.00
Short-2M5, Varying	0.87 approx	0.77	1.22
Long-2M5, Varying	1.02 approx	0.34	1.40

We have seen how the different types of sequences compare in two constant-frequency test maneuvers. The results have proven to be quite consistent with the theory. When the frequencies are very well known, as in the first experiment, sequences generated from simple-constraints alone yield acceptable results. As the modelling error of the frequencies grows, the sequences with derivative constraints prove to be more robust to these errors. Not all the data appears to be consistent with the theory, however. The tests

show that the 1M4--convolved, three-impulse sequence--with 81 impulses, does not reduce the vibrations as much as the direct-solution sequences, with many fewer impulses.

We have also seen that the adaptive method of command shaping does not perform as well as the constant-valued sequences when the sequences are tuned to the correct position. Once the system has varied from the tuned position, the adaptive sequences show an improvement over the constant shapers. The ability of the adaptive sequences to reduce vibration during a move with varying frequencies will be discussed in the next section.

5.4 Varying-Frequency Moves

The next step in comparing the different methods of implementing command input shaping is performing maneuvers that causes the system frequencies to vary. Two different tests will be completed. In the first test, the base joint will move from 30° to -30°, the shoulder will move from 60° to 10° and the elbow will move from 10° to 60°. This test will be repeated at three different joint velocities: 15°/sec, 30°/sec, and 50°/sec. The Flexbot will pass directly through the tuned-frequency position during this maneuver. The second test will be performed well away from the tuned-frequency position. The second maneuver will move the base joint from 0.0° to 30° while the shoulder and elbow both move from 80° to 45°. This test was performed with a joint velocity limit of 50°/sec. The actual paths of the robot in the frequency-space of the system are shown in Figure 5-13. The test paths are marked to show how the third frequency will change during the slews.

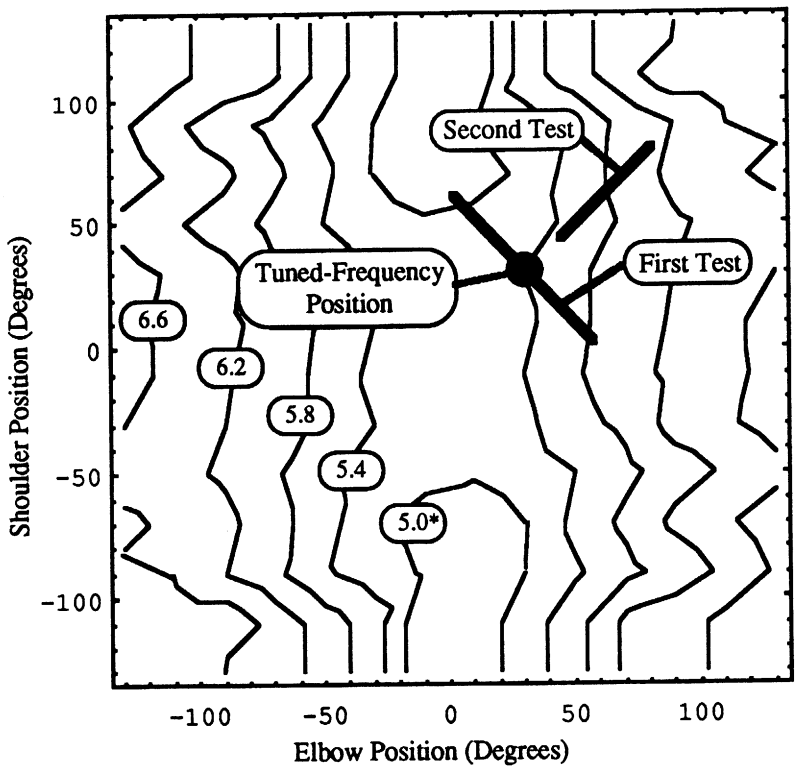

Figure 5-13: Variation of Third Frequency with Position with Testing Paths Marked. * Frequency in Hz.

Before viewing the test results, let's examine how one of the shaping sequences actually varies during a slew. Figure 5-14 shows the variation in one of the two-mode, three-impulse sequences of the Long-2M3 filter during a 50°/sec run of the first test. A slice of the three-dimensional figure at a specific move-time corresponds to a plot of a sequence' s impulses, as in Figure 4-15. Figure 5-14 shows the impulses varying significantly during the move. Each of the three impulses in the sequence is discretized using the method described in Section 4-5. As the frequency varies during the move, both the timing and the amplitude of the impulses change. The frequencies for this sequence are 6.23 and 7.55 Hz at the beginning of the move and 5.35 and 7.05 Hz at the end of the move. This variation in frequency causes a lengthening of the sequence from 0.145 sec. to 0.161 sec. At our digital time

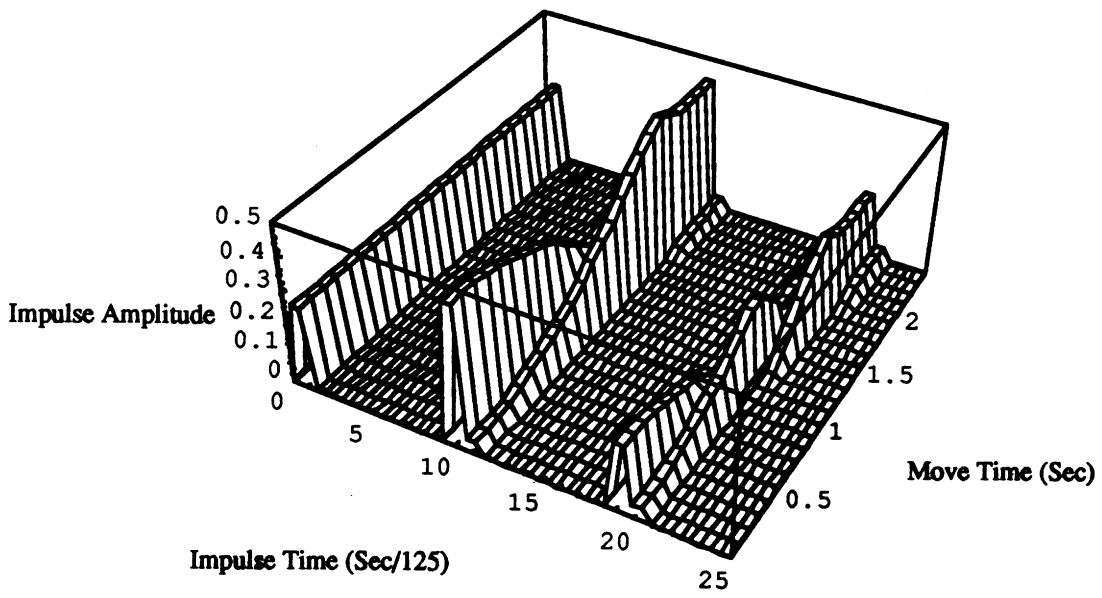

Figure 5-14: Variation in Filtering Sequence During 30°/sec Slew from {30,60,10} to {-30,10,60}.

frequency of 125 Hz, the change in time delay moves the last impulse from the 18th and 19th time steps to the 20th and 21th time steps. The discretization of the impulses insures that the change in the sequences is smooth as the frequency varies.

5.4.1 Varying-Frequency Move Close to Tuned-Frequency Position

The first varying-frequency test consists of a slew of all three axes concurrently. The base joint will move from 30° to -30°, the shoulder will move from 60° to 10° and the elbow will move from 10° to 60°. The tuned-frequency position is located within the trajectory of this slew, as seen in Figure 5-13. All the sequences in Table 5-1 were tested at 15°/sec and 30°/sec. The results are listed in Table 5-4. The results offer no conclusive

evidence that varying the shapers reduces the residual vibration more than using a constant-valued shaper, as several different tests are within the idle noise limit. The two best sequences were the 4M9--a direct-solution sequence for four modes--and the varying Long-2M3, both of which keep both modes of vibration below 10% of the unshaped value. The Long-2M3 has the benefit of being 38% shorter than the 4M9 (0.528 sec compared to 0.848 sec), as well as being calculated in real time. Acceleration data are shown for three different moves in Figures 5-15 to 5-17.

Table 5-4: Vibration Reduction in Variable Frequency Move, {30,60,10} to {-30,10,60} at 15°/sec.

Type of Shaper	Time Delay (sec)	3.3 Hz Residual Vibration (%)	7.0 Hz Residual Vibration (%)
Unshaped	0.00	100	100
Short-2M3	0.440	2.47	37.78
Long-2M3	0.528	6.88	24.13
Short-2M5	0.872	2.44	10.84
Long-2M5	1.016	6.33	21.67
4M9	0.848	4.44	7.38
1M3	1.048	2.81	44.77
Short-2M3, Varying	0.44 approx	5.15	30.27
Long-2M3, Varying	0.52 approx	6.51	6.93
Short-2M5, Varying	0.87 approx	0.29	19.23
Long-2M5, Varying	1.02 approx	8.61	10.44

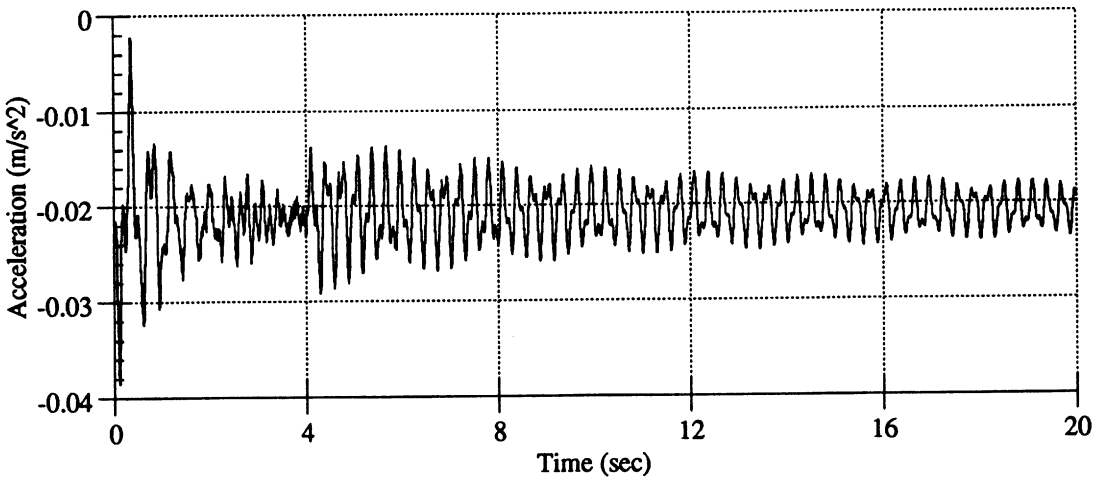

Figure 5-15: Acceleration of Unshaped, 15°/sec Slew from {30,60,10} to {-30,10,60}

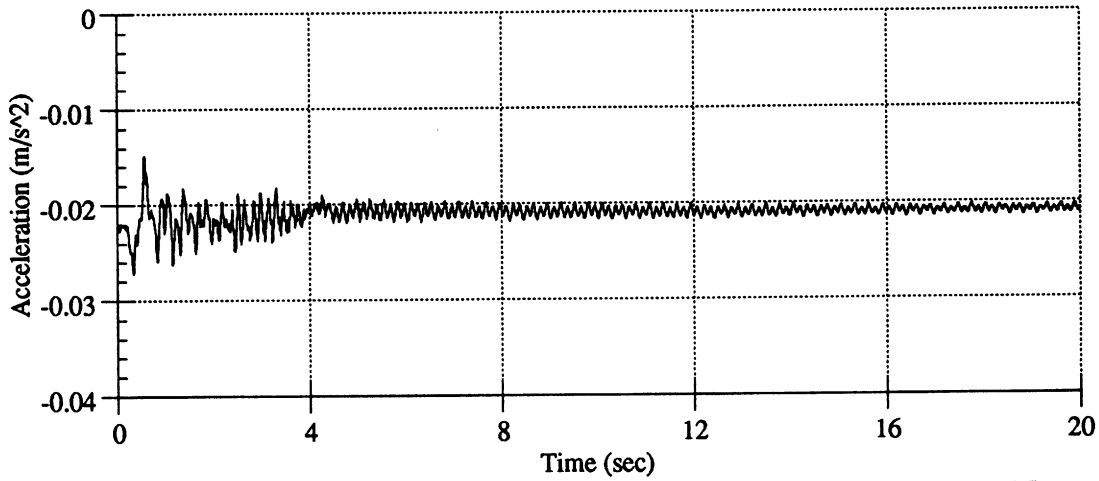

Figure 5-16: Acceleration of Shaped, 15°/sec Slew Using Long-2M3 Sequence, from {30,60,10} to {-30,10,60}.

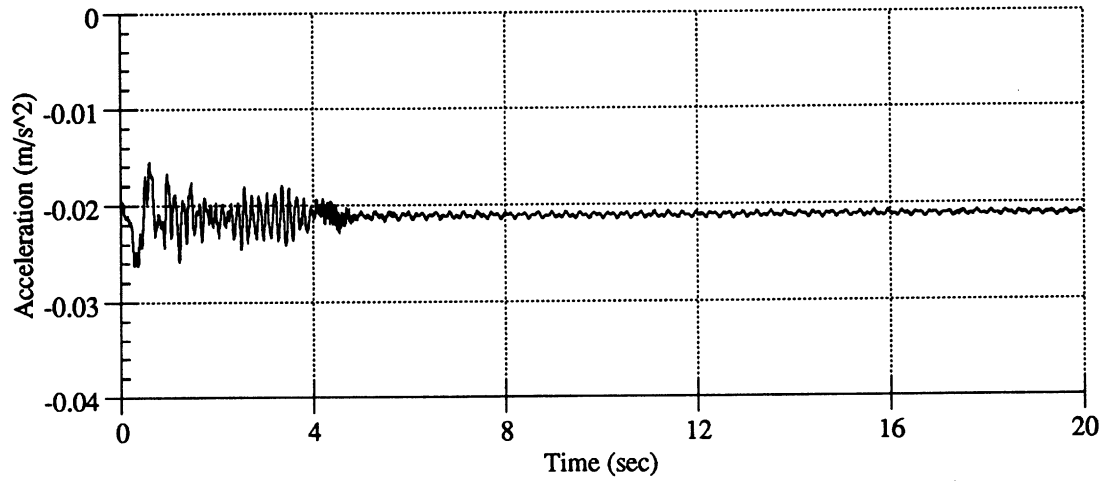

Figure 5-17: Acceleration of Shaped, 15°/sec Slew, Using Adaptive Long-2M3 Sequence, from {30,60,10} to {-30,10,60}

When the velocity limit is increased and the same test is performed, the results, shown in Table 5-5, are similar. Most of the sequences give good results. We do notice that the shortest sequences--the Short-2M3--give the poorest results. The longest sequences tend to be unable to eliminate the 7.0 Hz mode.

Table 5-5: Vibration Reduction in Variable Frequency Move, {30,60,10} to {-30,10,60} at 30°/sec.

Type of Shaper	Time Delay (sec)	3.3 Hz Residual Vibration (%)	7.0 Hz Residual Vibration (%)
Unshaped	0.00	100	100
Short-2M3	0.440	12.31	24.60
Long-2M3	0.528	4.97	4.77
Short-2M5	0.872	6.53	14.20
Long-2M5	1.016	7.25	15.15
4M9	0.848	7.68	18.95
1M3	1.048	3.32	24.90
Short-2M3, Varying	0.44 approx	16.48	16.42
Long-2M3, Varying	0.52 approx	10.76	10.76
Short-2M5, Varying	0.87 approx	5.41	2.16
Long-2M5, Varying	1.02 approx	8.04	39.37

At this point we will present some of the accelerometer data from the in-plane accelerometer. Due to a large amount of backlash in the elbow joint and the damping in the elbow and shoulder controllers, the signal from the in-plane accelerometer is not as crisp as the out of plane. Figures 5-18 -- 5-20 show accereration time-traces for the unshaped, Long-2M5, and Adaptive-Long-2M5 filters during the 30°/sec move from {30,60,10} to {-30,10,60}. The vibrations dissipate much faster than those seen by the out of plane accelerometer. The time history graphs show significant reduction of vibration when the input is shaped. However, the gain on the FFT is not as clear, as can be seen in Figures 5-21 -- 5-23, which show the FFT magnitude for the residual vibration for these same tests. The lack of clear peaks on the FFT Magnitude for the unshaped maneuver can be attributed to backlash in the elbow joint. When the vibration amplitude is large, the joint will bounce back and forth across the backlash. During a shaped maneuver, the vibration amplitude will be too small to overcome the preload on the joint due to gravity, and the joint will not pass through the backlash during the vibration. This phenomenon can explain the presence of sharp peaks in shaped slews where there are broad peaks in the unshaped slews. Backlash in the elbow will cause this phenomenon during the final set of varying-frequency tests.

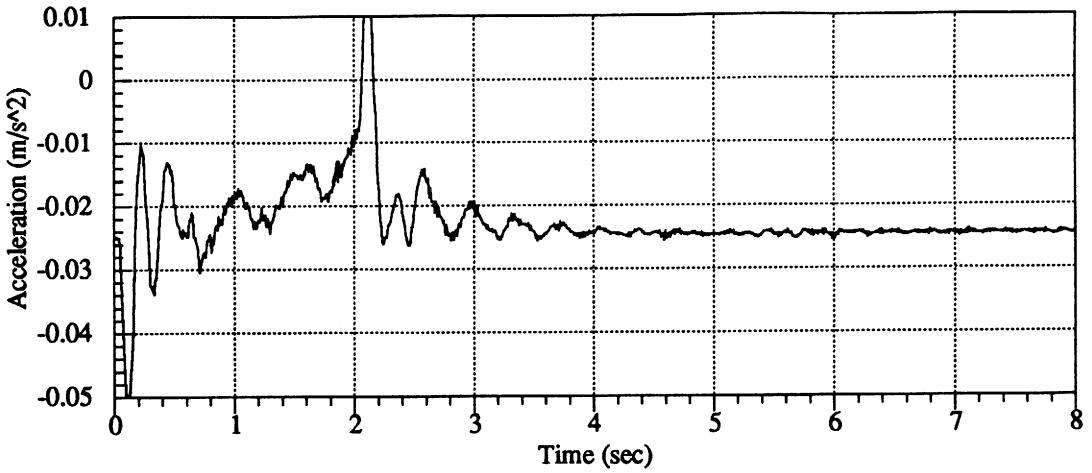

Figure 5-18: In-Plane Acceleration from Unshaped move from {30,60,10} to {-30,10,60} at 30°/sec.

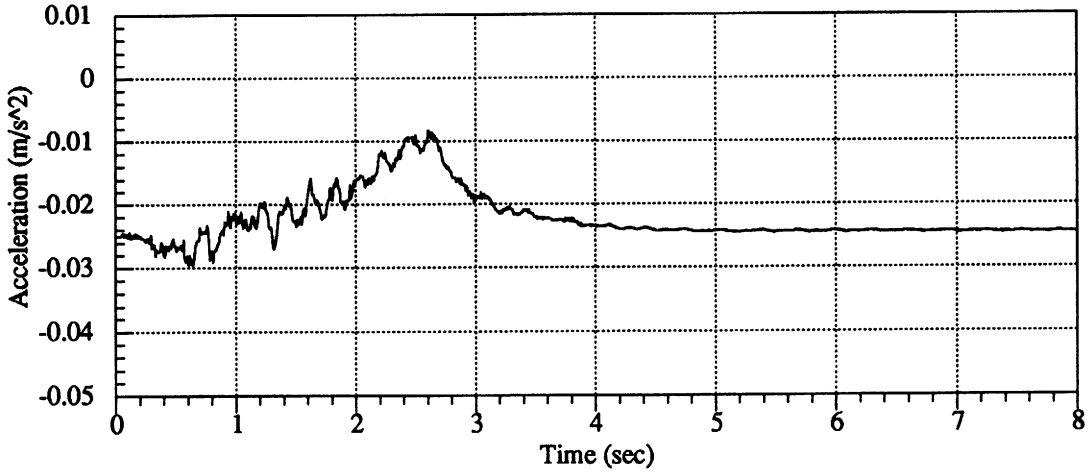

Figure 5-19: In-Plane Acceleration from Long-2M5 move from {30,60,10} to {-30,10,60} at 30°/sec.

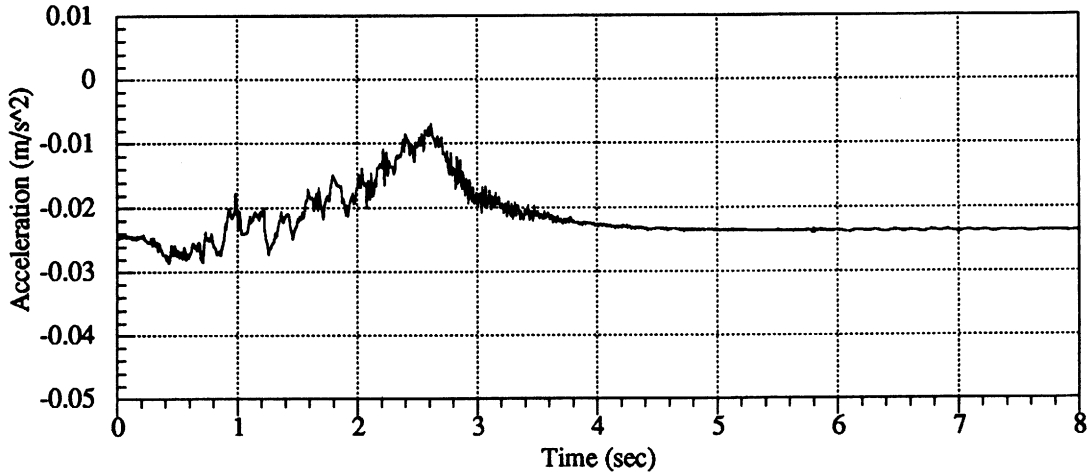

Figure 5-20: In-Plane Acceleration from Adaptive-Long-2M5 move from {30,60,10} to {-30,10,60} at 30°/sec.

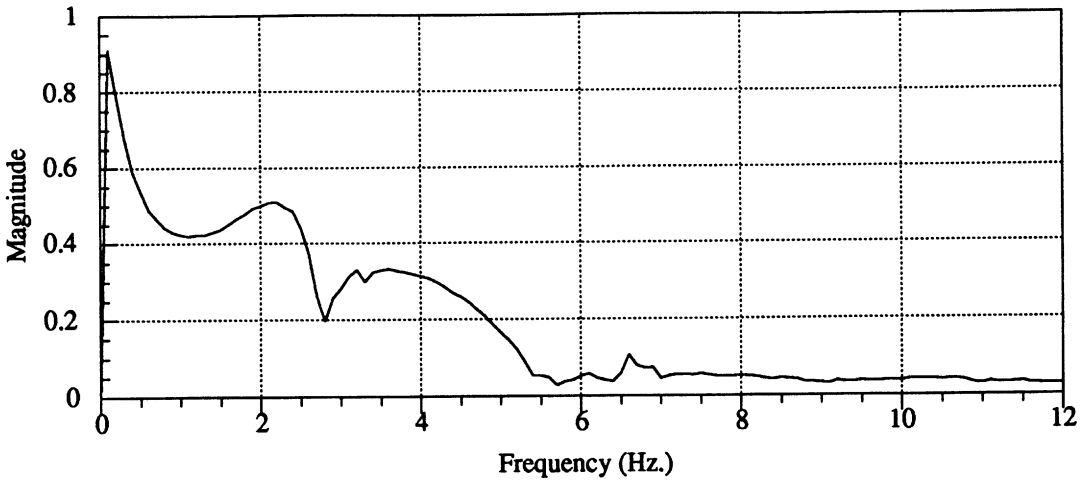

Figure 5-21: FFT Magnitude of In-Plane Acceleration of Unshaped Move from {30,60,10} to {-30,10,60} at 30°/sec.

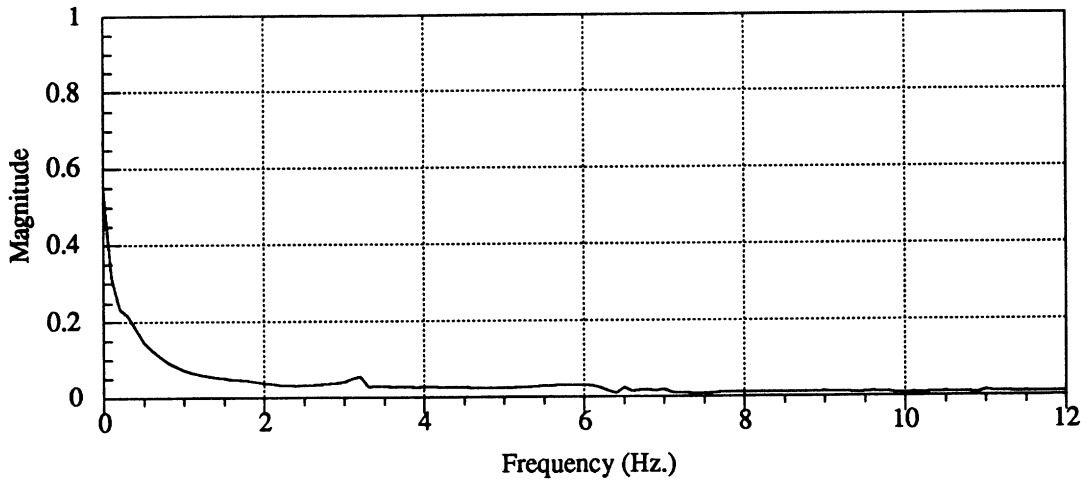

Figure 5-22: FFT Magnitude of In-Plane Acceleration of Long-2M5 Move from {30,60,10} to {-30,10,60} at 30°/sec.

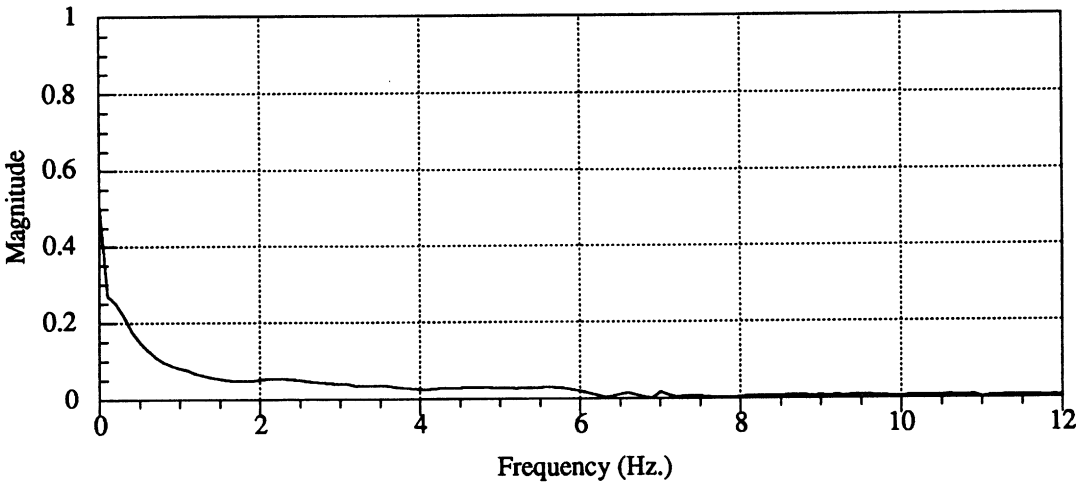

Figure 5-23: FFT Magnitude of In-Plane Acceleration of Adaptive-Long-2M5 Move from {30,60,10} to {-30,10,60} at 30°/sec.

Table 5-6: Vibration Reduction in Variable Frequency Move, {30,60,10} to {-30,10,60} at 50°/sec.

Type of Shaper	Time Delay (sec)	3.3 Hz Residual Vibration (%)	7.0 Hz Residual Vibration (%)
Unshaped	0.00	100	100
Long-2M3	0.528	13.77	3.22
Short-2M5	0.872	14.52	6.75
Long-2M3, Varying	0.52 approx	9.97	12.24
Short-2M5, Varying	0.87 approx	5.43	8.46

5.4.2 Varying-Frequency Move not at Tuned-Frequency Position

The final tests were performed at a different configuration of the system, where the tuned-frequency position is not within the trajectory. This maneuver moves the base joint from 0° to 30° while the shoulder and elbow move from 80° to 45°. The velocity limit is set to 50°/sec. This slew ends almost at the tuned-frequency position. Figure 5-24 shows the FFT magnitude for the unshaped response. We see that the FFT for this maneuver is no longer the sharp spike seen in all the above responses. It shows a large amount of noise from the in-plane vibration. The shaped response for an Adaptive-Long-2M3 slew is shown in Figure 5-25, and the response for a Long-2M3 slew is shown in Figure 5-26. The data is difficult to tabulate, as the shaped response virtually eliminates the wide-frequency band of noise, but produces a spike at a frequency that was not excited during the unshaped move. The shaped-frequency response produces spikes at the

frequencies predicted by the frequency mapping exercise of Section 4.4. These results show that the adaptive filtering is less effective than constant-valued filtering. The other filters perform similarly, with the adaptive filters leaving more residual vibration than the constant-valued shapers.

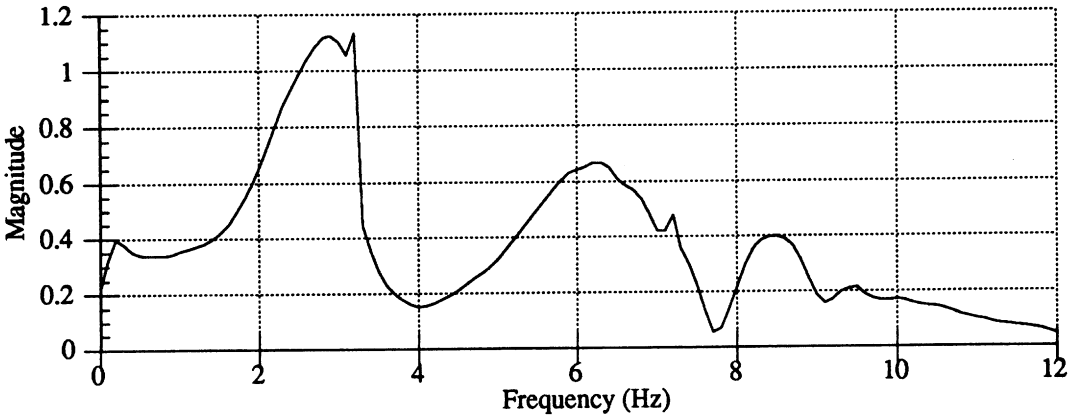

Figure 5-24: FFT Magnitude of Unshaped Response: 50°/sec Velocity Move from {0,80,80} to {30,45,45}.

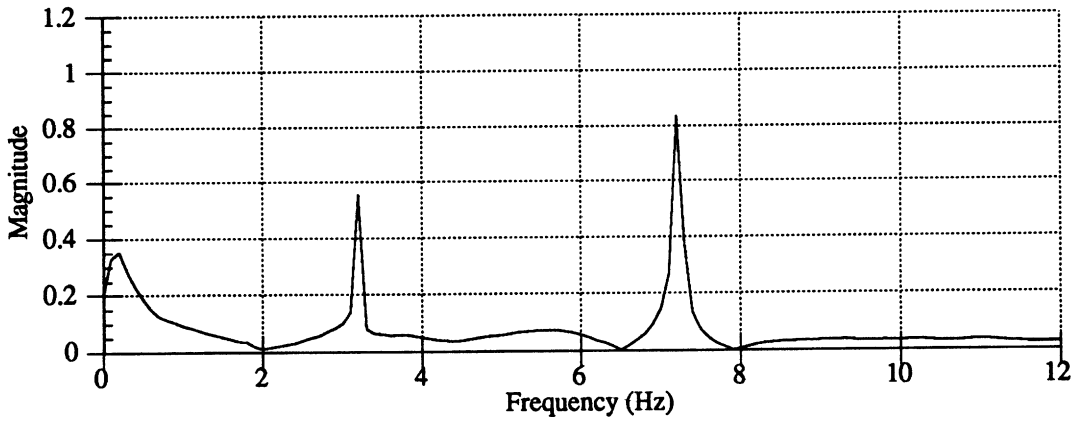

Figure 5-25: FFT Magnitude of Adaptive-Long-2M3 Shaper: 50°/sec Velocity Move from {0,80,80} to {30,45,45}.

5.5 Effect of Varying Prefiltering Sequences

The adaptive shaping technique developed shows promise in reducing the residual vibration in systems with large frequency variations. The method needs further work before it can be used with confidence. One issue that has not been addressed is stability. With the adaptive shaping technique, the

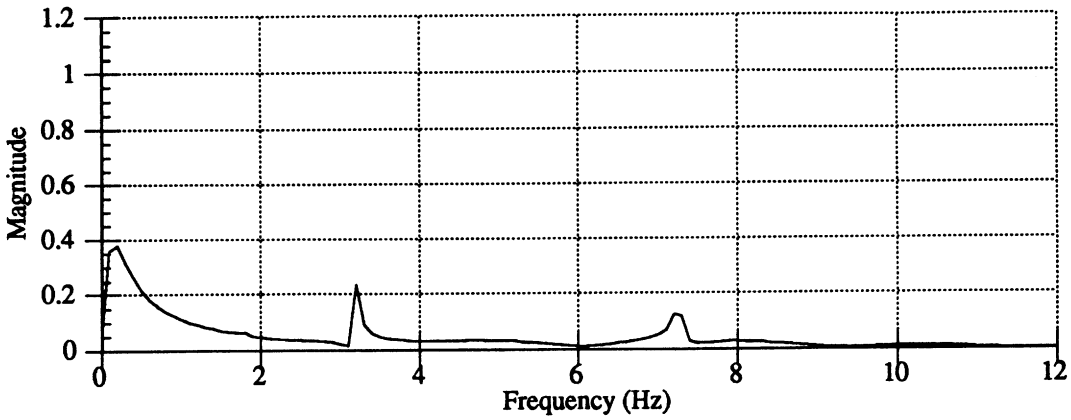

Figure 5-26: FFT Magnitude of Long-2M3 Shaper:
50°/sec Velocity Move from {0,80,80} to {30,45,45}.

input shaping is inside a feedback loop, so stability can be a problem. The slow variation of the shaping sequence with position suggests that the chance of instability is small. As the rate of change in frequency as a function of position rises, the sequences will vary faster, increasing the possibility of instability. While testing the method, the varying method only caused problems near the limit of the workspace, where the frequencies change fastest.

5.6 Comparison of Windowing Sequences.

In Chapter 3, we showed that input shaping algorithms are similar to Parzen and square windows. Several tests were performed comparing an input shaping window resembling a Parzen window. The sequence used is shown in Figure 5-27. The results of the testing are shown in Table 5-7. The triangular sequence has a time delay of 0.959 sec., an 8.5% savings over the 1M3 sequence. The triangular sequence could prove to be useful when many different frequencies need to be canceled. The Parzen window has been commonly used for this purpose in the past in windowing data without aliasing data [17]. Due to the large time delay when compared to the Short-

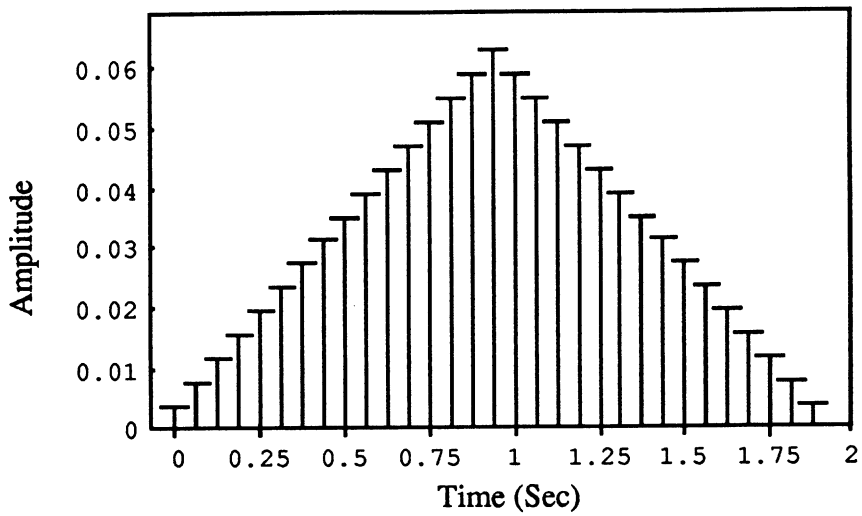

Figure 5-27: Sequence for Window Tests: Three-Impulse Sequences for 1.983, 3.966, 7.932, and 15.864 Hz

Table 5-7: Results of Windowing Tests.

Type of Move	3.3 Hz Residual Vibration (%)	7.0 Hz Residual Vibration (%)
15°/sec {-30,30,30} to {30,30,30}	4.02	7.72
50°/sec {-30,80,80} to (30,80,80}	2.17	0.54
15°/sec {30,60,10} to {-30,10,60}	2.66	6.56
30°/sec {30,60,10} to {-30,10,60}	14.61	8.36

2M3, Long2M3, or Short-2M5 sequences, the proper implementation may be to convolve a single two-impulse filter (Figure 2-3) with a Parzen window, to eliminate many different frequencies.

5.7 Conclusions

The results of the tests show that the direct-solution sequences developed in Chapter 3 reduce the residual vibration as well as the direct-solution

sequences that Hyde developed[10]. In many tests, short sequences performed well compared to longer, supposedly more robust, sequences. The highest frequency, the 7.0 Hz mode, is often difficult to control. Chang [5] shows that controller bandwidth has a strong effect on the ability to reduce vibrations. Previous experience with the Flexbot showed that with a low-damping, low-bandwidth, controller on the base joint, the shaping algorithms gave very poor results.

The new adaptive shaping technique was able to significantly reduce residual vibrations in some tests. The Long-2M3 and Short-2M5 were the adaptive sequence most successful in reducing vibrations. Experimental evidence does not show that the results are improved for all types of motions.

sequences that Hyde developed [8] in many tests, short sequences performed well compared to longer, supposedly more robust, sequences. The highest frequency, the 7.0 Hz mode, is often difficult to control. Chang [5] shows that controller bandwidth has a strong effect on the ability to reduce vibrations. Previous experience with the Flexbot showed that with a low-damping, low-bandwidth, controller on the base joint, the shaping algorithms gave very poor results.

The new adaptive shaping technique was able to significantly reduce residual vibrations in some tests. The Long-ZMS and Short-ZMS were the adaptive sequence most successful in reducing vibrations. Experimental evidence does not show that the results are improved for all types of motions.

Conclusions

Chapter 6

6.1 Summary

This document addressed several issues in implementing input command shaping techniques on flexible systems. First, an analytical solution was derived for calculating input command shaping sequences for two, undamped modes of vibration. The new sequences can be calculated for a wide range of frequencies. A method was developed to find approximate solutions for systems with two, damped frequencies. The limitations of the new solution method are addressed with attention focused on the frequency range that is applicable to the method and the time savings of the new sequences. The equations for calculating multiple mode sequences (more than two) are analyzed and some possible solution methods are proposed. The two-mode sequences were shown to have comparable robustness to modelling errors as previously-developed sequences, while providing a significant time savings. A simple analysis of negative-impulse sequences that can be found by adjusting the all-positive-valued-impulse constraint was performed,

addressing the issues of insensitivity to modelling errors and time savings. Also, a comparison between several standard data windowing techniques and input shaping sequences was performed. Two window shapes that are commonly used for data windowing can be applied in the same manner as input shaping sequences to reduce residual vibrations.

Second, problems involving the application of input command shaping to physical systems were addressed. A new shaping technique was developed to compensate for the large variation in system frequency over the workspace that exists in many systems. The adaptive shaping technique calculates a new shaping sequence at each time step of the digital controller. The sequences are calculated based upon the current system position, using an on-line map of the system frequencies. Discretization problems were discussed and a method for eliminating discretization errors was developed.

Finally, the new-sequences and the adaptive shaping technique were tested on the Flexbot, a three-degree-of-freedom, flexible manipulator located in the MIT Artificial Intelligence Laboratory. The new sequences were shown to be more effective at reducing residual vibration than comparable convolved sequences, while providing a significant time savings. The adaptive shaping technique successfully reduced the vibrations. Compared to constant-valued shapers, adaptive shaping provided improved performance in several tests, comparable vibration reduction for others tests, and worse results for some. Stability remains as an issue that needs to be addressed. Accuracy of the frequency map, speed of the move, and rate of change of frequency with position all effect the performance of the adaptive system. Several sequences designed to mimic data windows were tested and found to provide good results, although not as good as most of the sequences.

6.2 Suggested Work

The success of the two-mode sequences in reducing residual vibration suggests that effort be continued in finding easier methods of calculating sequences for higher mode systems. Also, an investigation of the nature of the negative-impulses sequences that are generated by the direct-solution technique was performed. Negative sequences will be shorter than positive sequences, but will excite other frequencies and, as a result, will have poor robustness to modelling errors.

The adaptive shaping technique show definite promise. The current implementation is not perfect. The experimental results show that it can be effective in certain configurations. Several issues to address are stability of the system and how velocity, servo rate, and frequency variation affect the stability; possible implementations that reduce the short drift that presently occurs at the end of a move; and on line identification of frequencies an in Tzes and Yurkovich [23] to allow for greater flexibility of the system.

Other important issues remain to be addressed. Designing systems to take the most advantage of the vibration reduction ability of preshaping, the effectiveness of command shaping on non-linear systems, and the effect of the closed-loop dynamics on the ability to successfully control vibrations all remain to be investigated fully.

6.2 Suggested Work

The success of the two-mode sequences in reducing residual vibration suggests that effort be continued in finding easier methods of calculating sequences for higher mode systems. Also, an investigation of the nature of the negative-impulses sequences that are generated by the direct-solution technique was performed. Negative sequences will be shorter than positive sequences, but will excite other frequencies and, as a result, will have poor robustness to modelling errors.

The adaptive shaping technique show definite promise. The current implementation is not perfect. The experimental results show that it can be effective in certain configurations. Several issues to address are stability of the system and how velocity, servo rate, and frequency variation affect the stability; possible implementations that reduce the short drift that presently occurs at the end of a move; and on line identification of frequencies as in Tzes and Yurkovich [28] to allow for greater flexibility of the system.

Other important issues remain to be addressed. Designing systems to take the most advantage of the vibration reduction ability of preshaping, the effectiveness of command shaping on non-linear systems, and the effect of the closed-loop dynamics on the ability to successfully control vibrations all remain to be investigated fully.

References

1 Asada, H., Ma, Z., and Tokumaru, H., "Inverse Dynamics of Flexible Robot Arms for Trajectory Control," Modeling and Control of Robotic Manipulators and Manufacturing Processes Session, ASME Winter Annual Meeting, 1987.

2 Aspinwall, D. M., "Acceleration Profiles for Minimizing Residual Response." *Journal of Dynamic Systems, Measurement, and Control*, Vol. 102, March, 1980.

3 Avery, Brian L., *A Force Control Analysis of a Harmonic Drive Robot*, Master of Science Thesis, Massachusetts Institute of Technology, 1992.

4 Brooke, Kendrick, and Meeraus, *GAMS: A User's Guide*, Redwood City, CA: The Scientific Press, 1988.

5 Chang, Kenneth W., *Shaping Inputs to Reduce Vibration in Large Flexible Space Structures*, Master of Science Thesis, Massachusetts Institute of Technology, 1992.

6 Christian, Andrew D., *Design and Implementation of a Flexible Robot*, Massachusetts Institute of Technology Artificial Intelligence Laboratory Technical Report No. 1153, 1989.

7 Eisler, G. R., Segalman, D. J., and Robinett, R. D., "Approximate Minimum-Time Trajectories for Two-Link Flexible Manipulators," American Control Conference, San Diego, California, May, 1989.

8 Farrenkopf, R. L., "Optimal Open-Loop Maneuver Profiles for Flexible Spacecraft," *Journal of Guidance and Control*, Vol. 2, No. 6, Nov.-Dec., 1979.

9 *HP 3563A Operating Manual: Control Systems Analyzer*, HP Part No. 03563-90000, Everett, WA: Hewlett-Packard Company, 1990.

10 Hyde, James, M., *Multiple Mode Vibration Suppression in Controlled Flexible Systems*, Massachusetts Institute of Technology Artificial Intelligence Laboratory Technical Report No. 1295, 1991.

11 Magee, David P., *Dynamic Control Modification Techniques in Teleoperation of a Flexible Manipulator*, Master of Science Thesis, Georgia Institute of Technology, 1991.

12 Meckl, Peter H., *Control of Vibration in Mechanical Systems Using Shaped Reference Inputs*, Massachusetts Institute of Technology Artificial Intelligence Laboratory Technical Report No. 1018, 1988.

13 Miller, D. W., Sepe, R. B., Rey, D., Saarmaa, E., and Crawley, E. F., "The Middeck Active Control Experiment (MACE)," Fifth NASA/DOD Controlled Structures Interaction Technology Conference, Lake Tahoe, NV, March, 1992.

14 Murphy, B. R., and Watanabe, I., "Digital Shaping Filters for Reducing Machine Vibration," *IEEE Transactions on Robotics and Automation*, Vol. 8, No. 2, April, 1992.

15 *MVME147S MPU VMEmodule User's Manual*, Motorola, Inc.

16 Narasimhan, S, Siegel, D., *The Condor Programmer's Manual-Version II*, Massachusetts Institute of Technology Artificial Intelligence Laboratory Working Paper No. 297, July, 1987.

17 Press, W., Flennery, B, Teukolsky, S. and Vetterling, W, *Numerical Recipes in C: The Art of Scientific Computing*, Cambridge: Cambridge UP, 1990.

18 Singer, Neil C., *Residual Vibration Reduction in Computer Controlled Machines*, Massachusetts Institute of Technology Artificial Intelligence Laboratory Technical Report No. 1030, 1989.

19 Singhose, William, "Shaping Inputs to Reduce Vibration: A Vector Diagram Approach," Massachusetts Institute of Technology Artificial Intelligence Laboratory Memo No. 1223, March, 1990.

20 Smith, O. J. M., *Feedback Control Systems*, New York: McGraw-Hill, 1958.

21 Swigert, C. J., "Shaped Torque Techniques." *Journal of Guidance and Control*, Vol. 3, No. 5, Sept.-Oct., 1980.

22 Turner, James D., and Junkins, John L., "Optimal Large-Angle Single-Axis Rotational Maneuvers of Flexible Spacecraft," *Journal of Guidance and Control*, Vol. 3, No. 6, Nov.-Dec., 1980.

23 Tzes, Anthony P., and Yurkovich, Stephen, "Application and Comparison of On-Line Identification Methods for Flexible Manipulator Control," *Proceedings 1989 International Conference on Advanced Robotics*, Columbus, OH, June, 1989.

24 Tzes, Anthony P., Englehart, Matthew J., and Yurkovich, Stephen, "Input Preshaping With Frequency Domain Information For Flexible-Link Manipulator Control," AIAA Guidance, Navigation and Control Conference, August, 1989.

25 *User Manual for DT1401 Series 12-Bit Resolution Analog/Digital I/O Systems for the VMEbus*, Document UM-05012-F, Marlboro, MA: Data Translation, Inc., 1987.

26 *User Manual for DT1406 Series 12-Bit Resolution Digital to Analog Converter Subsystems for the VMEbus*, Document UM-05076-A, Marlboro, MA: Data Translation, Inc., 1987.

27 *VME Bus Series Dual Channel Incremental Encoder Interface: User's Manual, Model VME-3570*, Ann Arbor, MI: Whedco Inc., 1987.

28 *VXWorks: Programmer's Guide*, Alameda, CA: Wind River Systems, 1990.

29 *VXWorks: Reference Manual*, Alameda, CA: Wind River Systems, 1990.

30 Wolfram, Stephen, *Mathematica: A System for Doing Mathematics by Computer, Second Edition*, Redwood City, CA: Addison-Wesley, 1991.

31 Banerjee, Arun K., "Dynamics and Control of the WISP Shuttle-Antenna System," Lockheed Palo Alto Research Lab, 1992.

32 Keene, Donald, "Improved Shuttle Manipulator Control Using Derived End-Point Feedback," C. S. Draper Laboratory Intralab Memo, August, 1991.

33 Newsom, J., Layman, W., Waites, H., and Hayduk, R., "The NASA Controls-Structures Interaction Technology Program," The 41st Congress of International Astronautical Foundatiaon, Dresden, GDR, Oct., 1990.

34 Seth, N., Rattan, K., and Brandstetter, K., "Vibration Control of a Coordinate Measuring Machine," Wright State University, Dayton, OH, 1992.

CS-TR Scanning Project
Document Control Form

Date : 5 / 11 / 95

Report # AI-TR-1371

Each of the following should be identified by a checkmark:
Originating Department:

☒ Artificial Intellegence Laboratory (AI)
☐ Laboratory for Computer Science (LCS)

Document Type:

☒ Technical Report (TR) ☐ Technical Memo (TM)
☐ Other:_____

Document Information

Number of pages: 120(127-IMAGES)
Not to include DOD forms, printer intstructions, etc... original pages only.

Originals are:
☐ Single-sided or
☒ Double-sided

Intended to be printed as :
☐ Single-sided or
☒ Double-sided

Print type:
☐ Typewriter ☐ Offset Press ☒ Laser Print
☐ InkJet Printer ☐ Unknown ☐ Other:_____

Check each if included with document:

☒ DOD Form ☐ Funding Agent Form ☒ Cover Page
☒ Spine ☐ Printers Notes ☐ Photo negatives
☐ Other: _____

Page Data:

Blank Pages(by page number): BACK OF TITLE PAGE, 4, 6, 8, 16

Photographs/Tonal Material (by page number): 24-, 27, 35-38

Other (note description/page number):

Description :	Page Number:
IMAGE MAP	(1-2)
UNNUM'ED TITLE AND BLANK	(3-120)
PAGES NUM'ED	3-120
SCANCONTROL, COVER, SPINE, DOD	(121-124)
TRGTS (3)	(125-127)

Scanning Agent Signoff:

Date Received: 5/11/95 Date Scanned: 5/15/95 Date Returned: 5/18/95

Scanning Agent Signature: Michael W. Cook

REPORT DOCUMENTATION PAGE

Form Approved
OBM No. 0704-0188

Public reporting burden for this collection of information is estimated to average 1 hour per response. Including the time for reviewing instructions, searching existing data sources, gathering and maintaining the data needed, and completing and reviewing the collection of information. Send comments regarding this burden estimate or any other aspect orf this collection of information, including suggestions for reducing this burden, to Washington Headquarters Services, Directorate for Information Operations and Reports, 1215 Jefferson Davis Highway, Suite 1204, Arlington, VA 22202-4302, and to the Office of Management and Budget, Paperwork Reduction Project (0704-0188), Washington, DC 20503.

1. AGENCY USE ONLY (Leave Blank)	2. REPORT DATE	3. REPORT TYPE AND DATES COVERED
	June 1992	

4. TITLE AND SUBTITLE
Minimizing Residual Vibrations in Flexible Systems

5. FUNDING NUMBERS

6. AUTHOR(S)
B. Whitney Rappole, Jr.

7. PERFORMING ORGANIZATION NAME(S) AND ADDRESS(ES)
Massachusetts Institute of Technology
Artificial Intelligence Laboratory
545 Technology Square
Cambridge, Massachusetts 02139

8. PERFORMING ORGANIZATION REPORT NUMBER
AITR 1371

9. SPONSORING/MONITORING AGENCY NAME(S) AND ADDRESS(ES)
Office of Naval Research
Information Systems
Arlington, Virginia 22217

10. SPONSORING/MONITORING AGENCY REPORT NUMBER
AD-A290074

11. SUPPLEMENTARY NOTES
None

12a. DISTRIBUTION/AVAILABILITY STATEMENT
DISTRIBUTION UNLIMITED

12b. DISTRIBUTION CODE

13. ABSTRACT (*Maximum 200 words*)

Residual vibrations degrade the performance of many systems. Due to the lightweight and flexible nature of space structures, controlling residual vibrations is especially difficult. Also, systems such as the Space Shuttle remote Manipulator System have frequencies that vary significantly based upon configuration and loading. Recently, a technique of minimizing vibrations in flexible structures by command input shaping was developed. This document presents research completed in developing a simple, closed-form method of calculating input shaping sequences for two-mode systems and a system to adapt the command input shaping technique to known changes in system frequency about the workspace. The new techniques were tested on a three-link, flexible manipulator.

14. SUBJECT TERMS
input shaping, vibration suppression, robots, space structures, adaptive

15. NUMBER OF PAGES
122

16. PRICE CODE

17. SECURITY CLASSIFICATION OF REPORT	18. SECURITY CLASSIFICATION OF THIS PAGE	19. SECURITY CLASSIFICATION OF ABSTRACT	20. LIMITATION OF ABSTRACT
UNCLASSIFIED	UNCLASSIFIED	UNCLASSIFIED	UNCLASSIFIED

Scanning Agent Identification Target

Scanning of this document was supported in part by the **Corporation for National Research Initiatives,** using funds from the **Advanced Research Projects Agency** of the **United states Government** under Grant: **MDA972-92-J1029.**

The scanning agent for this project was the **Document Services** department of the **M.I.T Libraries.** Technical support for this project was also provided by the **M.I.T. Laboratory for Computer Sciences.**

Scanned

Date: 5/15/1995

M.I.T. Libraries
Document Services